A Study of Load Responses towards the Pavement Edge

Jostein Aksnes

Thesis submitted to the Faculty of Engineering Science and Technology, Norwegian University of Science and Technology, in partial fulfilment of the requirements for the Dr.ing. degree

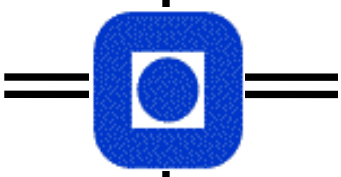

Department of Road end Railway Engineering

Norwegian University of Science and Technology

NTNU

August, 2002

URN:NBN:no-3347

The committee for appraisal of this thesis was comprised of the following members:

Professor, **Ulf Isacsson**
Department of Highway Engineering,
Royal Institute of Technology,
Stockholm, Sweden

Senior engineer, Dr.ing. **Tore Slyngstad**
Norwegian Public Roads Administration
Oslo, Norway

Professor, Dr.ing. **Steinar Nordal**
Department of Geotechnical Engineering
Norwegian University of Science and Technology,
Trondheim, Norway

Advisors during the study have been:

Professor emeritus, **Rasmus S. Nordal**,
Department of Road and Railway Engineering
Norwegian University of Science and Technology,
Trondheim, Norway

Associate professor, Dr.ing. **Helge Mork**,
Department of Road and Railway Engineering
Norwegian University of Science and Technology,
Trondheim, Norway

Research scientist, Dr.ing. **Inge Hoff**,
SINTEF Civil and Environmental Engineering, Roads and Transport,
Trondheim, Norway

URN:NBN:no-3347

ABSTRACT

A major part of the national and county road network in Norway consists of two-lane roads with relatively narrow shoulders. The width of the roadway is limited, forcing heavy trucks to drive close to the pavement edge. This represents a considerable deteriorating effect on these pavements, which typically consist of granular base materials and thin asphalt surfacing. The result is often premature cracking and deformations along the pavement edge. Despite the fact that pavement edge damages represent a great problem for the Norwegian road network, little research has been performed on this topic. This is the main background for the present thesis work to focus on pavement edge damages and load responses towards the pavement edge.

Chapter 2 gives a brief presentation of the basic theory of continuum mechanics together with some elastic constitutive material models. The general elasto-plastic theory is also described. Further, methods and programs based on elastic layer theory developed for structural analysis of pavements are presented. Finally, advantages and basic principles for the finite element method are discussed.

In *Chapter 3* the different types of pavement edge damages are described. Further, the factors influencing the strength of the pavement edge and damage development are discussed. To get information of the variation of bearing capacity over the cross section of existing roads, own FWD measurements are performed at different sites in Sør-Trøndelag county. As expected, a considerable decrease in bearing capacity towards the pavement edge was found. Also a minor field study on the effect of varying side slope is accomplished. The structural effect of gradually steepening the side slope is measured by FWD and plate loading tests. Chapter 3 also contains the findings from a literature review on measurement and calculation of pavement edge effects. Only a small number of articles on these subjects were found.

A full-scale pavement test has been performed at Sandmoen near Trondheim. Two pavements with different subbase materials were constructed, one of them instrumented for the measurement of stresses and strains in the base and subbase

layers at different offsets from the pavement edge. The construction work, materials, sensor types and positions are thoroughly described in *Chapter 4*.

Results from Sandmoen test field are presented in *Chapter 5*. Responses to three different types of loading have been measured. These are controlled wheel loading, FWD and plate loading. Vertical stresses have been successfully measured at the bottom of both the base and the subbase layers. Independent of loading type, the results show increasing vertical stresses as loads are applied closer to the pavement edge. This effect is evident at the bottom of the base layer for load positions closer than approximately one meter from the edge. Increasing horizontal stress is recorded at the bottom of the base layer when a load is applied on the pavement surface. Deformation measurements show large plastic strains in granular materials, especially for load application close to the pavement edge. Parts of these strains recover when the load position is changed.

Theoretical modelling and analysis of the Sandmoen test field are dealt with in *Chapter 6*. Both multilayered elastic and three dimensional finite element analyses are performed. In all calculations, the load is modelled as a uniformly distributed vertical pressure over a circular area, and all materials are modelled as linear elastic with material parameters found from laboratory testing. When linear elastic material models are used, the three dimensional finite element calculations show only insignificant differences in stresses, strains and deformations as the load is moved towards the pavement edge. Best correlation between measured and calculated load responses are found for vertical stress and strain in the base layer for the case of static plate loading being applied in the inner wheel path. Beyond this, the comparisons of measured and calculated load responses show considerable discrepancies.

ACKNOWLEDGEMENTS

This work has been carried out at the Department of Road and Railway Engineering at the Norwegian University of Science and Technology, which at the beginning of the study was known as the Norwegian Institute of Technology. Until his retirement in 1998, Professor Rasmus S. Nordal was my advisor. He encouraged me to apply for the scholarship and to start the doctoral study. After Nordal's retirement, Associate professor Helge Mork became my advisor. I would like to thank both Rasmus and Helge for their support and guidance.

Through the whole study I have had a valuable co-operation with Dr. ing. Inge Hoff, who finally was appointed to be my co-advisor. I owe Inge great thanks for his help and advice, which has been of vital importance for the accomplishment of the study.

I am very grateful to the staff at the Department of Road and Railway Engineering and the "Lab-gang" at SINTEF Civil and Environmental Engineering, Roads and transport for all their help. Especially I want to thank Einar Værnes for essential contribution regarding built-in instrumentation and signal conditioning, and Stein Hoseth and Tore Menne for help with the construction work and field measurements at the Sandmoen test field.

The Norwegian Public Roads Administration (NPRA) has been an important contributor to the present work. NPRA was giving the scholarship and has since 1996 been my employer. I am particularly grateful to NPRA, Sør-Trøndelag county for important contributions to the field testing projects and for allowing me to finalise my doctoral study.

Last but not least I will give thanks to my wife, Hanne, and our children, Siri and Vegard, for being precious sources of joy and recreation at leisure time, and for their love and patience during this work.

TABLE OF CONTENTS

LIST OF SYMBOLS AND ABBREVIATIONS

Latin symbols

A	Plastic resistance number
a	Attraction or load radius
B	Strain displacement matrix
B_1, B_2, B_3	Model parameters in the Boyce model
c	Cohesion ($c = a \cdot \tan\phi$)
C_u	Coefficient of uniformity
D	Dilatancy parameter or plate diameter
D	Stress-strain matrix, stiffness matrix, constitutive matrix
$\mathbf{D}_{ep}$	Elasto-plastic stiffness matrix
d	Deflection
E	Young's modulus
e	Matrix representation of the deviatoric strain tensor
e_{ij}	Deviatoric strain component (i, j = 1, 2, 3)
F	Factor of safety ($F = \tan\phi/\tan\rho$) or yield surface
F	Body force
f	Degree of shear mobilization ($f = 1/F = \tan\rho/\tan\phi$)
G	Shear modulus
g	Acceleration of gravity
g_0	Non-dimensional shear deformation modulus number
h	layer thickness
I_i	Stress invariants (i = 1, 2, 3)
I_1^{ε}	First strain invariant
J_i	Deviatoric stress invariants (i = 1, 2, 3)
J_2^{ε}	Second deviatoric strain invariant
K	Bulk modulus
K_0'	Coefficient of earth pressure at rest ($K_0' = \sigma_{h0}'/\sigma_{v0}'$)
k	Element stiffness matrix
k_0	Non-dimensional bulk modulus number
k_1, k_2	Model parameters in the K-θ model
M_r	Resilient modulus

N	Matrix of interpolation polynomials in space for the displacements
n	Porosity or stress dependency exponent
P	Force applied to the core in the split cylinder test or surface load
p	Pressure
Q	Potential surface
q	Deviator stress (σ_1 - σ_3)
R	Distance from point load to element in the Boussinesq model ($R^2=r^2+z^2$)
r	Radius under axial symmetry
S	Nodal force vector
$\mathbf{S}_F^0$	Body force vector
$\mathbf{S}_T^0$	Surface force vector
S_t	Tensile strength of bituminous materials found from the split cylinder test
S_σ	Part of the surface where surface traction is acting
s	Matrix representation of the deviatoric stress tensor
s_u	Undrained shear strength
t	Time or layer thickness
U	Energy
u	Vector of displacement
u	Radial displacement
V	Volume
v	Vector of nodal displacements
v	Displacement in r- or x-direction
W^p	Dissipated energy
w	Displacement in z-direction
w_{opt}	Optimum water content
x, y, z	Cartesian coordinates

Greek symbols

α	Angle
Δ	Symbol denoting a change in the parameter that follows
δ_{max}	Maximum dry density
$\boldsymbol{\varepsilon}$	Matrix/vector representation of a strain tensor

$\varepsilon_1, \varepsilon_2, \varepsilon_3$	Principal strains
ε^e	Elastic strain
ε^p	Plastic strain
ε_m	Mean strain, $\varepsilon_m = (\varepsilon_1+\varepsilon_2+\varepsilon_3)/3$
ε_s	Shear strain
ε_v	Volumetric strain, $\varepsilon_v = \varepsilon_1+\varepsilon_2+\varepsilon_3 = 3\varepsilon_m$
ϕ	Effective angle of internal friction, $\tan\phi = \tau_f/(\sigma'+a)$
γ	Angle
κ	State variable in elasto-plastic theory
λ	Plastic proportionality factor in elasto-plastic theory
ν	Poisson's ratio
θ	Bulk stress = $\sigma_1+ \sigma_2+ \sigma_3$ or angle
ρ	Mobilized friction angle, $\tan\rho = \tau_c/(\sigma'+a)$, or density of soil
$\boldsymbol{\sigma}$	Matrix/vector representation of a stress tensor
σ	Total stress
σ'	Effective stress, $\sigma' = \sigma-u$
$\sigma_1, \sigma_2, \sigma_3$	Principal stresses, $\sigma_1 \geq \sigma_2 \geq \sigma_3$
σ_a	Reference stress (σ_a = 100 kPa)
σ_d	Deviatoric stress, $\sigma_d = \sigma_1-\sigma_3$
σ_m	Mean stress, $\sigma_m = (\sigma_1+ \sigma_2+ \sigma_3)/3$
τ	Shear stress
τ_c, τ_f	Critical shear stress and shear strength according to a Coulomb criterion

Abbreviations

AADT	Annual average daily traffic
$AADT_h$	Annual average daily traffic of heavy vehicles
AC	Asphalt concrete
BC	Bearing capacity
CBR	California Bearing Ratio
DCP	Dynamic cone penetrometer
DMD	Dynaflect maximum deflection

ECMT	European Conference of Ministers of Transport
FE	Finite element
FEM	Finite Element Method
FWD	Falling Weight Deflectometer
HDT	Horizontal deformation transducer
HPC	Horizontal pressure cell
ITRD	International Transport Research Documentation
LVDT	Linear variable differential transducer
LWA	Light-weight aggregate
ME	Multilayered elastic
NPDM	The Norwegian Pavement Design Manual
NPRA	The Norwegian Public Roads Administration
NTH	The Norwegian Institute of Technology (former name of NTNU)
NTNU	The Norwegian University of Science and Technology
OECD	Organisation for Economic Co-operation and Development
SCI	Surface curvature index
SINTEF	The Foundation for Scientific and Industrial Research at the Norwegian University of Science and Technology
SDT	Soil deformation transducer
TRB	Transportation Research Board
TRIS	Transportation Research Information Services
VDT	Vertical deformation transducer
VPC	Vertical pressure cell

DEFINITION OF THE PAVEMENT EDGE

In the figure below it is poited out what is ment by the pavement edge throughout the thesis. The pavement edge and the edge of the surfacing are identical only in the case of no unpaved shoulder.

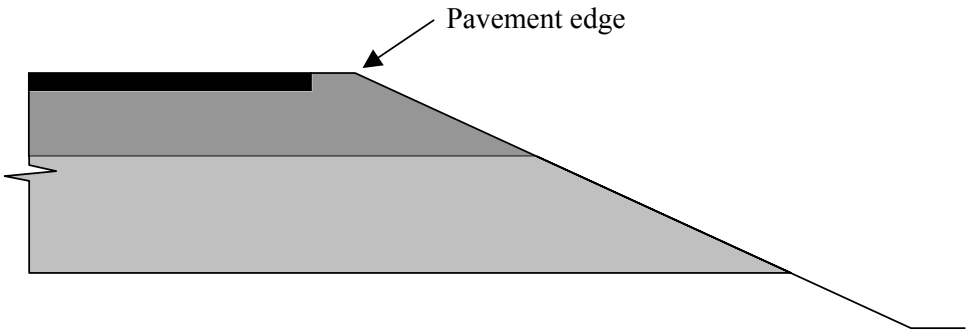

1 INTRODUCTION AND SCOPE

1.1 Background

The Norwegian Public Roads Administration is the national agency responsible for planning, construction, rehabilitation and maintenance of the national and county road network which has a total length of 53988 km (2002) /25/. The overall trend during the last 10-15 years is reduced allocation of money to maintain and rehabilitate these roads, while the traffic volumes are continuously increasing. This situation involves great demands for using the funds effectively, and cost-effective maintenance actions together with optimal design of rehabilitation projects and new pavements are more needed than ever. The aim is to construct pavements with optimal strength and durability to withstand the climatic and traffic loads. This requires high competence on the behaviour of materials and pavement structures under different loading conditions, and especially thorough knowledge about the principal deteriorating mechanisms.

Traffic countings show that a major part (89 %) of the Norwegian national and county road network consists of two-lane roads with relative low traffic volumes (AADT<3000). These roads typically have narrow roadway (5-6 m) and shoulders (often <0.5 m), and the normal design practice implies the use of open ditches and relatively thin bituminous surfacing, and granular base materials. Even though the traffic volumes on these roads often are low, the axle loads might be high. At present, 95 % of the national roads and 52 % of the county roads have 10 tons permitted axle load throughout the year. The remaining part has a permitted axle load limit of 8 tons /25/.

Not surprisingly, the combination of narrow roads and heavy axle loads has resulted in plenty of pavement edge damages. Registrations of pavement deterioration on different parts of the Norwegian low volume road network /20/ demonstrate that longitudinal cracking and settlements near the pavement edge represent a considerable

problem, and in many cases are the triggering factors for structural maintenance. Of the total registered road length, 11 % is reported to have cracking along the pavement edge. This is, together with cracks due to frost heave, the most common pavement defect. Despite of this, little research has been performed in Norway on this subject. This is the main background for the choice of topic in the present thesis work.

1.2 Scope of the thesis

The main objective for this thesis is to give a better understanding of pavement edge effects. Focus is put on the measurement of load responses towards the pavement edge, and the following central topics are included:

- Review of commonly used material models and methods for structural design
- Description of typical pavement edge damages
- Literature review on pavement edge effects
- Measurement of surface load responses over the cross section of existing roads
- Construction and instrumentation of a test field
- Results from measurements of load responses towards the pavement edge
- Comparison of measured and calculated load responses

In the conclusions drawn, an evaluation of the Norwegian design practice with respect to pavement edge stability is included, together with suggestions for further research.

2 STRUCTURAL ANALYSIS OF PAVEMENTS

2.1 Introduction

This chapter gives a short presentation of the basic theory of continuum mechanics, some commonly used models for pavement materials, and methods and programs developed for structural analysis of pavements.

Structural analysis of pavements is a demanding task. A pavement structure consists of several layers of different materials with complex behaviour. The stiffness of granular materials is primarily dependent of the stress level, while the moduli of bitumen stabilised materials also vary with both temperature and frequency of load. However, to be able to calculate stresses and strains it has been common to make the assumption that the materials act like continuous, homogenous and isotropic materials, and linear elasticity is still the most commonly used material model.

Different computer programs based on these principles are developed for pavement analysis, of which some are mentioned in this chapter. Nevertheless, application of the Finite Element Method gives the opportunity to model complex structures and to use more realistic material models than linear elasticity.

2.2 Continuum mechanics

Even though materials for road construction are not strictly continuous, one normally is forced to make this assumption, but promising attempts have been made to describe such materials with interactive discrete elements for each particle /35/. However, for practical purposes the number of particles involved is so large that the capability of normal computers is exceeded.

2.2.1 Stress and strain definitions

The stress state in a material might be described by stress components of an infinitesimal cubic element oriented according to a Cartesian coordinate system, see *Figure 2-1*.

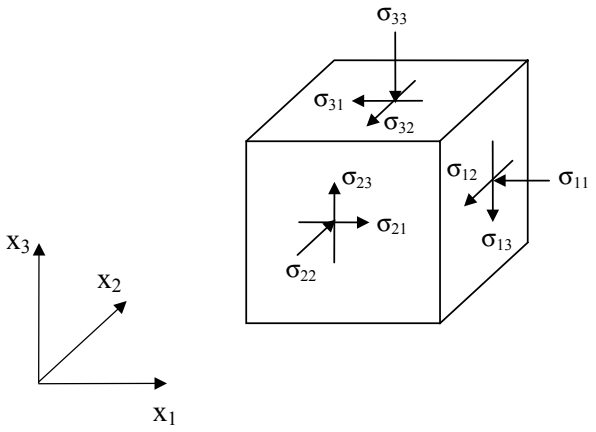

Figure 2-1: Stress components on a cubic element

The stress components are often given by a matrix:

$$\boldsymbol{\sigma} = \begin{bmatrix} \sigma_{11} & \sigma_{12} & \sigma_{13} \\ \sigma_{21} & \sigma_{22} & \sigma_{23} \\ \sigma_{31} & \sigma_{32} & \sigma_{33} \end{bmatrix} \qquad \textit{Eq 2-1}$$

where σ_{ii} are normal stresses and $\sigma_{ij,}$ $i \neq j$, are shear stresses.

Moment equilibrium of the cubic element gives $\sigma_{12} = \sigma_{21}$, $\sigma_{31} = \sigma_{13}$, $\sigma_{32} = \sigma_{23}$, i.e. $\boldsymbol{\sigma}$ is symmetric and contains six independent stress components.

Deviatoric and mean stress, $\mathbf{s}$ and $\boldsymbol{\sigma}_\mathbf{m}$, are defined as:

$$\mathbf{s} = \boldsymbol{\sigma} - \boldsymbol{\sigma}_\mathbf{m}$$

$$\begin{bmatrix} s_{11} & s_{12} & s_{13} \\ s_{21} & s_{22} & s_{23} \\ s_{31} & s_{32} & s_{33} \end{bmatrix} = \begin{bmatrix} \sigma_{11} & \sigma_{12} & \sigma_{13} \\ \sigma_{21} & \sigma_{22} & \sigma_{23} \\ \sigma_{31} & \sigma_{32} & \sigma_{33} \end{bmatrix} - \begin{bmatrix} \sigma_m & 0 & 0 \\ 0 & \sigma_m & 0 \\ 0 & 0 & \sigma_m \end{bmatrix} \qquad \textit{Eq 2-2}$$

where $\sigma_m = \frac{1}{3}(\sigma_{11} + \sigma_{22} + \sigma_{33})$ *Eq 2-3*

Assuming small deformations, the continuum mechanics theory defines the conventional engineering strain as:

$$\varepsilon_{ij} = -\frac{1}{2}\left(\frac{\partial u_i}{\partial x_j} + \frac{\partial u_j}{\partial x_i}\right) \qquad i, j = 1, 2, 3 \qquad \textit{Eq 2-4}$$

where u_i is the displacement in the x_i-direction.

The strain matrix becomes:

$$\boldsymbol{\varepsilon} = \begin{bmatrix} \varepsilon_{11} & \varepsilon_{12} & \varepsilon_{13} \\ \varepsilon_{21} & \varepsilon_{22} & \varepsilon_{23} \\ \varepsilon_{31} & \varepsilon_{32} & \varepsilon_{33} \end{bmatrix} \qquad \textit{Eq 2-5}$$

From the strain definition we see that $\varepsilon_{21} = \varepsilon_{12}$, $\varepsilon_{31} = \varepsilon_{13}$, $\varepsilon_{32} = \varepsilon_{23}$, i.e. the strain matrix is also symmetric and contains six independent strain components.

Volumetric and deviatoric strain, $\boldsymbol{\varepsilon}_\mathbf{v}$ and $\mathbf{e}$, are defined as:

$$\mathbf{e} = \begin{bmatrix} e_{11} & e_{12} & e_{13} \\ e_{21} & e_{22} & e_{23} \\ e_{31} & e_{32} & e_{33} \end{bmatrix} = \begin{bmatrix} \varepsilon_{11} & \varepsilon_{12} & \varepsilon_{13} \\ \varepsilon_{21} & \varepsilon_{22} & \varepsilon_{23} \\ \varepsilon_{31} & \varepsilon_{32} & \varepsilon_{33} \end{bmatrix} - \frac{1}{3}\begin{bmatrix} \varepsilon_v & 0 & 0 \\ 0 & \varepsilon_v & 0 \\ 0 & 0 & \varepsilon_v \end{bmatrix} \qquad \textit{Eq 2-6}$$

where $\varepsilon_v = \varepsilon_{11} + \varepsilon_{22} + \varepsilon_{33} = 3\varepsilon_m$ *Eq 2-7*

For a cubic unity element with volume V= 1*1*1, *Figure 2-2*, the presence of a one-dimensional tensile stress will cause an elongation Δ_1 along the stress direction and a contraction Δ_2 along the two perpendicular directions.

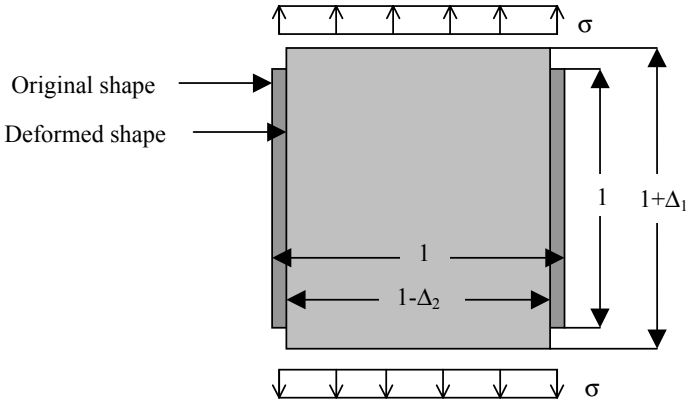

Figure 2-2: Unity element exposed to a one-dimensional tensile normal stress

The Poisson's ratio is defined as:

$$\nu = -\frac{\varepsilon_2}{\varepsilon_1} = -\frac{\Delta_2}{\Delta_1} \qquad \textit{Eq 2-8}$$

(The last sign of equality is valid only for the case of a unity element.)

For the cubic unity element in *Figure 2-2,* the strain in the load direction is $\varepsilon = \Delta_1$, and the displacement along the perpendicular directions becomes $-\Delta_2 = -\nu\varepsilon$. Assuming only small strains, i.e. $\varepsilon >> \varepsilon^2$, the change of volume caused by the normal stress σ then is:

$$\Delta V = (1+\varepsilon)(1-\nu\varepsilon)(1-\nu\varepsilon)-1 \approx \varepsilon - 2\nu\varepsilon \qquad \textit{Eq 2-9}$$

It is not likely that a uniform tension stress will cause volume decrease. This statement requires $\nu < 0.5$. Conventional road building materials are normally assumed to have $0.35 < \nu < 0.5$.

2.2.2 Fundamental laws of statics

A method that seeks to find the primary response of a static load need to fulfil the following three fundamental laws of statics:

- Kinematic compatibility
- Static equilibrium
- Material model

This is illustrated in *Figure 2-3*:

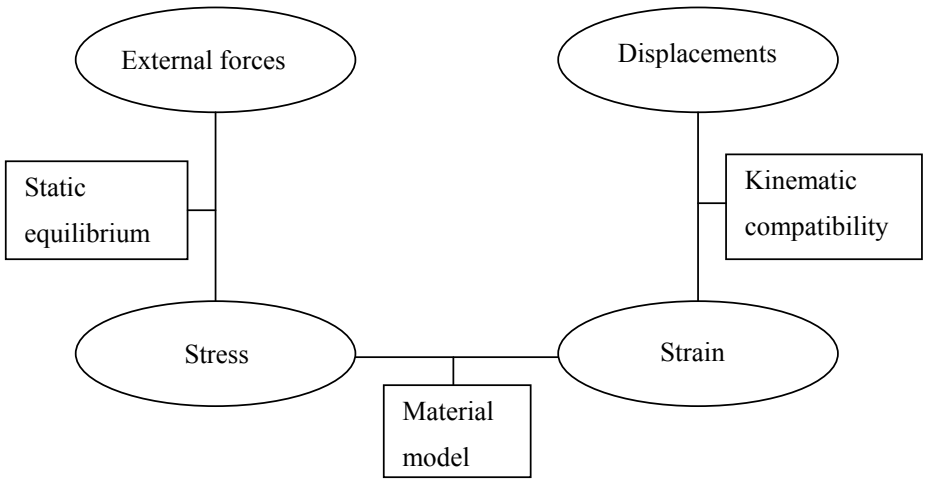

Figure 2-3: Illustration of the fundamental laws of statics

Kinematic compatibility implies that there must be conformity between displacements and strains, i.e. unintended gaps or discontinuities can not appear in the structure. This requirement provides the geometric connection in the structure.
The mathematical formulation of this requirement is that every strain component and its derived functions until at least the second order exist and are continuous.
Static equilibrium implies balance between internal forces or stresses and external loads. There must be balance for the whole structure and for all parts of it.

For a given material there are different models that describe the strain or deformation caused by an applied stress, temperature, creep or other effects. The *material model* must be satisfied everywhere in the structure.

2.3 Material models

A material model describes how a material deforms when it is exposed to an external force. The model is expressed as a set of equations relating stresses and strains, and is controlled by material parameters normally calibrated against laboratory tests. The simplest model (linear elasticity) has two parameters, while some of the more advanced models could have a lot more. Advanced material models also include high requirements to the quality and extent of the laboratory test and to the equipment used.

2.3.1 Linear elasticity

Due to simplicity, the linear elastic theory is widely used in structural design systems in civil engineering, including structural analysis of pavements. This is done although most materials used in pavement structures do not behave according to linear elasticity, at least not for the entire stress regime. Nevertheless, for some purposes this theory offers a simple and useful material model for such analyses.

Three basic conditions are characteristic for elastic behaviour of a continuum:

1. The stress is a unique function of the strain
2. A continuous strain energy function exists
3. The material recovers completely its original shape when the load is removed

The material is called *linear elastic* if the relation between stress and strain is linear as shown in *Figure 2-4*. The relationship is called *Hook's law,* and defines *Young's modulus,* E:

$$\sigma = E \cdot \varepsilon \qquad \textit{Eq 2-10}$$

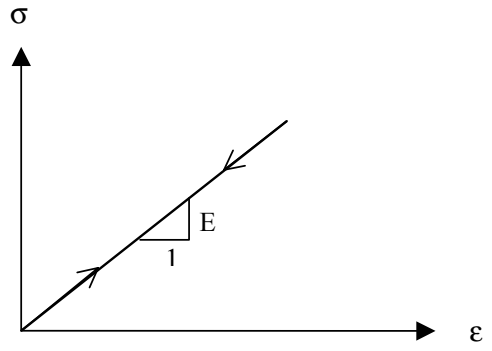

Figure 2-4: One-dimensional stress-strain relationship for a linear elastic material

As shown in *Chapter 2.2*, the general three dimensional stress state is defined by six independent stress tensor components. Similarly, six independent components define the strain. The stresses and strains relate linearly to each other, and a general relationship in matrix form is:

$$\begin{bmatrix}\sigma_{11}\\ \sigma_{22}\\ \sigma_{33}\\ \sigma_{12}\\ \sigma_{13}\\ \sigma_{23}\end{bmatrix} = \begin{bmatrix} D_{11} & D_{12} & D_{13} & D_{14} & D_{15} & D_{16} \\ & D_{22} & D_{23} & D_{24} & D_{25} & D_{26} \\ & & D_{33} & D_{34} & D_{35} & D_{36} \\ & & & D_{44} & D_{45} & D_{46} \\ & SYM. & & & D_{55} & D_{56} \\ & & & & & D_{66} \end{bmatrix} \begin{bmatrix}\varepsilon_{11}\\ \varepsilon_{22}\\ \varepsilon_{33}\\ 2\varepsilon_{12}\\ 2\varepsilon_{13}\\ 2\varepsilon_{23}\end{bmatrix} \qquad \textit{Eq 2-11}$$

or $\boldsymbol{\sigma} = \mathbf{D} \cdot \boldsymbol{\varepsilon}$

The symmetry of the stress-strain matrix, **D,** appears from energy considerations of a material element where the existence of a strain energy function is required /23/.

A material is called *homogenous elastic* if the elastic properties are the same at every point, and *isotropic elastic* if the elastic properties are the same independent of direction. Soils and road construction materials are usually neither perfectly homogenous nor isotropic, but in structural analysis one generally makes this assumption.

In terms of E and ν and in the case of homogeneity and isotropy, the stiffness matrix **D** simplifies to:

$$\mathbf{D} = \frac{E}{(1+\nu)(1-2\nu)} \begin{bmatrix} (1-\nu) & \nu & \nu & 0 & 0 & 0 \\ & (1-\nu) & \nu & 0 & 0 & 0 \\ & & (1-\nu) & 0 & 0 & 0 \\ & & & \frac{(1-2\nu)}{2} & 0 & 0 \\ & SYM. & & & \frac{(1-2\nu)}{2} & 0 \\ & & & & & \frac{(1-2\nu)}{2} \end{bmatrix} \qquad \textit{Eq 2-12}$$

It is often convenient to separate the volumetric and shear response, and to express the stiffness by the bulk modulus, K, and the shear modulus, G. The stiffness matrix can then be written as:

$$\mathbf{D} = \begin{bmatrix} K+\frac{4}{3}G & K-\frac{2}{3}G & K-\frac{2}{3}G & 0 & 0 & 0 \\ & K+\frac{4}{3}G & K-\frac{2}{3}G & 0 & 0 & 0 \\ & & K+\frac{4}{3}G & 0 & 0 & 0 \\ & & & G & 0 & 0 \\ & SYM. & & & G & 0 \\ & & & & & G \end{bmatrix} \qquad \textit{Eq 2-13}$$

K and G, or E and ν, are two alternative ways to express the elastic stiffness. If one of the sets of parameters is known, the other set can be determined by the following equations:

$$K = \frac{E}{3(1-2\nu)} \qquad \textit{Eq 2-14}$$

$$G = \frac{E}{2(1+\nu)} \qquad \textit{Eq 2-15}$$

$$E = \frac{9K}{1+3K/G} \qquad \textit{Eq 2-16}$$

$$\nu = \frac{1}{2}\left(1 - \frac{1}{K/G + 1/3}\right) \qquad \textit{Eq 2-17}$$

From *Equation 2-13* it can be shown that the relationship between volumetric strain and mean stress is given by:

$$\sigma_m = K \cdot \varepsilon_v \qquad \textit{Eq 2-18}$$

where: $\sigma_m = 1/3(\sigma_{11}+\sigma_{22}+\sigma_{33})$ and $\varepsilon_v = \varepsilon_{11}+\varepsilon_{22}+\varepsilon_{33}$

By expressing the deviatoric stress, **s**, as a function of deviatoric strain, **e**, it can be derived that:

$$s_{ij} = 2G \cdot e_{ij} \qquad \textit{Eq 2-19}$$

where: $s_{ij} = \sigma_{ij} - \sigma_m$ and $e_{ij} = \varepsilon_{ij} - \varepsilon_v/3$

The decomposition of the response into a volumetric part and a shear part, uniquely related to mean stress changes and deviatoric stress changes, respectively, is fundamental for isotropic elasticity. Here shear stresses cause no volume change, and isotropic compression provides no shear deformation. However, in soils and materials for road construction shear stresses may cause volume changes (dilatation). This subject is further discussed in *Chapter 2.3.2*.

2.3.2 Non-linear elasticity

Pavement materials do normally not behave perfectly linear elastic. Especially granular materials show non-linear stress dependent properties. In order to obtain higher accuracy in the calculations of load responses in a pavement than the linear elasticity can offer, it is necessary to use more advanced material models like non-linear elasticity. New powerful computers and the use of the Finite Element Method make this possible.

In non-linear elasticity the elastic modulus is replaced by the *resilient modulus*, M_r, and is no longer a constant, but depends on the stress level, see *Figure 2-5*.

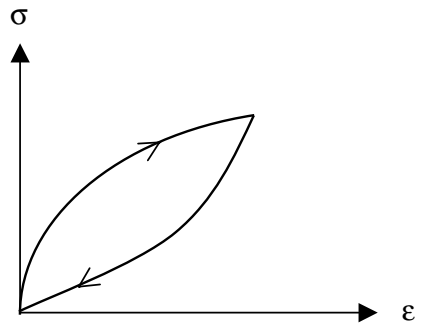

Figure 2-5: Non-linear elastic behaviour of a one-dimensional material

The resilient properties are usually determined by performing repeated load triaxial tests with constant or varying confining pressure. In this case, the resilient modulus and Poisson's ratio are defined by:

$$M_r = \frac{\Delta(\sigma_1 - \sigma_3)}{\varepsilon_{1,r}} \qquad \textit{Eq 2-20}$$

$$\nu = -\frac{\varepsilon_{3,r}}{\varepsilon_{1,r}} \qquad \textit{Eq 2-21}$$

Here σ_1 and σ_3 are major and minor principal stress, and $\varepsilon_{1,r}$ and $\varepsilon_{3,r}$ are major and minor recoverable axial and horizontal strain, respectively.

Several stress dependent models for granular materials have been proposed since the early 1960'ies. The majority of these models are based on curve-fitting procedures, using data from triaxial testing. In Lekarp et. al. /19/ several of these models are placed together in two different groups:

1. Mathematical expressions for resilient modulus and Poisson's ratio
2. Mathematical expressions for volumetric and shear stress-strain relationships

The most frequently used model of group 1 is known as the ***K-θ model*** (*Equation 2-22*), in which the resilient modulus is expressed as a function of the bulk stress, and the Poisson's ratio is assumed to be constant. The earliest reference to this type of model is Biarez /3/.

$$M_r = k_1\theta^{k_2} \quad \text{or} \quad M_r = k_1\sigma_a\left(\frac{\theta}{\sigma_a}\right)^{k_2} \qquad \textit{Eq 2-22}$$

M_r: resilient modulus

θ: bulk stress = $\sigma_1+\sigma_2+\sigma_3$

σ_a: reference pressure (e.q. 100 kPa)

k_1 and k_2 are model parameters

Due to it's simplicity the K-θ model is widely used for describing non-linear resilient response of granular materials, and it has been implemented in several computer programs for pavement design, e.g. IlliPave. However, it has some shortcomings, primarily that the Poisson's ratio is assumed to be a constant, and that the shear, or deviator, stress dependency of the resilient modulus is not taken into account.

Among the resilient models for volumetric and shear stress-strain relationship, the ***Boyce model*** /5/ is perhaps the most commonly used. The expressions for volumetric and shear response are as shown in *Equations 2-23 and 2-24*.

$$\varepsilon_v = p^{B_1}\left[\frac{1}{B_3} - \frac{1-B_1}{6B_2}\left(\frac{q}{p}\right)^2\right] \qquad \textit{Eq 2-23}$$

$$\varepsilon_s = \frac{p^{B_1}}{3B_2}\frac{q}{p} \qquad \textit{Eq 2-24}$$

q: deviatoric stress = σ_1-σ_3

p: mean normal stress = $(\sigma_1+\sigma_2+\sigma_3)/3$

B_1, B_2 and B_3 are model parameters

During his dr.ing. study, Hoff /13/ developed a new constitutive model for granular materials. This model belongs to group 2: volumetric and shear stress- strain relationship. It is based on hyperelasticity, which provides the existence of a strain energy function and includes the effect of resilient dilatancy in unbound granular materials.

The proposed strain energy function is:

$$U = \frac{1}{2}K\left(I_1^{\varepsilon}\right)^2 + D \cdot I_1^{\varepsilon} \cdot J_2^{\varepsilon} + 2G \cdot J_2^{\varepsilon} \qquad \textit{Eq 2-25}$$

I_1^{ε} is the first strain invariant (volumetric strain)

J_2^{ε} is the second deviatoric strain invariant

The dilatancy is included through the term $D \cdot I_1^{\varepsilon} \cdot J_2^{\varepsilon}$, which relates volumetric strains to shear strains.

The relation between stresses and strains is found by taking the derivatives of the energy function:

$$\sigma_i = \frac{\partial U}{\partial \varepsilon_i} \qquad i = 1,2,3 \qquad \textit{Eq 2-26}$$

This gives the following stress-strain relationship expressed by principal stresses and strains:

$$\begin{bmatrix} \sigma_1 \\ \sigma_2 \\ \sigma_3 \end{bmatrix} = \begin{bmatrix} K + \frac{4}{3}G + D\varepsilon_1 & K - \frac{2}{3}G - \frac{1}{2}D\varepsilon_3 & K - \frac{2}{3}G - \frac{1}{2}D\varepsilon_2 \\ K - \frac{2}{3}G - \frac{1}{2}D\varepsilon_3 & K + \frac{4}{3}G + D\varepsilon_2 & K - \frac{2}{3}G - \frac{1}{2}D\varepsilon_1 \\ K - \frac{2}{3}G - \frac{1}{2}D\varepsilon_2 & K - \frac{2}{3}G - \frac{1}{2}D\varepsilon_1 & K + \frac{4}{3}G + D\varepsilon_3 \end{bmatrix} \cdot \begin{bmatrix} \varepsilon_1 \\ \varepsilon_2 \\ \varepsilon_3 \end{bmatrix} \qquad \textit{Eq 2-27}$$

2.3.3 Elasto-plasticity

The theory of elasto-plasticity is thoroughly described in several textbooks. Nordal /23/ gives a good introduction to this subject, and the main points are included here.

The theory of elasto-plasticity claims that in case of plastic loading the total strain is made up of both an elastic and a plastic component:

$$d\boldsymbol{\varepsilon} = d\boldsymbol{\varepsilon}^e + d\boldsymbol{\varepsilon}^p \qquad \textit{Eq 2-28}$$

The elastic strain is given by:

$$d\boldsymbol{\varepsilon}^e = \mathbf{D}^{-1} d\boldsymbol{\sigma} \qquad \textit{Eq 2-29}$$

where **D** is the stiffness matrix in the case of linear elasticity, defined in *Equation 2-12.*

The plastic strain is controlled by a *yield criterion*, a *flow rule* and a *hardening rule*.

The *yield criterion* defines the stress states where plastic strain may develop. It is an equation in stress tensor components and state variables, usually denoted:

$$F(\boldsymbol{\sigma}, \kappa) = 0 \qquad \textit{Eq 2-30}$$

where κ is a state variable, for example the degree of mobilization

This equation must be satisfied for any plastic strain to develop.

The six independent stress tensor components, σ_{ij}, define a six-dimensional stress space. In this stress space the yield criterion defines a yield surface. For low stress levels, situated inside the yield surface, the response is usually assumed to be elastic. Initially, the stress state must lie inside or on the yield surface. Any stress increment that tries to bring the stress state outside the surface will cause development of plastic strains. Such an elasto-plastic stress increment moves the yield surface so that the new stress state always lies on the surface. The yield surface may only expand to a certain limit, -the *failure surface*. The failure surface distinguishes obtainable from unobtainable stress states.

A surface in a six-dimensional space is hard to imagine, thus, often the yield criterion is visualised in the three-dimensional principal stress space. In *Figure 2-6* two commonly used criteria for soils, the Mohr-Coulomb and the Drücker-Prager criterion, are illustrated in the π-plane.

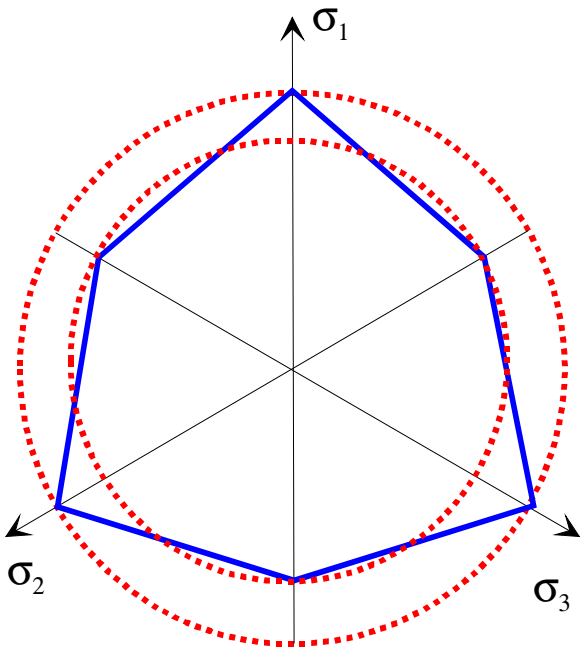

Figure 2-6: Mohr-Coulomb (solid line) and Drücker-Prager (dotted lines) yield surfaces illustrated in the π-plane /13/

The *flow rule* determines the plastic deformation mode for the plastic strain components, $d\boldsymbol{\varepsilon}^p$, due to a given stress state, $\boldsymbol{\sigma}$, and a stress increment, $d\boldsymbol{\sigma}$. It was proposed by von Mises in 1928 /39/. For this purpose he introduced a potential function, denoted $Q(\boldsymbol{\sigma})$:

$$d\boldsymbol{\varepsilon}^p = d\lambda \cdot \frac{\partial Q}{\partial \boldsymbol{\sigma}} \qquad \textit{Eq 2-31}$$

The *hardening rule* provides the resistance against plastic strain development, and determines the size of the plastic strain increment during plastic loading, i.e. the size of the parameter $d\lambda$ in the flow rule. It is expressed as:

$$d\lambda = \frac{1}{A} \cdot \frac{\partial F}{\partial \boldsymbol{\sigma}} d\boldsymbol{\sigma} \qquad \textit{Eq 2-32}$$

where A is a plastic resistance number:

$$A = -\frac{\partial F}{\partial \kappa}\frac{\partial \kappa}{\partial \bar{\varepsilon}^{p}}\frac{\partial \bar{\varepsilon}^{p}}{\partial \lambda} \qquad \text{for strain hardening} \qquad \textit{Eq 2-33}$$

$$A = -\frac{\partial F}{\partial \kappa}\frac{\partial \kappa}{\partial W^{p}}\frac{\partial W^{p}}{\partial \lambda} \qquad \text{for work hardening} \qquad \textit{Eq 2-34}$$

Here $\bar{\varepsilon}^{p}$ is the amount of plastic strain, while W^{p} is dissipated energy.

When formulating the incremental elasto-plastic stress-strain relationship, the yield criterion, the flow rule and the hardening rule are combined. The result becomes:

$$d\boldsymbol{\sigma} = \mathbf{D}_{ep} \cdot d\boldsymbol{\varepsilon} \qquad \text{Eq 2-35}$$

Here the expression for the elasto-plastic stiffness matrix is:

$$\mathbf{D}_{ep} = \mathbf{D} - \frac{\mathbf{D}\left\{\frac{\partial Q}{\partial \boldsymbol{\sigma}}\right\}\left\{\frac{\partial F}{\partial \boldsymbol{\sigma}}\right\}^{T}\mathbf{D}}{\left(A + \left\{\frac{\partial F}{\partial \boldsymbol{\sigma}}\right\}^{T}\mathbf{D}\left\{\frac{\partial Q}{\partial \boldsymbol{\sigma}}\right\}\right)} \qquad \textit{Eq 2-36}$$

The matrix can be evaluated when the elastic parameters K and G plus the relationship between increase in degree of mobilisation and change in plastic strain, i.e. the κ-λ curve, are found from laboratory tests.

2.4 Methods and computer programs based on elastic layer theory

The tools for pavement design have evolved quite a lot since Boussinesq developed his well known equations. Burmister's solution for a two-layered system and Odemark's equivalent stiffness method for multilayered elastic systems were important contributions in this evolution, but the greatest step forward has been the development and exploitation of the finite element method.

2.4.1 Boussinesq's equations

In 1885 Boussinesq /4/ developed equations for the structural analysis of homogenous, isotropic, and elastic media exposed to a vertical point load on the surface. Results of his work have formed the basis for many subsequent stress analyses for pavements.

Boussinesq's structural model was a semi-infinite, axisymmetric elastic space with elastic modulus E and Poisson's ratio ν, *Figure 2-7*.

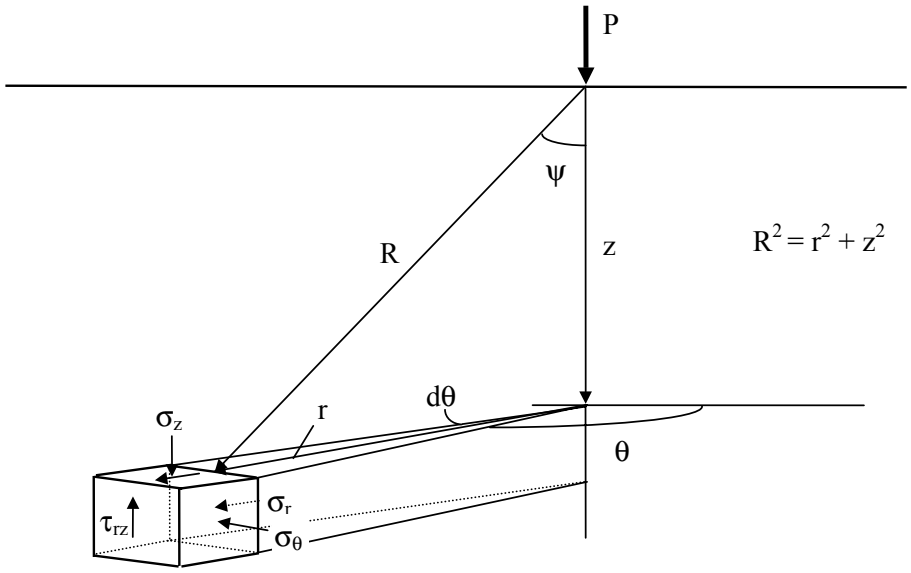

Figure 2-7: Stresses under a point load

The derivation of the equations is mathematical complicated, and only the results are presented here. The stresses on an element due to the surface load P are:

$$\sigma_z = \frac{3P}{2\pi} \cdot \frac{z^3}{(z^2 + r^2)^{5/2}} = \frac{3 \cdot P}{2\pi} \cdot \frac{z^3}{R^5} \qquad \textit{Eq 2-37}$$

$$\sigma_\theta = \frac{P}{2\pi} \cdot (1 - 2\nu) \cdot (\frac{1}{R(R+z)} - \frac{z}{R^3}) \qquad \textit{Eq 2-38}$$

$$\sigma_r = \frac{P}{2\pi} \cdot (\frac{3zr^2}{R^5} - \frac{1-2\nu}{R(R+z)}) \qquad \textit{Eq 2-39}$$

$$\tau_{rz} = \frac{3P}{2\pi} \cdot \frac{rz^2}{R^5} \qquad \textit{Eq 2-40}$$

The vertical and radial displacements are given by:

$$w = \frac{P(1+\nu)}{2\pi E} \cdot (\frac{z^2}{R^3} + \frac{2(1-\nu)}{R}) \qquad \textit{Eq 2-41}$$

$$u = \frac{P(1+\nu)}{2\pi E} \cdot (\frac{rz}{R^3} - \frac{r(1-2\nu)}{R(R+z)}) \qquad \textit{Eq 2-42}$$

It can be noticed that σ_z and τ_{rz} are independent of Poisson's ratio ν. The other quantities are dependent of ν. All the stress components are independent of E.

For an element on the axis of symmetry under the load, r=0 and R=z. The expression for σ_z then simplifies to:

$$\sigma_z = \frac{3}{2\pi} \cdot \frac{P}{z^2} \qquad \textit{Eq 2-43}$$

If z approaches zero in this expression, the vertical stress approaches infinity. This is caused by the definition of the load as a point load.

Boussinesq's solution for a point load can easily be integrated to give load responses under a uniformly distributed circular load.

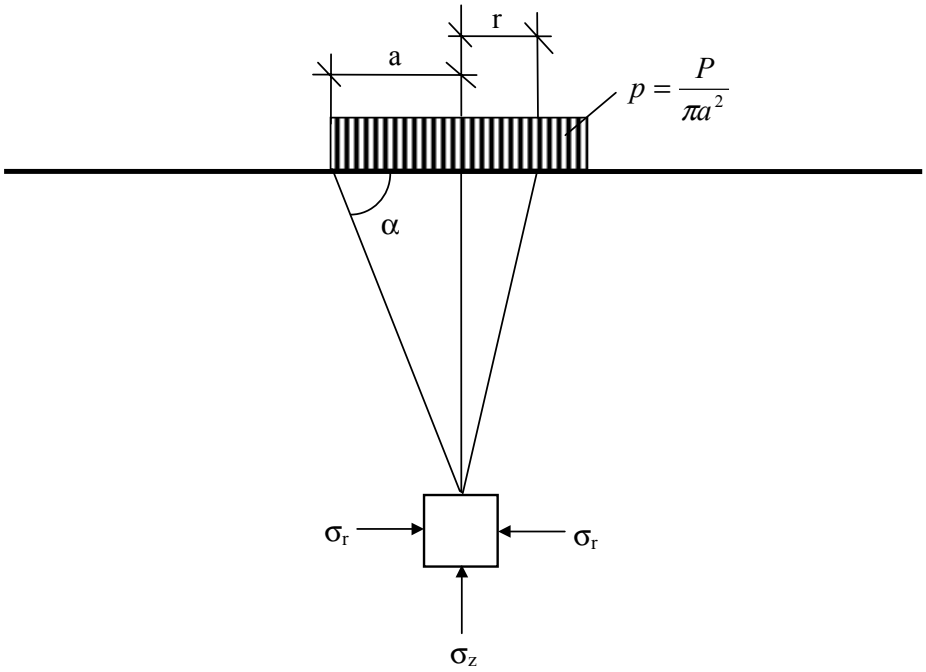

Figure 2-8: Stresses under a uniform circular load

The equations for stresses on the axis of symmetry then simplify to /32/:

$$\sigma_z = p(1 - \sin^3 \alpha) \qquad \textit{Eq 2-44}$$

$$\sigma_r = \frac{p}{2} \cdot (1 + 2\nu - 2(1+\nu)\sin\alpha + \sin^3 \alpha) \qquad \textit{Eq 2-45}$$

$$\tau_{rz} = \frac{1}{2}(\sigma_z - \sigma_r) \qquad \textit{Eq 2-46}$$

The expression for the surface deflection becomes:

$$w_0 = \frac{2pa(1-\nu^2)}{E} \qquad \textit{Eq 2-47}$$

2.4.2 Burmister's solution

A pavement structure is a layered system. Boussinesq's solution is valid only for a semi-infinite half-space, and was consequently insufficient for use in pavement design. The natural evolution was therefore to develop a solution for a layered system. This was not done until 1943, when Burmister /6/ came up with his theoretical solution for a two-layered system. The following assumptions were done:

- Uniformly distributed circular load
- Axisymmetric system
- Linear elastic, homogenous, isotropic and weightless materials
- Layer one: infinite in horizontal direction, parameters h_1, E_1, ν_1=0.5
- Layer two: infinite in both horizontal and vertical direction, parameters E_2, ν_2=0.5
- Full friction between the layers

Burmister later developed a solution for three-layered systems based on the two-layer solution. The equations he derived were so complicated that diagrams and tables had to be worked out in order to make practical use of the system. Consequently, diagrams and tables for several combinations of Young's modulus and layer thicknesses were developed.

2.4.3 Odemark's equivalent stiffness method

Odemark /24/ presented his equivalent stiffness method in 1949. This is actually a simplified version of Burmister's solution for two-layer systems, but can also be used for multi-layered systems.

The basic principle for the method can be explained in the case of a two-layer system. The upper layer with Young's modulus E_1 and thickness h_1, is substituted by an equivalent layer with Young's modulus E_m and thickness h_e, where E_m is the Young's modulus of the underlying layer.

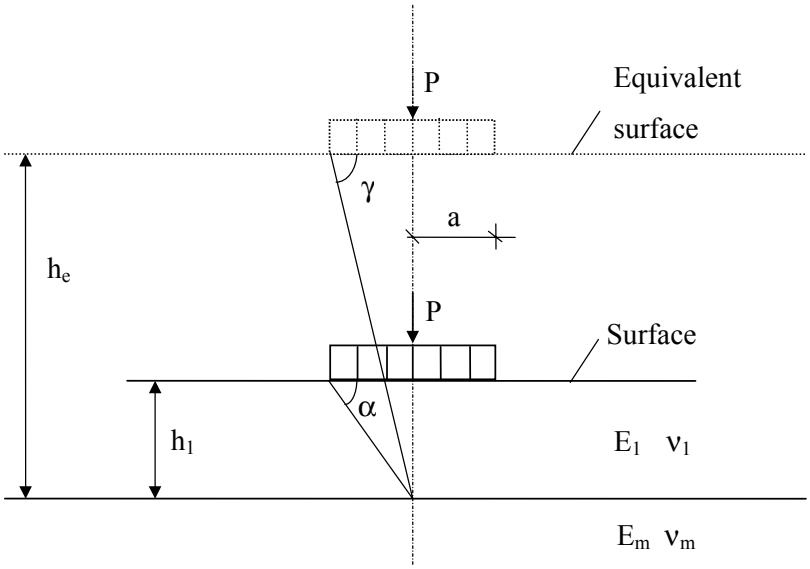

Figure 2-9: Odemark's equivalent method, two-layer system

The requirement controlling the equivalent thickness is that stresses and strains on top of the subgrade should remain unchanged, either the load is applied to the original surface or to the surface of the equivalent layer. This approximation is true if the bending stiffness of the original and the substituted layer is similar. The equivalent thickness can now be derived from the expression for the plate bending stiffness:

$$\frac{E_m h_e^3}{12(1-\nu_m^2)} = k\frac{E_1 h_1^3}{12(1-\nu_1^2)} \qquad \textit{Eq 2-48}$$

where *k* is a correction factor introduced because of the approximation made.

If $\nu_m = \nu_1 = 0.5$, and k=0.9 (which give good correlation with the Burmister solution for a two-layer system), one gets the well known expression for the equivalent layer thickness:

$$h_e = 0.9 \cdot h \cdot \sqrt[3]{\frac{E_1}{E_m}} \qquad \textit{Eq 2-49}$$

Load responses in the equivalent system can now be calculated using Boussinesq's equations for a circular load on a semi-infinite elastic space.

2.4.4 Chevron

In 1963, *California Research Corporation* developed a computer program for the analysis of load responses in a multi-layered elastic system. The work was done at request of the *Asphalt Development Group* of the *Chevron oil company*.

The program gives a numerical solution to the Burmister equations, and can calculate load responses for an arbitrary point within a multi-layered elastic system.

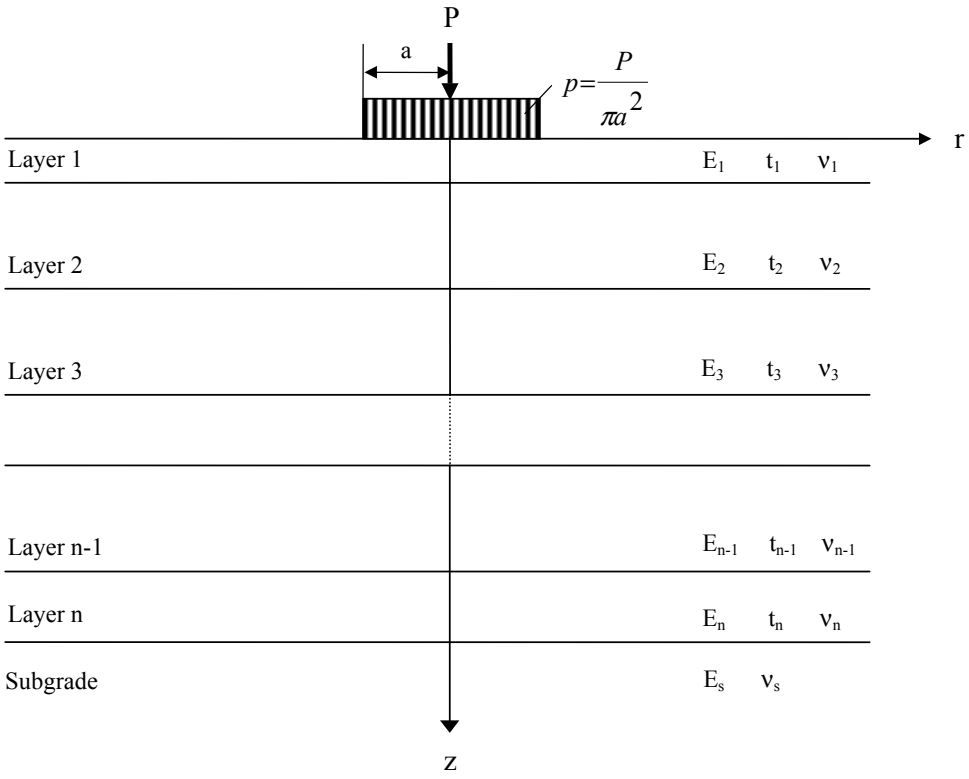

Figure 2-10: Multi-layered elastic system

The assumptions made in Chevron are:

- Weightless, homogeneous and isotropic materials
- Similar elastic properties for both tension and compression
- Uniformly distributed and circular normal load
- All layers have infinite horizontal extension and constant, finite thickness
- Full friction between the layers
- The subgrade has infinite extension both horizontally and downwards

The program can manage structures with up to 15 layers, the subgrade included. Calculation of responses from more than one load is not implemented in the original program, but could be done manually by utilizing the superposition principle.

The assumptions of a circular load area and infinite horizontal extension together make the model axisymmetric. In the calculation of load responses, Chevron therefore makes use of cylinder co-ordinates.

2.4.5 BISAR

BISAR (Bitumen Stress Analysis in Roads) is a program developed by Shell in 1972. It was originally suitable for mainframe computers only, but was adapted for use on personal computers in 1987.

With BISAR it is possible to calculate load responses at any position in a multi-layer system from several simultaneous loads. Also horizontal load components can be included. It is possible to vary the friction between the layers from full bonding to almost free slippage.

BISAR is defined by the following configuration and material behaviour:

- Similar material models as Chevron
- Up to 10 simultaneous normal loads

- All loads are uniformly distributed over a circular area, but can also have horizontal components
- Layers of uniform thickness extending infinitely in horizontal direction
- The maximum number of layers is 10
- The subgrade has infinite extension both horizontally and downwards

The BISAR program used for calculations within this thesis is version 3.0 from 1998.

2.5 The Finite Element Method

Structural analysis of flexible pavements by the use of the multilayered elastic method has some essential shortcomings. The structure is modelled as a series of layers, where each layer is assumed to consist of an isotropic, homogenous and linear elastic medium with finite thickness and infinite horizontal extension.

In reality, pavement materials exhibit non-linear elasticity and during the pavement life permanent deformations usually occur in one or more of the layers. The modulus of granular materials are particularly stress dependent while the modulus of bituminous materials are dependent of both temperature and frequency of loading.

Further, in a real pavement structure, the horizontal extension is restricted by the pavement edge. The confining pressure in a granular layer decreases towards the edge, and due to the stress dependent characteristics of granular materials, it is obvious that this is the weakest part of the pavement structure. A structural model with layers of infinite horizontal extension is therefore not suitable for the calculation of critical load responses in a pavement where heavy traffic loads might be situated close to the edge.

2.5.1 Advantages connected to the use of FEM

Finite element analyses represents an improved tool for calculating stresses, strains and displacements in a pavement structure. Here, modelling of the pavement edge is possible, either in a two- or a three-dimensional geometric model, and more realistic material models can be used for characterisation of the different layers of the structure. The Finite Element Method is therefore adopted in this work as a tool for analysing load responses near the edge of a pavement structure.

2.5.2 Basic principles of FEM

In the Finite Element Method, the structure to be analysed is divided into an assembly of elements with finite dimensions. Each element has a limited number of nodes in which the elements are connected. The continuous variation of displacements in the structure is represented by an assumed linear or quadratic function over each finite

element. For a given element geometry and constitutive equation of material, the element stiffness matrix relating unknown nodal displacements and applied forces at the nodes is then established by using the principle of virtual work. The global structural stiffness matrix for the entire finite element system is then formulated by superimposing the individual element stiffness matrices. As a result, a set of simultaneous equations, in terms of relationships between forces and displacements is formed. The system of linear equations is solved using Gaussian elimination for all nodal displacements. With the displacement of all nodal points known, strains can be calculated, and finally stresses can be calculated from the strains.

2.5.3 Finite element programs specially developed for pavement analysis

IlliPave is developed from a finite element program made by E. L. Wilson in 1965 /33/. The adaption for use in pavement analysis has mainly been done by the University of Illinois, hence the name IlliPave. The geometric model is an axisymmetric model with an uniformly distributed circular load placed in the centre. The nodes at the bottom of the cylinder are fixed, and the nodes at the edge and along the symmetry-axis are only free to move vertically. It is possible to use stress dependent models to describe resilient modulus. Failure criterion based on the Mohr-Coulomb theory is used for granular materials and fine-grained subgrade soils to modify calculated stresses so that they do not exceed the strength of the material.

MichPave is another finite element program developed for pavement analysis at Michigan State University in 1989 /21/. As in IlliPave, stress dependent material models can be used, and the correction of stresses follows the same principles based on the Mohr-Coulomb theory. The main difference between IlliPave and MichPave is that in MichPave the material below a lower boundary is considered to be linear elastic and with infinite extension both in vertical and horizontal direction.

2.5.4 The general finite element program ABAQUS

ABAQUS is a general purpose finite element program with possibilities to accomplish analyses of various kinds /11/. It has to some extent been used by NTNU and SINTEF for pavement analyses, and was also chosen for the FE-analysis within this thesis.

ABAQUS is a large program system, which requires a powerful computer. The pre-processor is divided into 10 modules, where each module defines a logical aspect of the modelling process, and contributes with data to form an input file to the solver. Here the calculations are performed, and an output database is generated. Finally, a post-processor is used to read the output database and to view the results.

The main advantage of *ABAQUS* compared to other available FE-programs is the advanced methods for modelling available in the preprocessor. This makes 3D modelling of the pavement structure a not too laborious task. One drawback of the program is the limited number of material models available for stress-strain analyses. For example, stress dependent material models suitable for granular materials have not yet been implemented.

3 PAVEMENT EDGE EFFECTS

3.1 Pavement edge damages

A major part of the Norwegian road network consists of relatively narrow two-lane roads with little or no shoulders outside the trafficked area. These roads are typically built with thin asphalt surfacing over granular base materials. Results from several investigations on pavement condition in different parts of Norway are summarised by Lerfald /20/. Here it is concluded that deterioration very often starts at or near the shoulder, and that damages related to the pavement edge is one of the most common causes for maintenance and reconstruction. Of the total investigated road length, 11 % is reported to have longitudinal edge cracks.

3.1.1 Permanent deformations / rutting

Deformations may occur in every layer of the pavement and in the subgrade. In a pavement with thin bituminous surfacing, deformations usually develop as a result of either consolidation or shear deformation in granular base and subbase materials, subgrade or fill. The spring thaw is usually the most critical period for permanent deformations to develop, and pavements with a poor drainage system are especially vulnerable.

Figure 3-1 shows a typical example of how rutting can develop in the outer wheel path on a pavement with narrow shoulder and insufficient drainage.

Figure 3-1: Example of severe deformation of outer wheel path

3.1.2 Longitudinal cracking

Longitudinal cracks are usually initiated by heavy traffic loads near the pavement edge causing deformations in underlying base layers and/or subgrade, as illustrated in *Figure 3-2*.

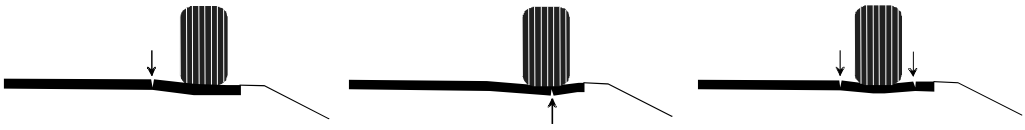

Figure 3-2: Longitudinal cracking close to the pavement edge

Typical examples of longitudinal cracking and deformation close to the pavement edge are shown in *Figure 3-3* and *Figure 3-4*.

Figure 3-3: Longitudinal cracking along the pavement edge

Figure 3-4: Deformation and longitudinal cracking

3.1.3 Crocodile cracking

Crocodile or alligator cracking is the common denotation of interconnected cracks forming a series of small polygons resembling a crocodile skin. Crocodile cracking near the pavement edge often occurs at sites where the granular base material is water saturated, and therefore has reduced shear strength. This may typically be found at road cuts with insufficient drainage system where ground water forces its way into the pavement structure, see *Figure 3-5*.

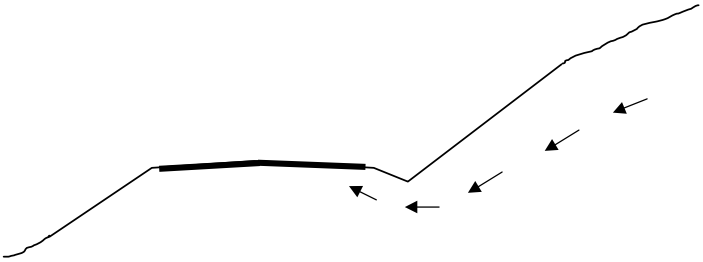

Figure 3-5: Flow of ground water into the pavement

Crocodile cracking may also be the advanced state of longitudinal cracking where several longitudinal cracks are interconnected by smaller transverse cracks.

Figure 3-6: Deformation and interconnected longitudinal cracking

3.1.4 Pavement edge drop-off

Heavy vehicles driving at the pavement edge of narrow roads may cause spalling of the bituminous surfacing. Deformation of the base layer is the main cause to these damages, and the surfacing is particularly vulnerable during the spring periods when the granular materials are saturated and the bituminous materials are brittle due to low temperatures.

Water running along the pavement edge may cause erosion of granular material beside and under the pavement edge, see *Figure 3-7*, resulting in spalling from the edge of the surfacing.

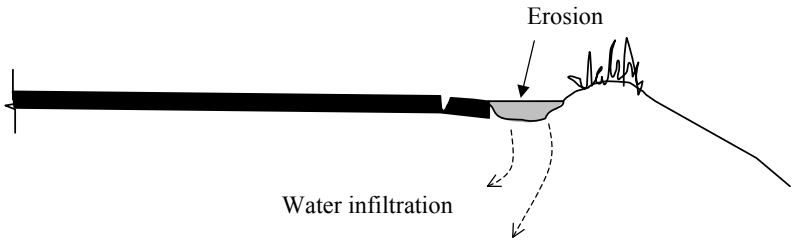

Figure 3-7: Erosion and water ingress outside the pavement edge

3.2 Factors influencing the pavement edge strength and damage development

In this chapter some factors assumed to be of high importance for the pavement edge strength and damage development are discussed. The aim is not to give a complete description of all factors that may have a possible influence, but rather to point out the most significant factors of the road cross section that are free to be varied in a pavement design process.

3.2.1 Width of the pavement and the shoulders

The width of the pavement and the shoulders is especially important for the strength of the pavement edge. A wide shoulder is favourable because:

- The base and subbase layers have greater side support and thus increased resistance against deformations
- The load carrying part of the pavement is less exposed to water ingress during critical periods

According to the Norwegian Pavement Design Manual (NPDM) /31/ and Road and Street Design Manual /30/, the requirement for the pavement and shoulder width is dependent on the traffic volume and the road classification. For a two-lane road in a rural area of Norway with an AADT less than 1500 vehicles, the requirement is a lane width of 2.75 m and a shoulder width of 0.5 m. Only half of the shoulder, i.e. 0.25 m, has to be paved, which implies that the total width of the paved surface in this case is only 6.0 m. When two trucks meet at a road like this, the pavement will obviously get heavy traffic loads near the edge, and the chances for the development of edge damages are high.

3.2.2 Drainage

A well functioning drainage system is essential for a pavement, and it should function under all weather and climatic conditions throughout the year. But even if the

condition of the drainage system is good, the pavement is normally not fully protected from ingress of water. In order to avoid damages to the pavement during critical wet periods, it is therefore important to reduce the consequences of saturation by using materials non-susceptible to moisture, and by using materials and methods avoiding granular materials to be crushed during the construction work or by traffic loads.

3.2.3 Road ditches

Another important factor is the design of the road ditches. For a two-lane Norwegian road there are two basic alternatives for drainage of the pavement; an open or a closed ditch. The geometrical design is as shown in *Figure 3-8*.

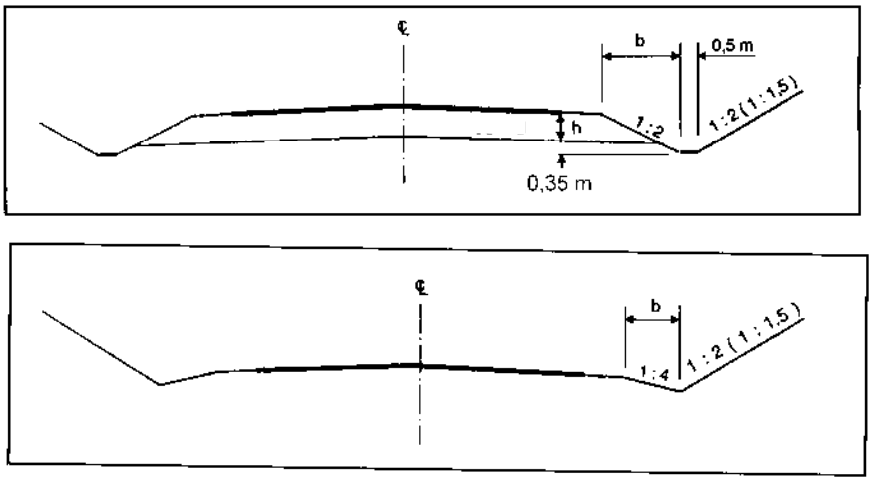

Figure 3-8: Required shape of a ditch according to the NPDM /31/

A closed ditch is favourable for the strength of the pavement edge, especially on roads with narrow shoulders. The gentle side slope for the closed ditch (1:4) is also positive with respect to traffic safety. Nevertheless, in rural areas of Norway, the normal tradition is to choose open ditches because they usually give the lowest investment costs, and they have satisfactory drainage properties. With respect to the strength of the pavement edge, open ditches do not have the same quality as closed ditches.
The required depth of the open ditch is defined by the total thickness of the pavement, and the side slope is fixed to 1:2.

3.2.4 Gradient of fill slope

A too steep gradient of the fill slope may give instability and settlements, especially in the outer part of the pavement. It may also cause unevenness of the pavement surface due to overloading of a soft subgrade soil. In the NPDM the maximum gradient of the fill slope is 1:1.25 for crushed rock, 1:1.5 for sand and gravel and 1:2 for other soils.

3.2.5 Material quality

From triaxial testing it is known that the stiffness and shear strength of granular materials is very dependent on the stress level. Reduced side support for granular base and subbase materials near the pavement edge means lower level of horizontal stress, and consequently reduced shear strength in this part of the pavement compared to the condition under the inner wheel path. Use of materials with good internal stability and high shear strength should therefore be emphasised in order to ensure sufficient stiffness and resistance against permanent deformations of the pavement edge.

3.2.6 The construction work

The performance of the construction work is of significant importance for the quality of the pavement. Construction methods and equipment should be well tested, and a thorough documentation of the construction work is necessary.

3.3 Literature review on measured pavement edge effects

A literature review on measured pavement edge effects has been performed. The review includes seeks in BIBSYS and TRANSPORT. BIBSYS is a library data center offering services to all Norwegian University Libraries, the National Library, all college libraries, and a number of research libraries. TRANSPORT is a bibliographic database produced by OECD, TRB and ECMT, and combines the following databases: TRIS, ITRD and TRANSDOC.

Even though pavement edge damages represent a considerable problem, especially for narrow roads, the literature review shows that there has not been done very much research on this topic. Only a few articles and reports are found, mainly from investigations accomplished in the Nordic countries. A short review of the main findings regarding measurements of deformations and elastic deflections in the road cross section is presented here.

3.3.1 The Vormsund test road

At Vormsund in the south-eastern part of Norway, a full-scale field test was carried out during the years 1958-68 /22/. The main object was to study frost action in frost susceptible sub-grade soils, and its effects on the pavement structure. Besides, the surface deflection and development of rutting both in the inner and the outer wheel paths were recorded.

The test road was built with eight different sections, each of approximately 100 m length. The pavements consisted of:

- Bituminous surfacing, 80 kg/m^2
- Crushed gravel base with primed surface, 20 cm thick
- Gravel subbase with varying thickness (20-65 cm)
- Silt and clay subgrade

One conclusion from the Vormsund test road was that rut depths in the outer wheel paths were much deeper than in the inner wheel paths. It was recorded that the rutting was caused by plastic deformations in the pavement and subgrade, and that the ruts mainly developed during the spring periods. The deepest ruts appeared at the sections with clay subgrade. Measured rut depths are shown in *Figure 3-9*.

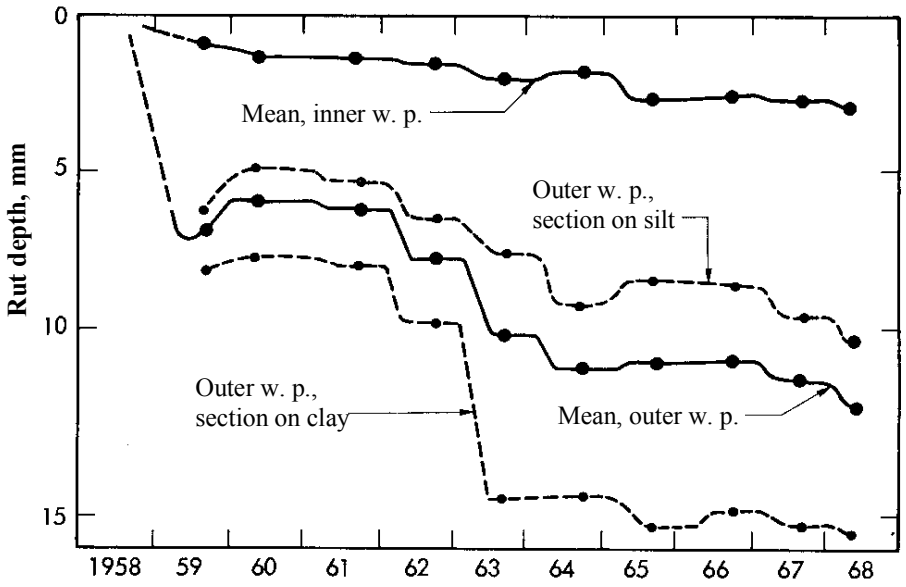

Figure 3-9: Development of average rut depths in inner and outer wheel path /22/

3.3.2 Full scale testing in Sweden

Results from full scale testing done by the Public Roads Administration in Sweden 1983 and 1985 are presented in the references /37/ and /38/.

The 1983 report /37/ contains findings from compaction tests carried out indoor in a big hall owned by Dynapac. The testing included density and FWD measurements on the base and subbase layers, plus registration of rutting resulting from a heavily loaded truck trafficking on pavements exposed to different compaction efforts.

The results show that the granular materials were well compacted both near the pavement edge and at the centre line. No significant differences in density were found

and the FWD-measurements showed just a minor decrease in bearing capacity towards the pavement edge. On the other hand, rutting after 20 passages of a truck was found to be 40 % higher 0.25 m from the pavement edge than at the centre line.

The second report /38/ presents data from density and FWD measurements carried out in Sweden 1985 on four different pavements. The main object of this project was to collect information on the variation in compaction and bearing capacity across the road cross section.

The lane width of the test pavements was 3.1 m, while the shoulder width ranged from 0.3 to 0.8 m in order to be able to investigate the effect of varying side support. The pavement structures of the test sections were identical and consisted of these layers:

- Bituminous surfacing: 100 kg/m^2
- Base: crushed gravel, 20 cm thick
- Subbase: gravel, 35 cm thick

The density measurements on the base layer showed that with the same compaction effort, the obtained value of density near the pavement edge was 93 % mod. Proctor compared to 110 % in the middle of the road.

The FWD measurements were carried out with a load of 50 kN, and the "E-modulus" (MPa) of the pavements was calculated using the following equation:

$$E = \frac{118.8}{d_0} \qquad \textit{Eq 3-1}$$

where d_0 is the deflection (mm) in the middle of the FWD-plate. (Any explanation of the origin of this equation is not found in the report.)

Evaluation of the results from the FWD-measurements on top of the bituminous surfacing shows that compared to the centre-line value, the "E-modulus" at the pavement edge is approximately 40 % lower. The value in the outer wheel path, 60

cm from the edge is found to be 15 % lower than the centre-line value. The FWD-measurements also indicate that increasing the shoulder width by 0.2-0.3 m gives approximately 5 % higher "E-modulus" at the pavement edge.

Mean values from calculations of "E-modulus" on three of the test pavements are shown in *Figure 3-10*. FWD measurements were done on top of both the base layer and the surface layer.

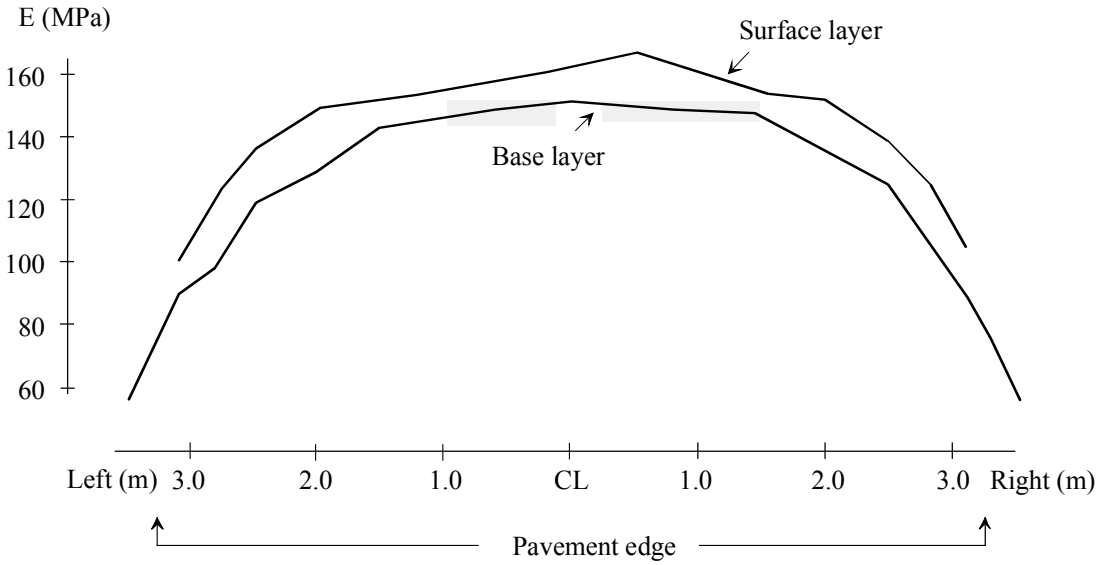

Figure 3-10: Results from FWD-measurements /38/

3.3.3 Dynaflect measurements in Norway

In his diploma work from Department of Road and Railway Engineering at NTH 1980, Gullberg /9/ presents results from deflection measurements at 23 different road sections. The roads selected for this investigation were all situated in the area around Hønefoss to the north-west of Oslo. A Dynaflect apparatus was used, and measurements were done at nine points for each cross section.

The results are presented as idealised profiles of DMD, SCI and the DMD/SCI-ratio over the road cross sections. DMD and SCI are defined as:

DMD = Dynaflect Maximum Deflection (10^{-3} mm)
SCI = Surface Curvature Index = DMD – d_{300}

where d_{300} is deflection 300 mm from the middle point between the steel wheels of the Dynaflect apparatus (10^{-3} mm).

Idealised profiles from one of the investigated sections are shown in *Figure 3-11*. The curves represent mean values from measurements in three different cross sections. Both the DMD and SCI-values increase considerably towards the pavement edge of the majority of the investigated road sections.

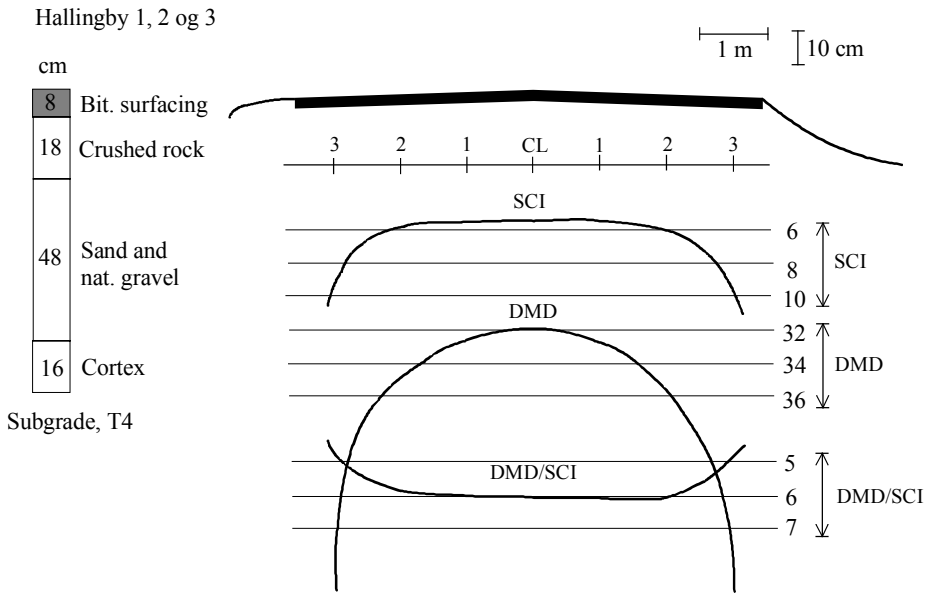

Figure 3-11: Idealised values from Dynaflect measurements, mean of three different cross sections /9/

3.3.4 Summary

Rather few references concerning measurements of the structural pavement edge effects are found in the literature.

At the Vormsund test road, deeper ruts were observed in the outer wheel path than in the inner, especially on test sections with clay subgrade. Most of the deformations developed during the spring thaw periods.

From full scale testing in Sweden, it is concluded that differences in structural strength between the edge and the centre line are evident from measurements of permanent deformation after passages of a truck. The differences are also clear from FWD measurements, but more difficult to see from density measurements.

Dynaflect measurements at roads north-west of Oslo confirms that the bearing capacity decreases towards the edge of the pavement.

The conclusions presented are all based on measurements of either surface deflection, rutting or density. Results from measurements of stresses, strains or deformations towards the pavement edge in different layers of the pavement structure are not found in the checked literature.

3.4 FWD measurements at different road cross sections in Sør-Trøndelag county

To investigate how the bearing capacity varies over the road cross-section, own FWD measurements were performed at eight different sites in Sør-Trøndelag county. These are all two-lane low volume roads with relatively thin asphalt surfacing, and granular base materials. The width of the asphalt surfacing at the sites was 5.0-7.0 m while the width of the unpaved shoulder varied from 0.30 to 0.85 m. The side slope varied from approximately 1:1.3 to 1:2.0.

The used Dynatest FWD equipment is owned by the Norwegian Public Roads Administration of Sør-Trøndelag county. The load plate diameter is 30 cm and the deflection sensors were placed 0, 20, 30, 40, 60, 90 and 150 cm from the load centre.

The results from the measurements are converted into bearing capacity, calculated by using the Norwegian empirical formula /31/:

$$BC = 11 \cdot \left(\frac{E_{\text{dim}}}{200} \right)^{0.6} \cdot \left(\frac{50}{AADT_h} \right)^{0.072} \text{ (tons)} \qquad \textit{Eq 3-2}$$

where: $AADT_h$ = average annual daily traffic of heavy vehicles, that is vehicles with allowed total weight > 3.5 tons

$$E_{\text{dim}}(MPa) = \frac{110 \cdot p}{(d_0 \cdot (d_0 - d_{20}))^{0.5}} \qquad \textit{Eq 3-3}$$

p = average contact pressure under the plate

d_0 = maximum deflection in the load centre (mm)

d_{20} = deflection 20 cm from the load centre (mm)

Results from all the measurements are collected in *Figure 3-12*. Here the bearing capacity towards the pavement edge is expressed as a percentage of the centre-line value. A logarithmic trend-line is added to the figure.

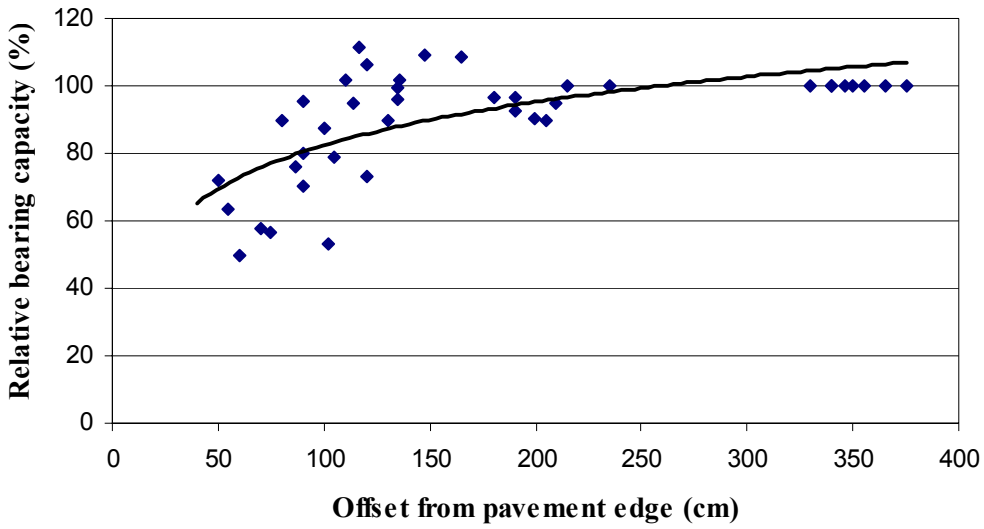

Figure 3-12: Mean relative bearing capacity in the road cross section based on FWD-measurements at eight sites in Sør-Trøndelag county.

The measurements show, as expected, a considerable decrease in bearing capacity towards the pavement edge. The edge effect is noticeable from an offset of about 1.0 m, and the bearing capacity 50 cm from the pavement edge is reduced by approximately 40 % compared to the centre line value.

URN:NBN:no-3347

3.5 A field study on the effect of varying side slope

In order to increase our knowledge on how varying side slope influences the bearing capacity properties of the pavement edge, a limited field test was accomplished at Fv 462 near Orkanger about 50 km south-west of Trondheim 1995.

Surface deflection measurements were carried out from the centre line and towards one side of the road. Initially there was almost no side slope or ditch at the chosen cross-section, but between the measurement series a gradually higher gradient of the side slope was established by excavation.

3.5.1 Geometry and material data

The cross-section geometry and layer thicknesses of the pavement are shown in *Figure 3-13* and *Figure 3-14*. The thickness of the bituminous layers was controlled by cores taken from the pavement, while the thickness of the subbase layer was found from excavation subsequent to the measurements. The 18 pavement cores showed an average total thickness of bituminous surface and base layer of 9.7 cm. Only small variations in thickness of the cores were observed, that is ±1.0 cm.
The average thickness was 3.1 cm for the surface layer and 6.6 cm for the base layer. The subgrade material at the site is a silty, fine-grained sand.

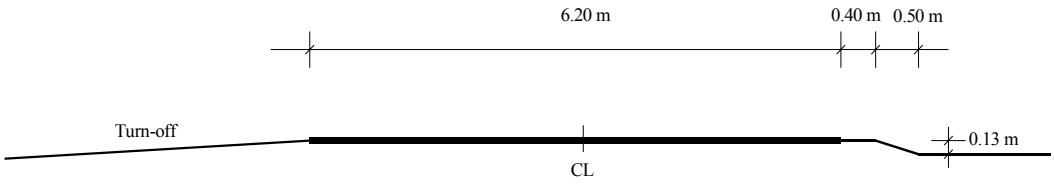

Figure 3-13: Original geometry of the chosen cross-section

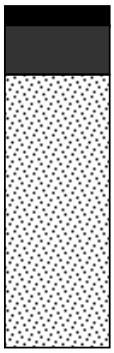

Surfacing: 3.1 cm asphalt concrete
Base: 6.6 cm bitumen stabilized gravel

Subbase: 80 cm gravel

Figure 3-14: Pavement structure

Indirect tensile tests /28/ were carried out on five specimens from both the surface and the base layers. The test temperature was set to 1.0 °C in order to have a good approximation of the field condition (during the measurements the surface temperature varied from –2 °C early in the morning to +5 °C at 3.00 p.m.). Calculated mean values of E-modulus are shown in *Table 3.1*. These values are calculated according to the following equation, originally developed for specimens tested at 25 °C /2/:

$$E = 6.1 \cdot S_t + 100 \quad \text{(MPa)} \qquad \textit{Eq 3-4}$$

where $S_t = \dfrac{2 \cdot P_{max}}{\pi \cdot t \cdot D}$ (N/m^2) *Eq 3-5*

P_{max} : maximum diametrical pressure force applied to the core (N)

t: thickness of the core (m)

D: diameter of the core (m)

Table 3.1: Results from indirect tensile testing

Layer	Mean E-modulus (MPa)	Standard deviation
Surface layer	16157	1376
Base layer	10162	1420

Grain size distributions of the subbase and subgrade materials are shown in *Figure 3-15*. Density and water content in these layers were found from nuclear density measurements. The mean value from three different measurements on each material is shown in *Table 3.2*.

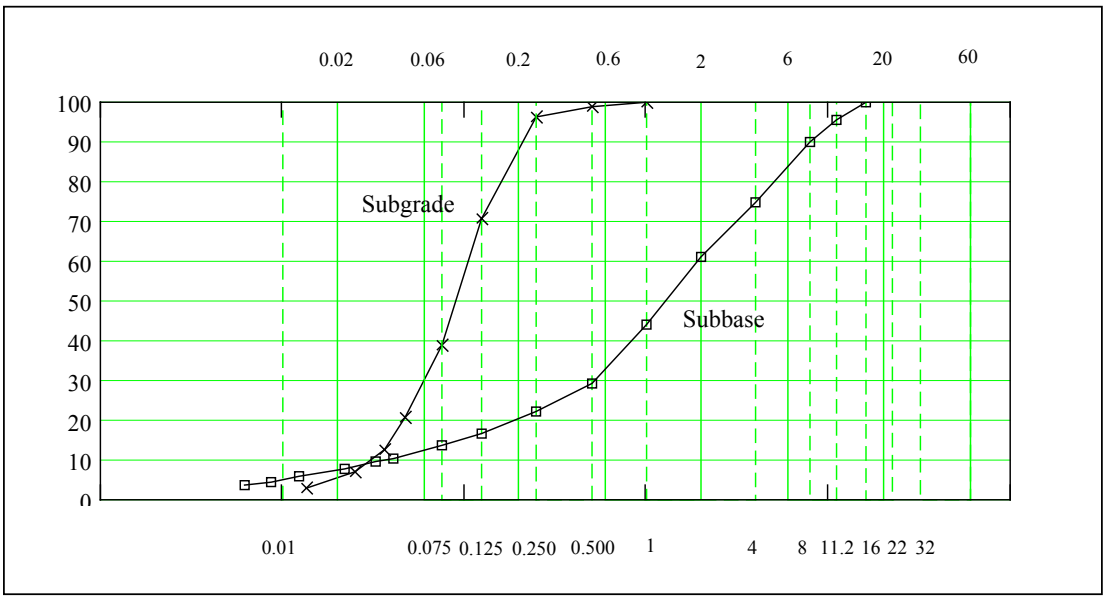

Figure 3-15: Grain size distribution for subbase and subgrade

Table 3.2: Results from nuclear density measurements

Material	Mean dry density (kg/m^3)	Mean water content (%)
Subbase	2089	6.6
Subgrade	1497	15.9

3.5.2 Field measurement program

Surface deflection measurements with both FWD and plate loading equipment were carried out according to the following plan:

- Six points located from the centre line towards the right edge of the pavement were marked at the surface:

Point no.	1	2	3	4	5	6
Distance from edge of surfacing (cm)	20	50	80	120	180	310 (centre line)

- The FWD equipment was placed crosswise to the road, and FWD measurements were performed at all six points, *Figure 3-16.*
- Plate loading test was performed at point number 1, 2, 3 and 6.
- An excavator was used for establishing a gradient of the side slope of 1:4 starting from the edge of the bituminous surfacing, *Figure 3-17*.
- The deflection measurements were repeated.
- Similar procedure was also carried out for gradients 1:2 and 1:1

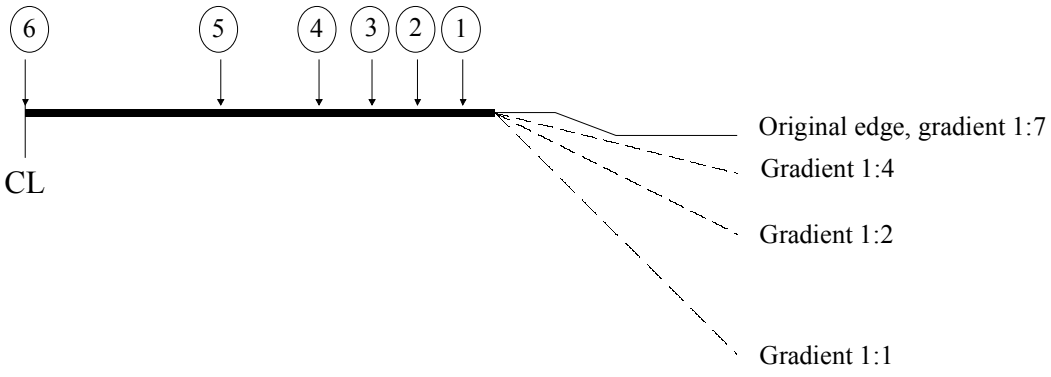

Figure 3-16: Location of measuring points in the cross section

Figure 3-17: Excavation from the side of the road at Fv 462

3.5.3 Results from FWD measurements

To be able to locate the load plate as close to the edge of the surfacing as was the intention, the FWD-apparatus had to be placed crosswise to the road. The followed measuring procedure was to apply threee drops, first a seating drop with a low load, immidiately followed by two measuring drops, each of approximately 55 kN.

Computed bearing capacity values from the second measuring drop are shown in *Figure* 3-18. The formula used for evaluation of bearing capacity is presented in *Equation 3-2*.

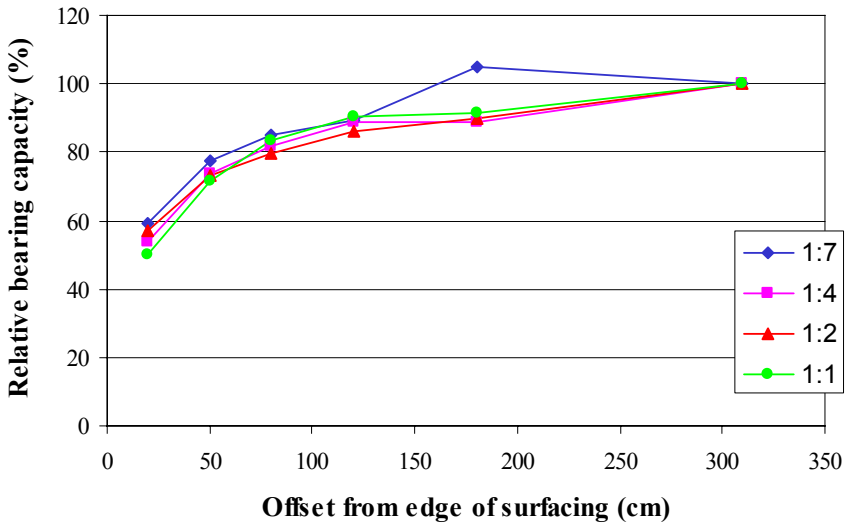

Figure 3-18: Relative bearing capacity based on FWD measurements

3.5.4 Results from plate loading tests

Plate loading tests were carried out at points 1, 2, 3 and 6 for each of the different slopes. The load was applied in the following steps (kPa): 0, 50, 150, 300, 450, 600, 0, 50, 150, 300, 450, 600, 0. (The plate loading equipment and test procedure is further described in *Chapter 5.4.*)

From the load-deflection curves, an average "E-modulus" for the pavement structure can be calculated using the Boussinesq expression for deflection under a uniformly distributed circular load (*Equation 2-47*). Assuming Poisson's ratio, ν = 0.5, the "E-modulus" formula becomes:

$$E = 0.75 \cdot \frac{\Delta p}{\Delta d} \cdot D \qquad \textit{Eq 3-6}$$

where: Δp = pressure difference (kPa)

Δd = deflection difference (m)

D = diameter of loading plate (0.3 m)

"E-modulus" can be evaluated from both loading and unloading. Obtained E2-values from the second loading sequence are shown in *Figure 3-19*.

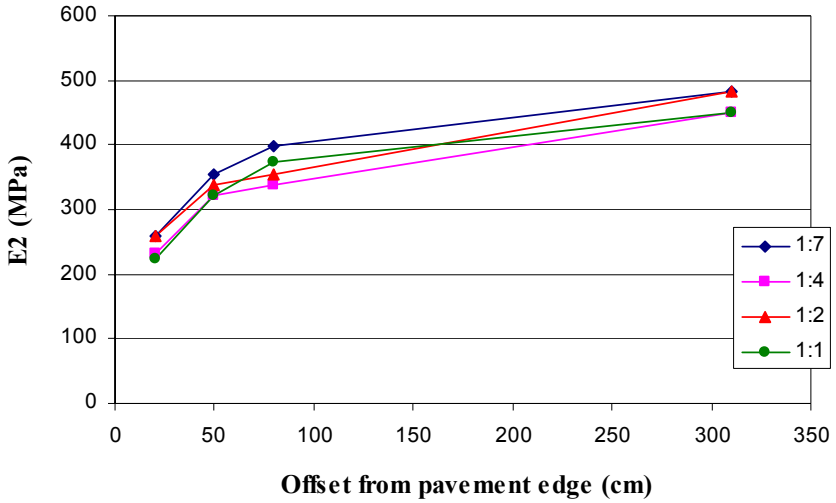

Figure 3-19: "E-modulus" from the second loading sequence

Calculated "E-modulus" values from unloading after the second loading sequence are shown in *Figure 3-20*. The values close to the pavement edge are somewhat higher than the corresponding values in *Figure 3-19*, while the differences at the centre line are very small.

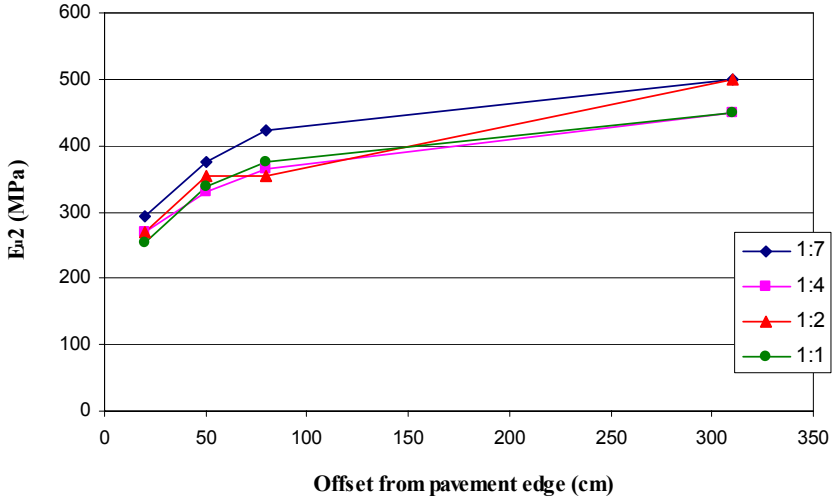

Figure 3-20: "E-modulus" from unloading after the second loading sequence

Information on permanent deformations can also be read from the plate loading results. *Figure 3-21* shows permanent deflection after the second loading sequence.

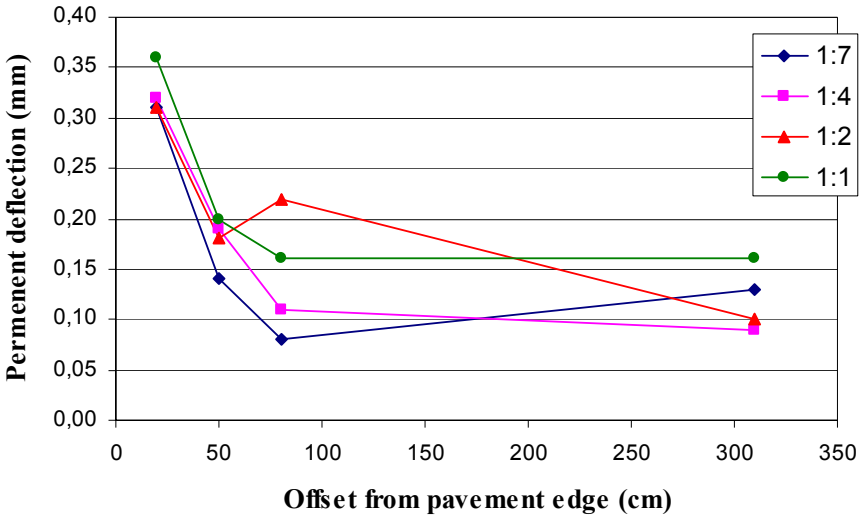

Figure 3-21: Permanent deflection after the second loading sequence

3.5.5 Discussion and conclusions

The field test at Fv 462 was accomplished to gain more information about the effect of varying side slope. The fact that a steeper side slope was established by excavating soil from the side of the road, implies that the assumed negative effect of reduced side support during construction and compaction of granular materials near the pavement edge, is not included. Still, the measurements should give good information about the effect of steepening the side slope by, for instance, ditch clearing.

It was expected that the effect of steepening the side slope should be more evident than the results from FWD and plate loading show. Excavation from the original side slope of 1:7 down to 1:2 seems to have very little influence on the measured elastic response close to the pavement edge. Further steepening to a slope of 1:1 is, however, noticeably for the measuring point 20 cm from the edge of the surfacing. Nevertheless, the measurements showed, independent of the side slope, a significant reduction of pavement stiffness towards the pavement edge.

3.6 Literature review on models for calculation of pavement edge effects

In addition to the reported measurements on pavement edge effects referred to in *Chapter 3.3*, the literature review also included models for calculation of pavement edge effects, or bearing capacity in the road cross section. The only findings regarding this subject were two Finnish projects reported in 1982 and -83.

3.6.1 Study at the Technical Research Centre of Finland

As a part of the Nordic research project called *"Taksering av eksisterende veger med tanke på opprusting for fremtidig bruk,"* Lampinen at the Technical Research Centre of Finland (VTT) in 1983 performed a study on two different methods for calculation of load bearing capacity in the road cross-section /17/.

The first method is a geotechnical approach to the problem, and is based on failure load theory. Here the pavement structure is assumed to be a homogenous one-layered system.

The second approach claims to be based on linear elastic theory and Burmister's solution for a two-layered system. Here Lampinen refers to calculations done by the Canadian Good Roads Association /7/.

In /17/ the pavement edge is described by the following variables; width of the shoulder, gradient of the slope and height of the embankment. It is from the theoretical calculations concluded that the load bearing capacity is mostly affected by the width of the shoulder.

3.6.2 Study at the Helsinki University of Technology in Finland

At the Helsinki University of Technology, a study of calculation methods was presented by Lehtipuu 1982 /18/. The paper describes alternative methods to increase

the bearing capacity of the shoulders, based on four different calculation criteria, see *Figure 3-22*.

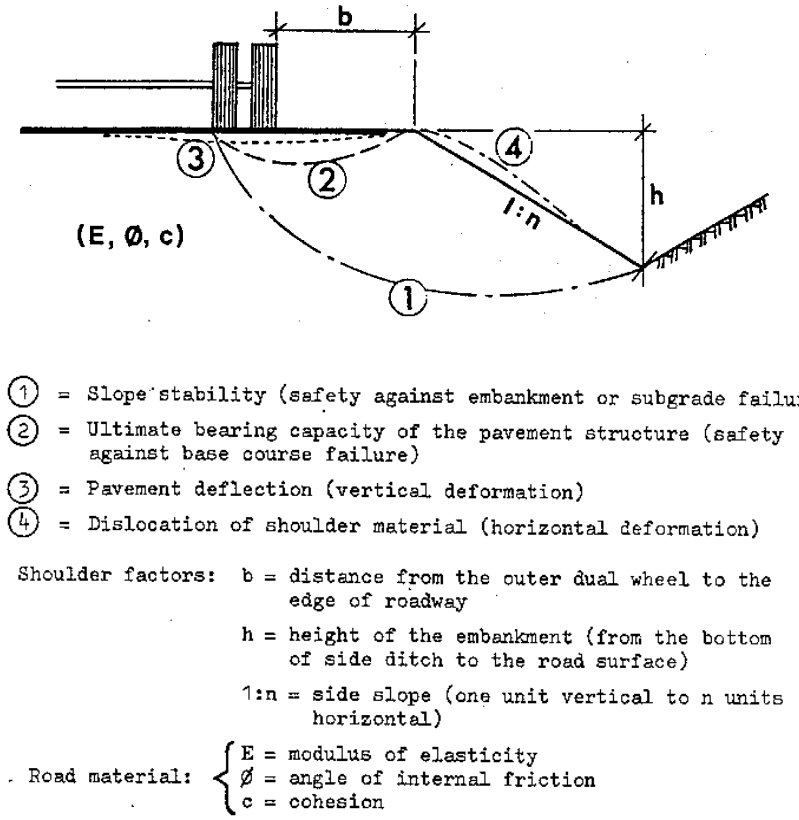

Figure 3-22: Four different criteria to study the bearing capacity of road shoulders /18/

The study is primarily based on geotechnical considerations, where the pavement is modelled as a homogenous one-layer system. Of the proposed criteria in *Figure 3-22,* Lehtipuu concludes that number 1 and 2 are best suited for comparison between different methods to strengthen weak road shoulders.

3.6.3 Comments on the Finnish studies

The conclusions in the reports /17/ and /18/ are partly based on theoretical analyses of the pavement modelled as a homogenous one-layer system. This might be a suitable

assumption for an old gravel road, but represents a considerable simplification of the pavement for a modern road with a layered structure and asphalt surfacing.

Lampinen /17/ also refers to calculations based on Burmister's solution for a two-layered system. As stated in *Chapter 2.5*, this solution is valid only for axisymmetric structures with layers of infinite horizontal extension. This implies that the Burmister model has no pavement edge, and consequently is not well suited as a basis for calculation of responses from a load situated near the pavement edge.

4 SANDMOEN TEST FIELD; CONSTRUCTION AND INSTRUMENTATION

4.1 Introduction

To get reliable measurements of edge effects for pavements with standardised base and subbase materials, it was decided to establish a full-scale pavement test field for the measurement of load responses from controlled wheel loading, FWD and static plate loading in different layers and at different offsets from the pavement edge. For this purpose, two different test sections were constructed (1 and 2 in *Figure 4-2*), of which one was instrumented.

The two main objectives of the current test sections were to:

- Measure load responses and bearing capacity at different distances from the pavement edge
- Compare the bearing capacity of two pavement structures with different subbase materials; crushed stone and natural gravel

Several alternative locations were evaluated for the test field. Finally, Sandmoen heavy vehicle control station was chosen. The main reasons for choosing this site were:

- It was close to Trondheim and NTNU
- Construction and testing could be performed without disturbing the traffic on highway E6, nor the control activities at the control station
- Power supply for the registration equipment was easily available

The control station is owned by the Norwegian Public Roads Administration and is located about 15 km south of Trondheim, close to the main highway E6, as shown on the map segment in *Figure 4-1*.

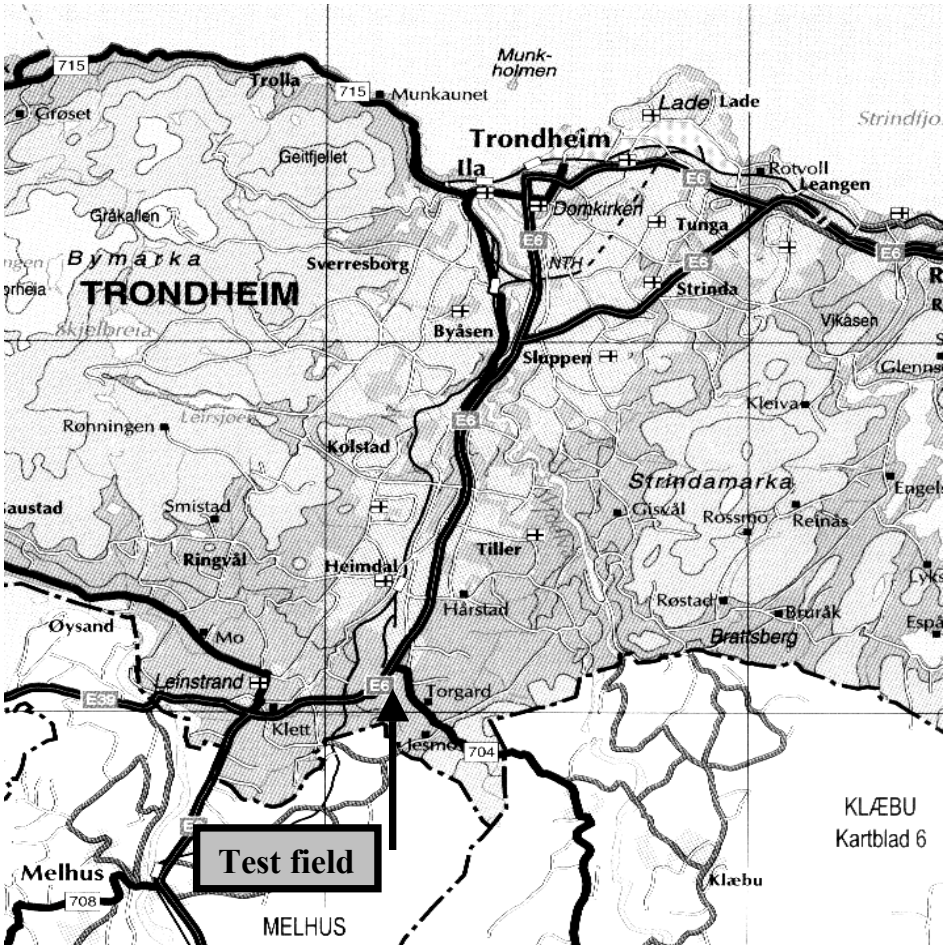

Figure 4-1: Map segment of the Trondheim region

In connection to another research project, two other test sections were built adjacent to the current ones to investigate the behaviour of lightweight aggregate (LWA) when used in a pavement structure. Construction of the test pavements at the same site but with different sections for each research purpose was beneficial to both projects, and made the financing easier by sharing the common costs. In this way, the test field was carried through by a co-operation between the Norwegian Public Roads Administration, NTNU and SINTEF.

Figure 4-2 shows a sketch of the area and the different sections at the test field. Sections 3 and 4 are constructed with base material of expanded clay as part of the LWA-project, further described in separate reports /12/, /14/ and /15/.

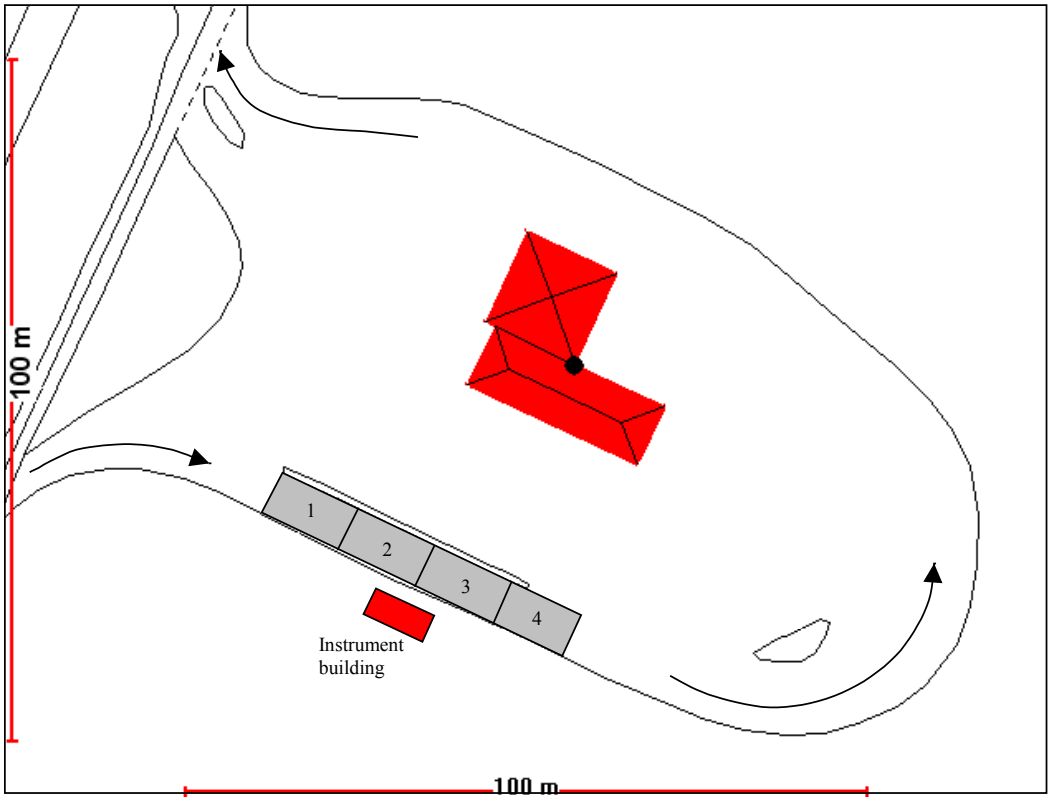

Figure 4-2: Test field with test sections 1-4 at Sandmoen control station

4.2 Description of the sections

The pavements at sections 1 and 2 are designed according to the NPDM /31/, with AADT=1000 and standard assumptions regarding other input variables for design of a two-lane national road. They have identical bituminous top layer and crushed rock base, but different subbase materials. Crushed rock is used as subbase at Section 1 and natural gravel is used at Section 2, see *Figure 4-3*. The chosen pavements are representative for the design of a large part of the existing Norwegian low-volume road network.

Section 2 is instrumented for the measurement of load responses at different depths and offsets from the pavement edge. This section is chosen for instrumentation because of its natural gravel subbase in which the different sensors can be more easily installed. Data from Section 1 is only collected by surface measurements.
The instrumentation is described in *Section 4.5*.

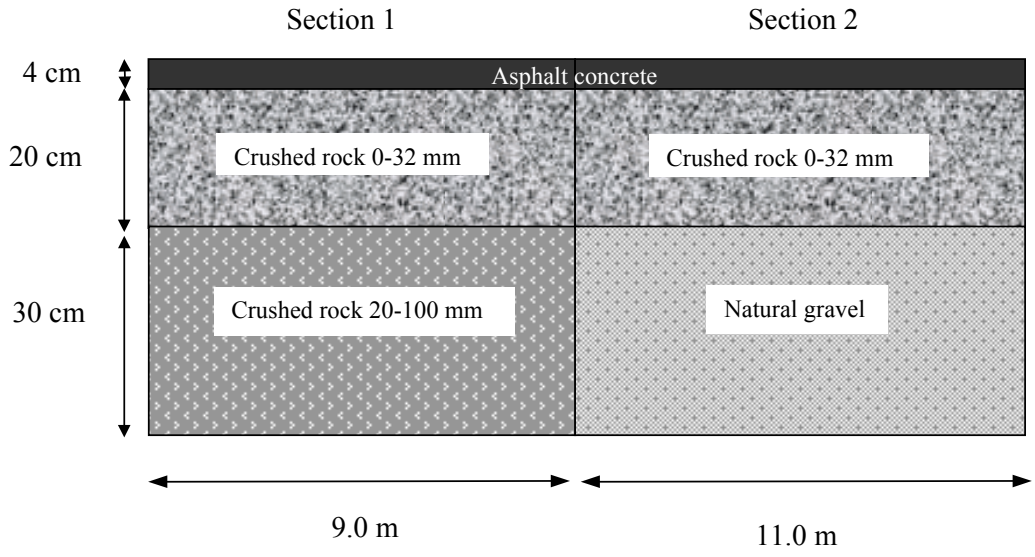

Figure 4-3: Pavement structures of the test sections

4.3 Construction

The original pavement at the site consisted of an asphalt top layer, a gravel base and a crushed rock subbase, with a total thickness of 80-100 cm. This structure was excavated and replaced by the test structures.

After the excavation, Dynamic Cone Penetrometer tests (DCP) and nuclear density measurements (Troxler) were performed on the subgrade at level 100 cm below the original surface. *Figure* 4-4 shows the results from the DCP measurements.
The nuclear density measurements gave an average dry density of 1971 kg/m^3, and average moisture content 12 %. The natural subgrade can be classified as sandy till.

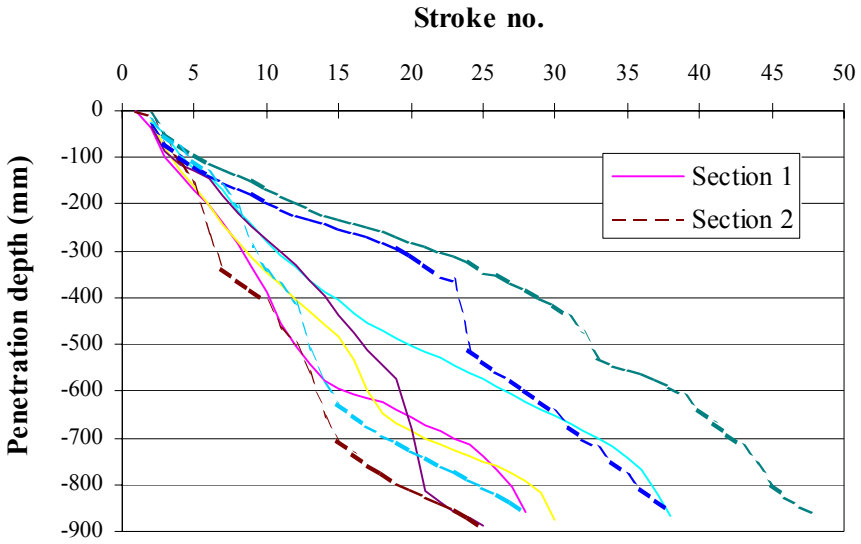

Figure 4-4: Results from DCP tests in the subgrade

The DCP measurements showed some scatter. It was therefore decided to further excavate down to a depth of 115 cm below the surface to include a layer of single graded fine sand with thickness 60 cm, acting as a homogenous subgrade material for the entire test field. The sand was filled in and levelled by an excavator, see
Figure 4-5. Compaction was carried out by the use of a vibrating plate mounted on the excavator.

Figure 4-5: Placement of the sand layer

The test field was constructed with 25 cm unpaved shoulder and side slope gradient 1:2. The width of the test field is 4.5 m. A cross-section sketch is shown in *Figure 4-6*.

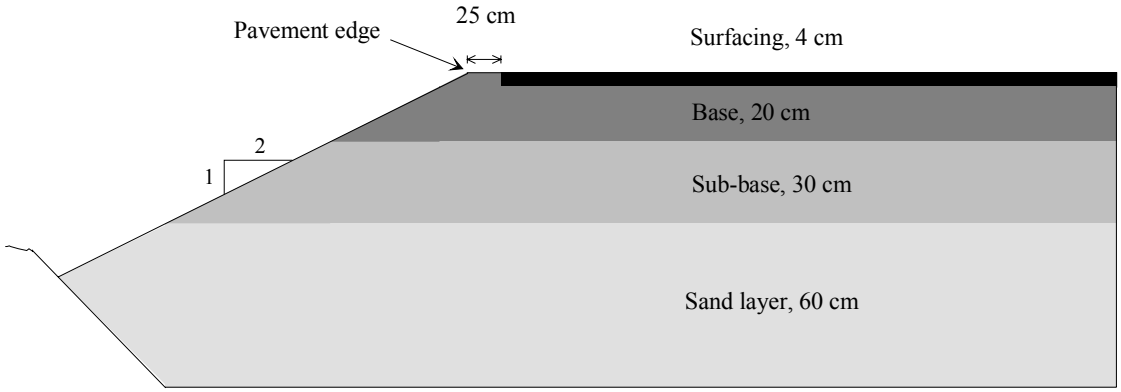

Figure 4-6: Cross-section of the pavement structure

The subbase materials at both sections were filled in and levelled by an excavator. Levelling of the base layer was done by a road grader. The level of the different layers was thoroughly controlled by utilising a levelling telescope.

To avoid any damage or disturbance of the instruments, a relatively small vibrating roller (1500 kg) was chosen for compaction of both the subbase and base layers.

Figure 4-7: Tipping of base material at Section 1 (in the lower left corner of the picture the surface of the subbase layer of Section 2 can be seen)

4.4 Materials

The different pavement materials have been tested both in the laboratory and in the field. The laboratory testing was performed on specimens taken from the test field and the results are presented here.

Grain size distributions for the unbound materials are shown in *Figure 4-8*.

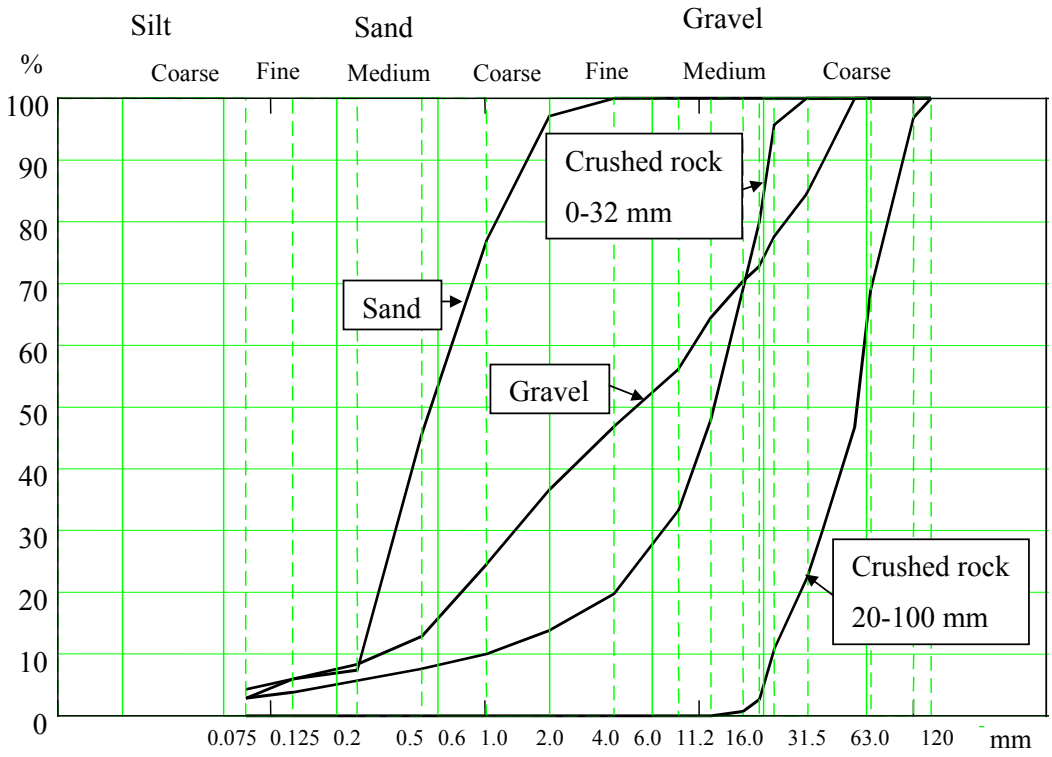

Figure 4-8: Grain size distributions for the unbound materials at the test field

4.4.1 Sand

The sand was delivered from a local gravel pit at Brøttem. The coarse grains have been removed from the gravel by sieving, and most of the fines have artificially been washed out. The result is a very single graded material, $C_u = D_{60}/D_{10} = 4.7$.

Measurement of water content and density in the field immediately after compaction gave the following mean values:

- Water content 5.9 %
- Dry density 1.71 kg/dm^3

The Modified Proctor compaction test was carried out in the laboratory to find the optimum water content and the corresponding maximum dry density. The results were:

- w_{opt} = 9.0 %
- δ_{max} = 2.00 kg/dm^3

CBR testing of a sample compacted to maximum density gave CBR = 20 %. The in-situ value was probably lower due to lower density.

Two samples for repeated load triaxial testing were compacted in the gyratory compactor to the same level of mean density as the density measured in the field. This density was achieved with relatively low compaction effort, as shown in *Figure 4-9*.

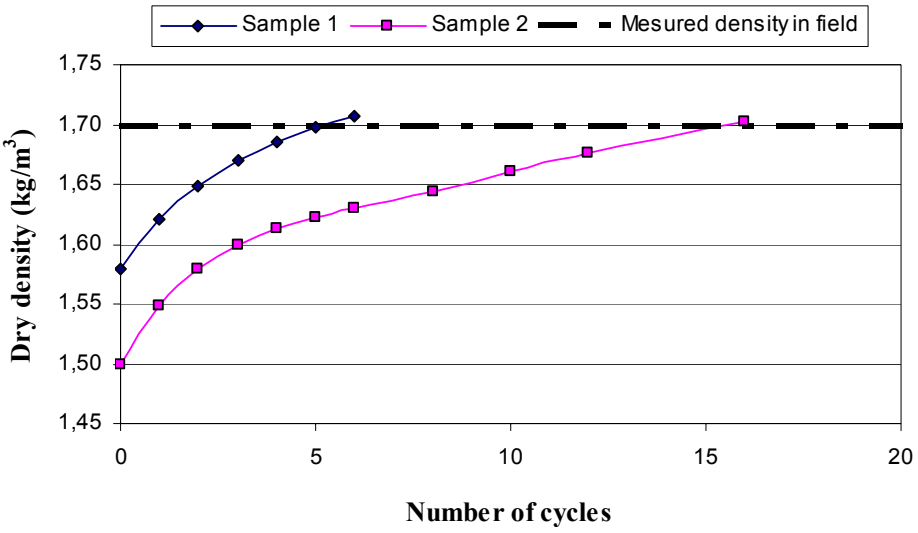

Figure 4-9: Gyratory compaction of sand

For both samples the gyratory angle was set to 1.0°. The applied vertical pressure was 200 kPa for Sample 1, and 100 kPa for Sample 2.

The repeated load triaxial tests were carried out at three different levels of confining pressure (100, 50 and 25 kPa). For each level of confining pressure, deviatoric stress was applied in increasing steps, each of 1000 load pulses with 10 Hz loading frequency, until excessive permanent deformations started to develop. *Figure 4-10* shows the resilient stiffness as function of mean stress level.

For the stress range this material is exposed to in the test field structures, it seems reasonable to use a fixed value for the E-modulus of 75 MPa.

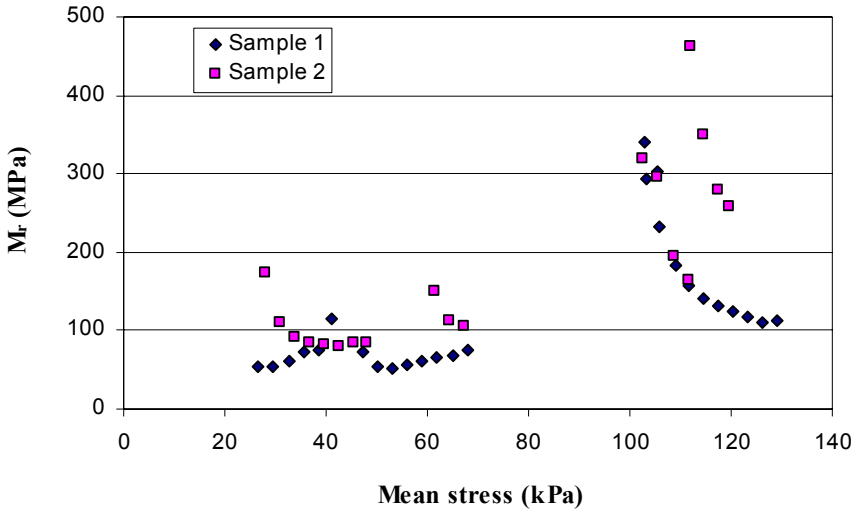

Figure 4-10: Resilient modulus for the sand as a function of mean stress

Figure 4-11 shows measured permanent deformation at the end of each loading step. Because the sand is a relatively loosely compacted, single graded material, it is rather sensitive to high shear mobilisation.

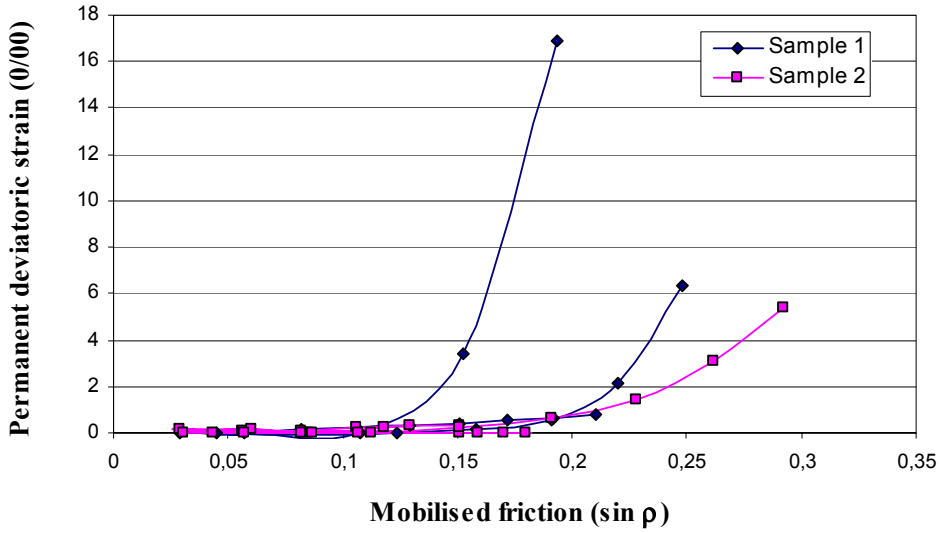

Figure 4-11: Permanent deformations for the sand during triaxial testing

4.4.2 Crushed rock in the subbase of Section 1

The crushed rock used as a subbase material at Section 1 was delivered from Vassfjellet quarry. It was a coarse material of fraction 20-100 mm, see *Figure 4-8*.

Rock from this quarry is of high quality, and the mechanical properties satisfy the requirements for the highest quality class (Steinklasse 1) in the Norwegian classification system. Testing (Norwegian methods) of laboratory crushed samples gave the following results:

Table 4-1: Mechanical properties of crushed rock from Vassfjellet quarry

English notation	Norwegian notation	Value
Flakiness	Flisighet	1.33
Brittleness	Sprøhet	25.5
Abrasion	Abrasjon	0.42

Modified Proctor, CBR and triaxial testing of a material with this particle size was not possible with the available laboratory equipment.

4.4.3 Natural gravel in the subbase of Section 2

The natural gravel used in the subbase of Section 2 was, like the sand, delivered from the gravel pit at Brøttem. It had a fines content of 6.0 % < 75 µm, and maximum particle size 53 mm, see *Figure 4-8*.

Measurement of water content and density in the field gave the following mean values:

- Water content: 4.8 %
- Dry density: 2.21 kg/dm^3

Because the gravel was relatively coarse grained (27.1 % > 19 mm), Modified Proctor and CBR tests in the laboratory have not been performed.

Three samples were prepared for repeated load triaxial testing. Results from the gyratory compaction are shown in *Figure 4-12*. For all samples, the gyratory angle was set to 1.0^o and the vertical pressure was 400 kPa.

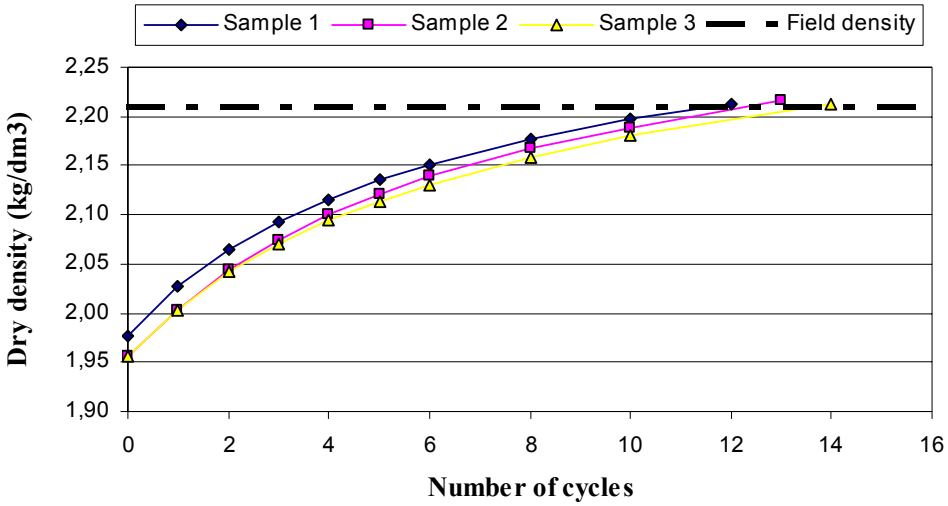

Figure 4-12: Gyratory compaction of gravel

Resilient modulus obtained from the repeated load triaxial testing is shown in *Figure 4-13*.

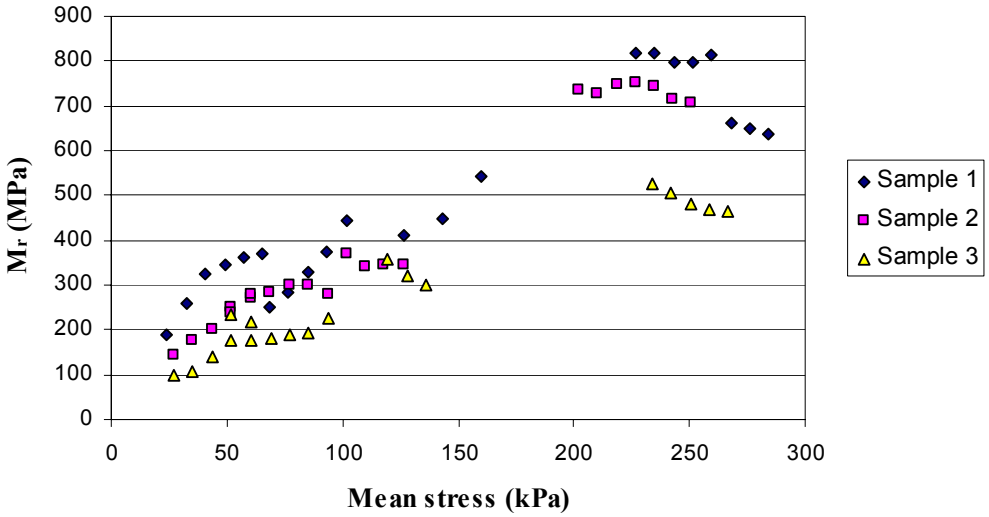

Figure 4-13: Resilient modulus for the gravel as a function of mean stress

Proposed E-moduli from the triaxial tests are given in *Table 4-2.*

Table 4-2: Proposed elastic moduli for the gravel at different levels of mean stress

Mean stress (kPa)	50	100	150	200	250
E-modulus (MPa)	250	350	450	600	700

The measured permanent deformation is shown in *Figure 4-14*. The data indicate that the shear mobilisation for the gravel should not exceed sin ρ = 0.30.

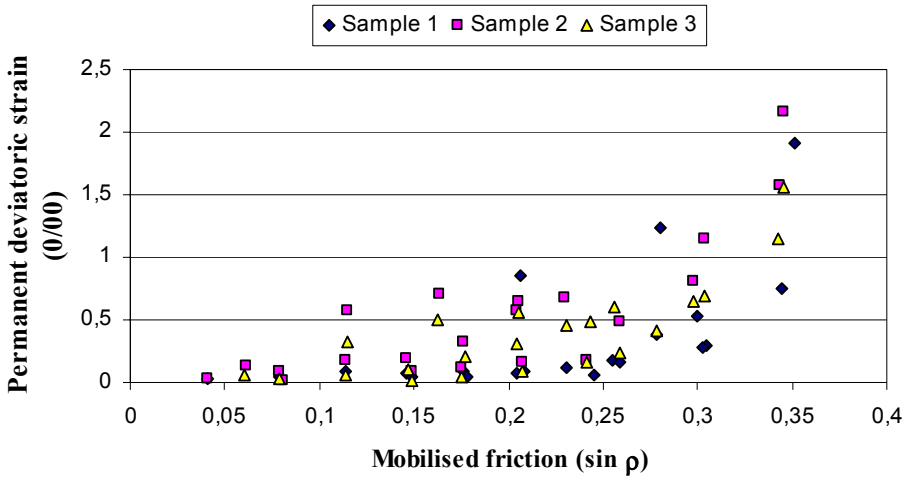

Figure 4-14: Permanent deformations for the gravel during triaxial testing

4.4.4 Crushed rock in the base layer

Like the crushed rock in the subbase layer of Section 1, the crushed rock used as a base material at both sections was delivered from Vassfjellet quarry. The fraction of this material was 0-32 mm. Quality parameters are given in *Chapter 4.4.2.*

Measurement of water content and density in the field gave the following mean values:

- Water content: 1.9 %
- Dry density: 2.19 kg/dm^3

Two samples for repeated load triaxial tests were compacted using the gyratory compactor with the following settings:

- Gyratory angle: 1.0°
- Vertical pressure: 400 kPa
- Fixed number of cycles: 400

Figure 4-15 shows the achieved density as a function of the number of cycles compared with the target density from the field measurement.

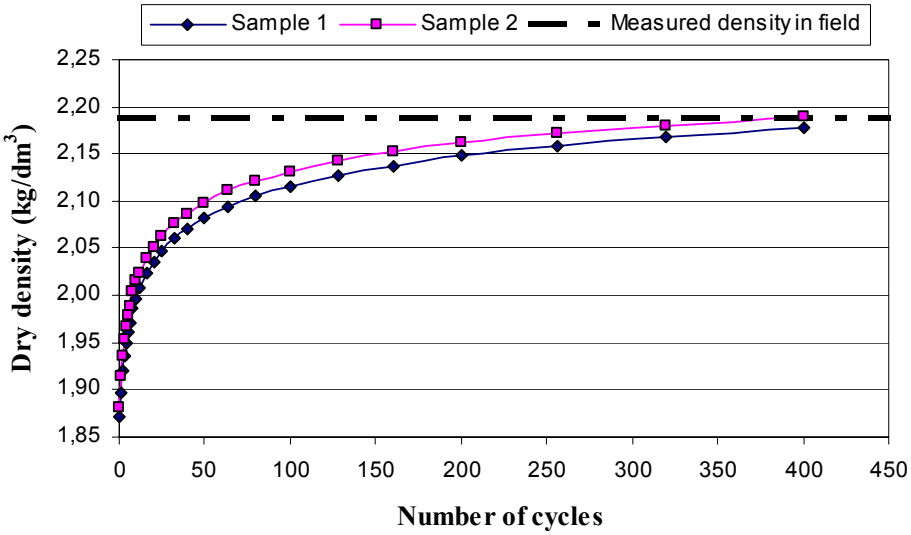

Figure 4-15: Gyratory compaction of crushed rock 0-32 mm

The material was tested at four different levels of confining pressure (100, 200, 50 and 25 kPa). *Figure 4-16* shows the results from repeated load triaxial testing.

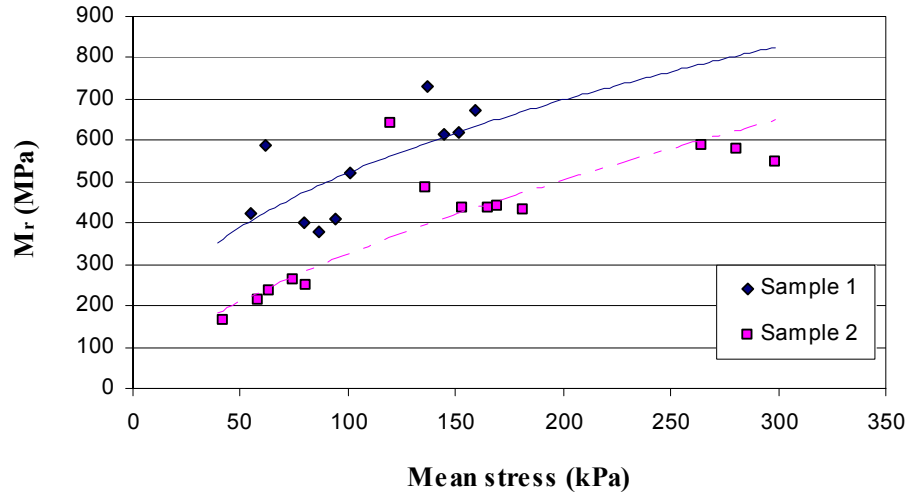

Figure 4-16: Resilient modulus as a function of mean stress for crushed rock 0-32 mm

As can be seen, some scatter between the results occur, but this is not more than could be expected for a coarse graded material like this.

Proposed E-moduli from the triaxial tests are given in *Table 4-3*.

Table 4-3: Proposed elastic moduli for the crushed rock 0-32 mm at different levels of mean stress

Mean stress (kPa)	50	100	150	200	250
E-modulus (MPa)	300	400	550	610	670

The development of permanent deformations during triaxial testing is shown in *Figure 4-17*. For each load step 3000 cycles are applied. Compared to the sand and gravel materials, the level of permanent deviatoric strain is low. The limit for shear mobilisation seems to be a little below sin ρ = 0.30.

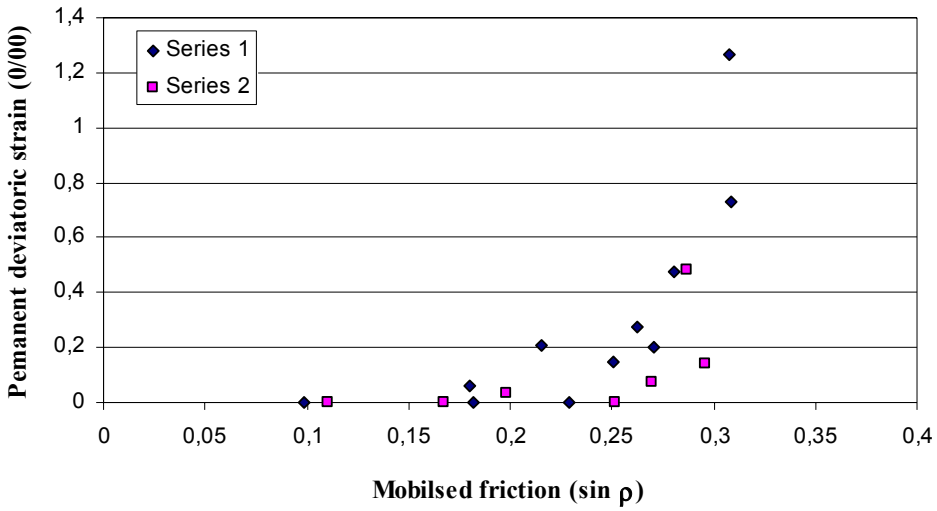

Figure 4-17: Permanent deformations for the crushed rock 0-32 mm during triaxial testing

4.4.5 Compaction control on top of the base layer

The compaction of the granular materials in the field was controlled by performing plate-loading and FWD tests on the top of the base layer at two different locations at each section. The average results are shown in *Table 4-4*. As expected, Section 1 with crushed rock subbase shows a stiffer behaviour than Section 2.

Table 4-4: Mean values from plate loading and FWD tests on the top of the base layer

Section	E1 (MPa)	E2 (MPa)	E2/E1	Bearing capacity (tons)
1	177.3	363.5	2.05	9.9
2	105.3	233.7	2.22	7.0

4.4.6 Asphalt concrete surfacing

The surfacing at the test field is a densely graded asphalt concrete with a maximum aggregate size 16 mm (in Norwegian terms: Agb16). The mix is composed of crushed rock, natural gravel and sand, and was planned to have a binder content of 5.6 % (180 pen.) and a void content of 4.5 %. Extraction analyses in the laboratory showed a mean binder content of 5.3 %. The density of the asphalt concrete was 2.45 kg/dm^3.

Table 4-5 shows results from indirect tensile testing of four cores taken from the surfacing. The test temperature was 25 ^{o}C. The elastic modulus is calculated according to *Equation 3.4*.

Table 4-5: Results from indirect tensile testing at 25 ^{o}C of specimens from the surfacing

Specimen no.	Height (mm)	E-modulus (MPa)
1	42.2	1803
2	43.5	1532
3	42.6	1750
4	37.7	2006
Mean values	**41.5**	**1773**

4.5 Instrumentation

Section 2 of the test field was instrumented for measurement of load responses in both horizontal and vertical direction in the base and subbase layers. Measurements of vertical stresses and strains were emphasised because this was considered to give the most reliable results.

A frost penetration sensor and temperature sensors at different depths were also installed, primarily used for reference measurements in connection with the LWA-project.

4.5.1 Instrument positions

An overview of the location of the instruments at Section 2 is shown in *Figure 4-18*. The instrumentation plan reflects the scope of the study, which was measurement of load responses at different offsets from the pavement edge. The instrumentation consisted of the following sensor types:

- VPC – Vertical Pressure Cell
- HPC – Horizontal Pressure Cell
- VDT – Vertical Deformation Transducer
- HDT – Horizontal Deformation Transducer
- F – Frost penetration sensor
- T – Temperature sensors

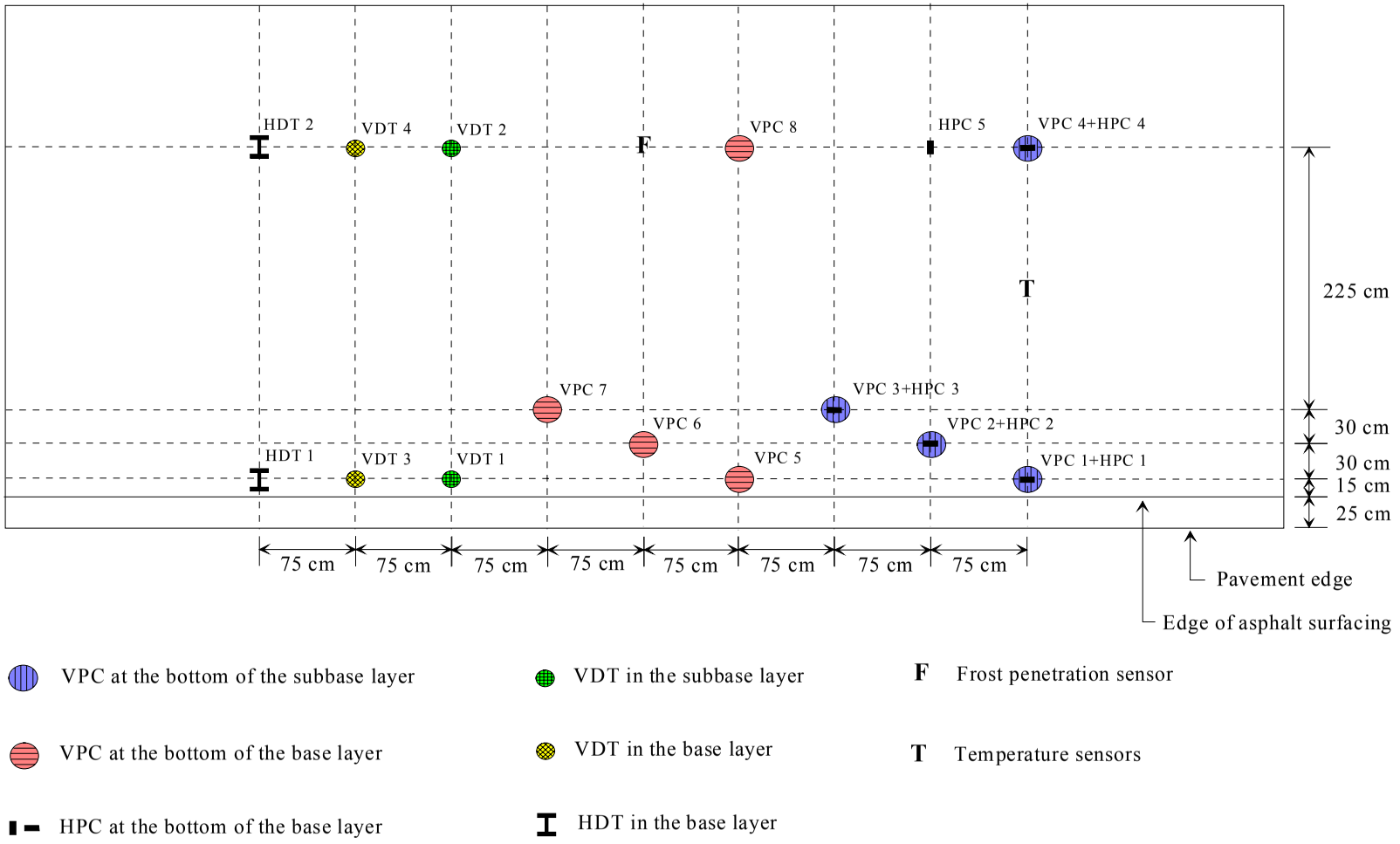

Figure 4-18: Horizontal location of sensors at Section 2

A local co-ordinate system was established before the construction of the test field with the x-axis pointing in the transverse direction, and the y-axis along the edge of the asphalt surfacing. Positive z-direction was vertically down with the zero point at the surface. Each sensor got its position according to this co-ordinate system, and the installation during construction was controlled using a total station (theodolite). To avoid that the sensors influenced on each other, the mutual horizontal spacing between the sensors was minimum 75 cm /40/.

4.5.2 Vertical Pressure Cell (VPC)

The type of pressure cell chosen for the measurements of vertical stresses was a Geokon 3500-100 Dynamic Soil Pressure Cell, *Figure 4-19*. This is a hydraulic-diaphragm type of cell with large diameter (225 mm) and small thickness (7 mm). The measurement range is 0-689 kPa (0-100 psi).

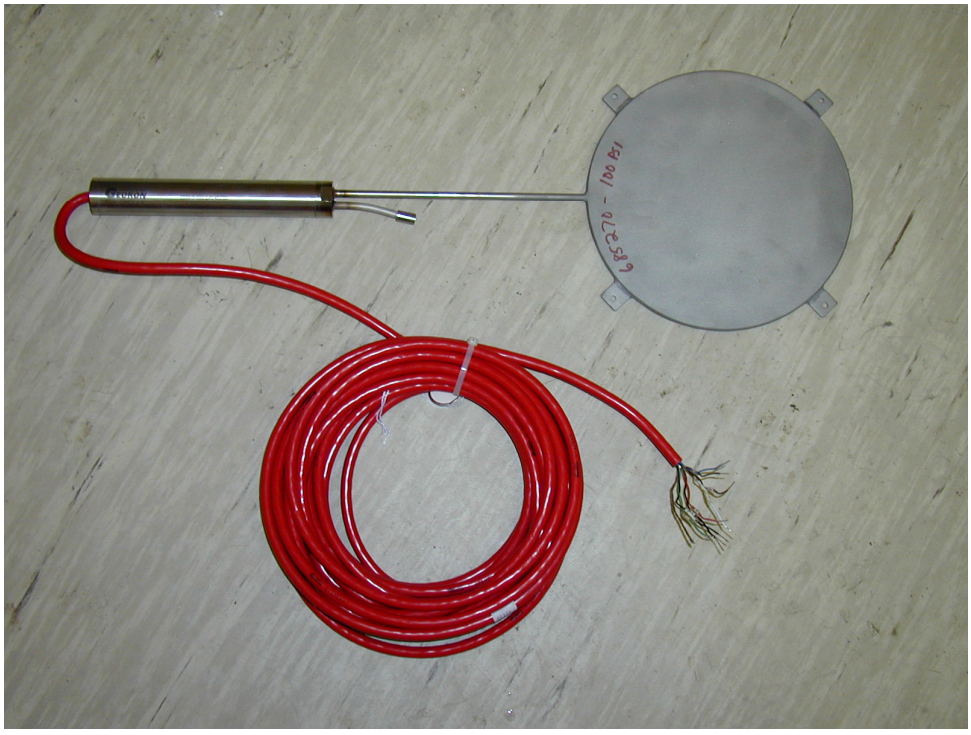

Figure 4-19: Geokon Soil Pressure Cell

The Geokon Soil Pressure Cell consists of two circular stainless steel plates welded together around their periphery and spaced by a narrow cavity filled with an antifreeze flid. A high-pressure, stainless steel tubing connects the cavity to a pressure transducer (semiconductor strain gauge instrumented diaphragm) housed inside a tube of 152 mm length and 19 mm diameter. External pressures acting on the cell are balanced by an equal pressure induced in the internal fluid. This pressure is converted into an electrical signal by the pressure transducer.

The primary advantage of this soil pressure cell is it's low aspect ratio, thickness/diameter = 0.03. Therefore, it is expected to have acceptable accuracy for the measurement of dynamic stresses in soils, independent of the soil stiffness /27/.

The Geokon cells were calibrated under hydrostatic water pressure condition in a tank. Readings were taken at increments of 1 m down to a maximum depth of 9 m. As expected, the relation between cell output and hydrostatic stress was linear.

Eight VPC's were installed; four at the bottom of the subbase layer (VPC 1 – VPC 4), and four at the bottom of the base layer (VPC 5 – VPC 8).

4.5.3 Horizontal Pressure Cell (HPC)

Horizontal stress within a layer varies over the layer thickness. Hence, small diameter soil pressure cells have to be used for such measurements. After some consideration, the final choice was the Kulite 0234-3 Soil Pressure Cell, *Figure 4-20*. The main reasons for choosing this cell were that other commercially available stress cells were considerably more expensive, and that this type of cell also was chosen at the Minnesota Road Research Project (Mn/Road) /1/.

The Kulite pressure cell has a total diameter of 55 mm, a thickness equal to 15 mm, and utilises a solid state silicone strain gauge bridge mounted on a flexible diaphragm as it's sensing element. The diaphragm is placed at the centre of the transducer housing behind a stainless steel plate. Silicone fills the cavity between the diaphragm and the plate. When the stainless steel plate deflects due to an applied pressure, load is

transferred to the diaphragm via the silicon. A rigid annulus surrounds the interior of the cell and serves to protect the transducer from lateral stresses. The measurement range is 0-103 kPa (0-15 psi).

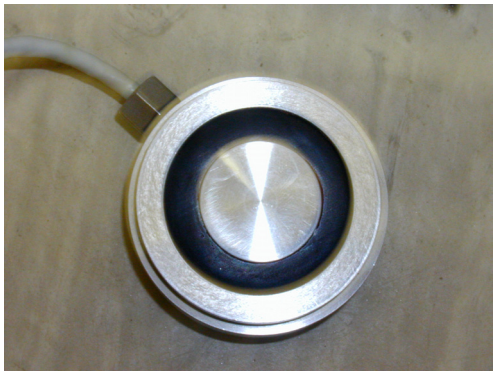

Figure 4-20: Kulite 0234 Soil Pressure Cell

Five HPC's were installed at the bottom of the base layer with the lower periphery at the top of the subbase; four for measurements in the transversal (HPC 1 – HPC 4) and one for measurements in the longitudinal direction (HPC 5).

4.5.4 Soil Deformation Transducer (SDT)

Soil Deformation Transducers (SDT's) were used for measuring dynamic strains and permanent deformations in the subbase and the base layer. In *Figure 4-18*, transducers for measurements in the vertical direction are denoted VDT, while transducers for measurement in horizontal direction are denoted HDT. Totally six SDT's were placed in the structure; two for measurements in the vertical direction in the subbase (VDT 1 and VDT 2), two for measurements in the vertical direction in the base layer and two for measurements in the transversal direction in the base layer (VDT 3 and VDT 4, and HDT 1 and HDT 2, respectively).

The SDT's were made at NTNU/SINTEF. A picture of a transducer is shown in *Figure 4-21*.

The circular end plates are made of aluminium, and the rod between the plates is made of brass. For the VDT's, the distance between the top and the bottom of the transducer was adjusted to the layer thickness; 200 mm for the base layer and 300 mm for the subbase layer. For HDT's the distance between the plates was 200 mm.

By the use of a Linear Variable Differential Transducer (LVDT), the change of distance between the plates by loading was recorded. The LVDT body was mounted inside the brass rod, which was screwed to the bottom circular plate. The LVDT core was connected to the top plate of the SDT, with the possibility of adjustment during installation, see *Figure 4-22*. The type of LVDT used was a Lukas-Schaevitz MHR-500, with a nominal linear range of ± 12.70 mm. The signal cable from the LVDT body was lead out through a sealed hole in the rod near the bottom plate of the SDT.

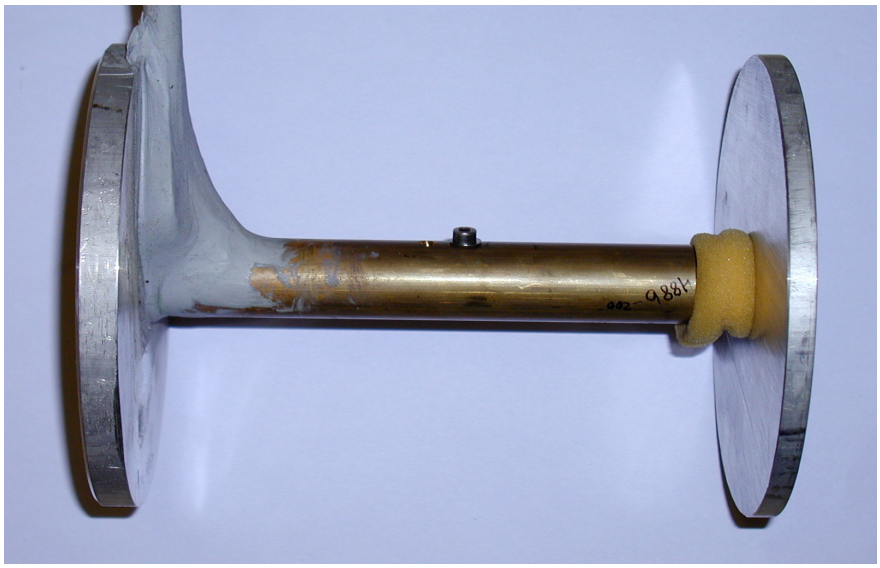

Figure 4-21: Soil Deformation Transducer

The VDT's, without the top plate and LVDT-core, were placed in correct position on the surface of the underlying layer with the signal cable stretched out to the edge. The rod opening was sealed, and base material filled by hand over the bottom plate and around the rod forming a cone of material over the sensor. The entire layer was then filled in, levelled and compacted with a vibrating roller. After compaction, the material over the rod was carefully removed, the top plate installed and the LVDT-

core adjusted, see *Figure 4-23*. The LVDT-core was greased to secure low friction and avoid corrosion. Finally, some material was put on top of the sensor and carefully compacted. Re-adjustment of the LVDT-core was necessary for some of the sensors.

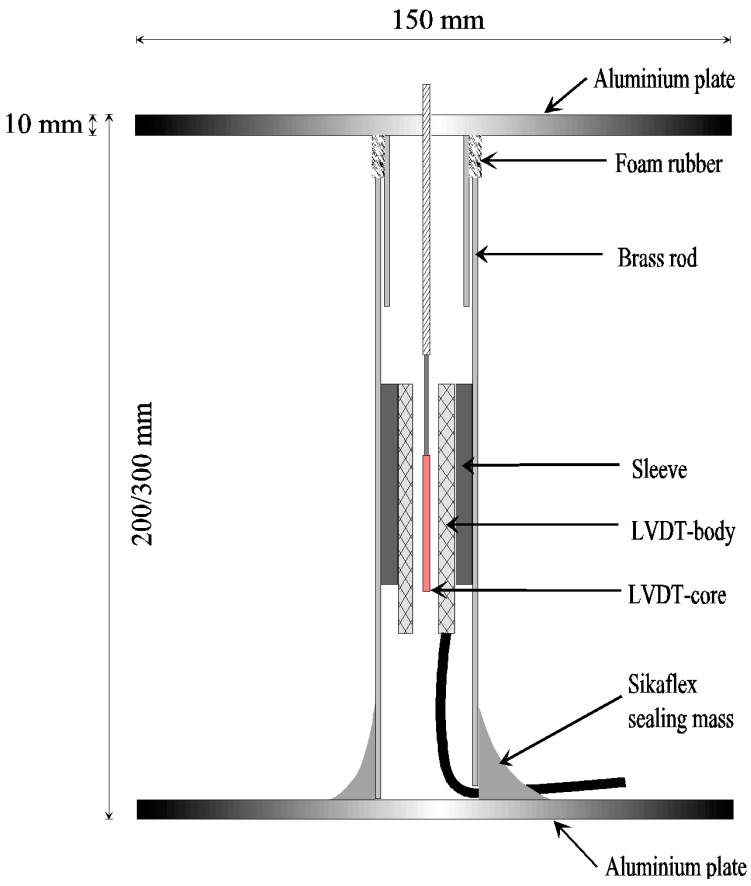

Figure 4-22: Sketch of a Soil Deformation Transducer

Figure 4-23: Installation of a VDT in the subbase layer

4.5.5 Temperature sensors

The registration of temperatures was primarily interesting as a reference for the LWA-project, in which documentation of the insulation properties of expanded clay was one of the main objectives. Nine temperature sensors were installed at different depths at section 2, see *Figure 4-24*. In addition, a sensor protected from radiation mounted outside the instrument building adjacent to the test field recorded the air temperature.

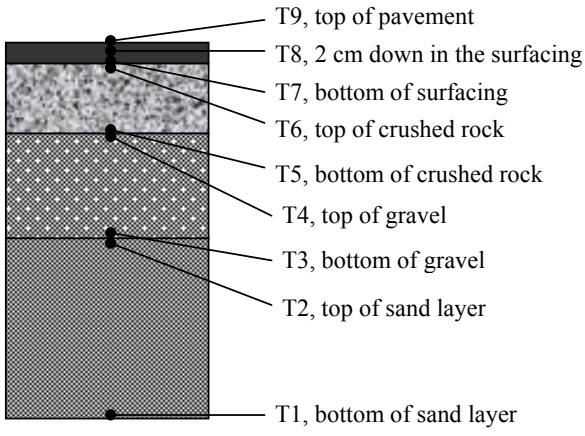

Figure 4-24: Placement of thermocouples at Section 2

The sensors were made of copper-constantan thermocouples, type T, and temperatures were logged every 10 min. by the use of a standard data-logger of type HP 34970 A.

4.5.6 Frost penetration sensor

A frost penetration sensor was installed for registration of ground frost during the winter. The sensor consists of a transparent tube inserted vertically into the pavement and filled with methylene-blue coloured water. The dye added to the water makes the distinction between frozen and non-frozen water in the tube to appear clearly. A further description of the frost penetration sensor is given in /29/.

4.5.7 Signal conditioning

Signals from built-in pressure cells and LVDT's were lead through sealed cables to an amplifier, type *Hottinger Spider 8*. Further, the signals were transmitted to a PC and processed by a program specially developed for this purpose. For truck loading, this program generated one data file for every vehicle passing over the test section and in the case of FWD loading, one data file was generated for every drop. All files were stored to disk, labelled according to date and time. In the case of static plate loading, the sensor outputs had to be written down from the computer screen for every loading step.

Temperature data were stored in a data-logger and frequently transmitted to a PC for disk saving and further analyses.

4.6 Evaluation and experience

The construction of the test field was carried out during approximately two weeks in June 1999. The weather was fortunately good, and all instruments could be installed as planned.

Accurate levelling of the granular layers by the use of the excavator was a challenge for the operators. Quite a lot of time was used to obtain an even surface of each layer, and a levelling telescope was used for control. The surface of the base layer was created by using a road grader.

The installation of the sensors was a laborious task and required a high degree of accuracy and control. The establishment of the local co-ordinate system and control of the lateral position of each sensor by use the of the total station was essential for this work.

To avoid disturbance of the sensors, a rather light vibration roller (1500 kg) was chosen for compaction. Possibly, a somewhat heavier roller could have been used to obtain a better compaction of the unbound materials and still avoiding any damage to the sensors.

5 RESULTS FROM SANDMOEN TEST FIELD

5.1 Introduction

Measurements were carried out at Sandmoen test field at several occasions both in 1999 and 2000, see *Table 5-1*, including the following three modes:

- Measurement of stresses and deformations from controlled wheel loading by using a specific truck driving over the test sections
- Measurement of stresses, deformations and surface deflections FWD tests
- Measurement of stresses, deformations and surface deflections from plate loading tests

Table 5-1: Performed measurements at Sandmoen test field

Date	Mode
1999-08-26	Controlled wheel loading
1999-09-28	FWD
1999-11-01	Controlled wheel loading
2000-03-28	Controlled wheel loading
2000-05-29	Controlled wheel loading
2000-06-15	FWD
2000-07-06	Plate loading

In this chapter the most interesting results from the different loading occations are presented.

5.2 Controlled wheel loading

By driving a specific truck over the test sections, responses from different combinations of wheel load and tyre pressure have been measured. Data for four different load/pressure combinations of the right front wheel are analysed and presented here. These are shown in *Table 5-2*.

Table 5-2: Analysed load characteristics for the right front wheel

Denotation	Date	Load (kN)	Tyre pressure (kPa)
A	1999-11-01	15,2	690
B	2000-05-29	29.4	690
C	1999-08-26	30.6	900
D	1999-08-26	42,9	900

Figure 5-1: Controlled wheel loading

As the pavement at the test field had granular base and subbase materials and only a thin asphalt surfacing (4 cm), varying temperature and speed were assumed to have only minor influence on the measured stresses and deformations in the granular base and subbase layers. Consequently, effects of variations in temperature and speed have not been studied.

Readings from the different sensors were taken while the truck was driving over the test field at low speed (about 15 km/h) and at different offsets from the pavement edge. The aim offsets from the pavement edge for the right front wheel were marked as longitudinal lines at the pavement surface, see Figure 5-1. This was necessary to enable the driver to position the truck, and was a very good help for visual control of the wheel position.

5.2.1 Vertical stress under wheel loading

Vertical stresses have been successfully measured at the bottom of both the base and the subbase layers. Figure 5-2 shows readings from VPC 2 and VPC 6, 70 cm from the pavement edge, for one certain passage of the two-axle truck with the right front wheel directly over the sensors. Load and tyre pressure for the front wheel was in this case 29.4 kN and 690 kPa, respectively (case B in Table 5-2).

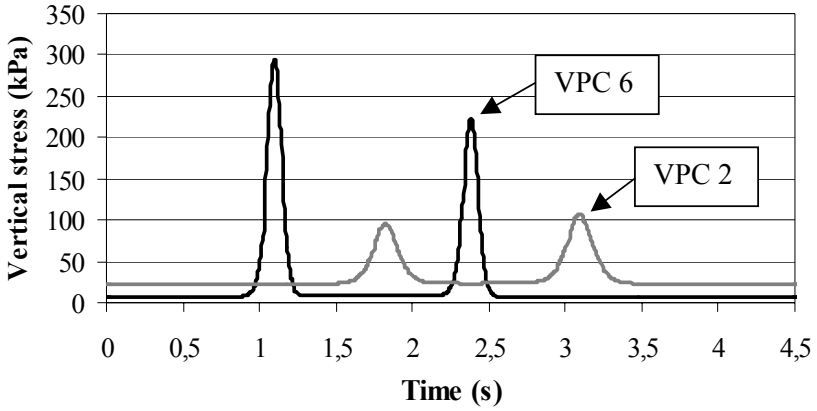

Figure 5-2: Example of logged vertical stress under the two-axle truck

Measured peak values of vertical stress at the bottom of the base and the subbase layers for the front wheel at different offsets from the pavement edge are shown in *Figure 5-3* and *Figure 5-4*. Duplicate readings are marked, and trend curves (2nd order polynomials) are added. The numbering of the curves relates to *Table 5-2*.

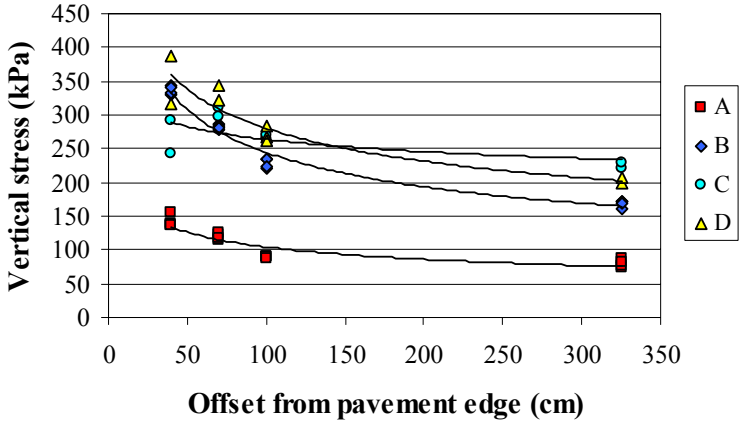

Figure 5-3: Measured vertical stresses directly under the right front wheel at the bottom of the base layer

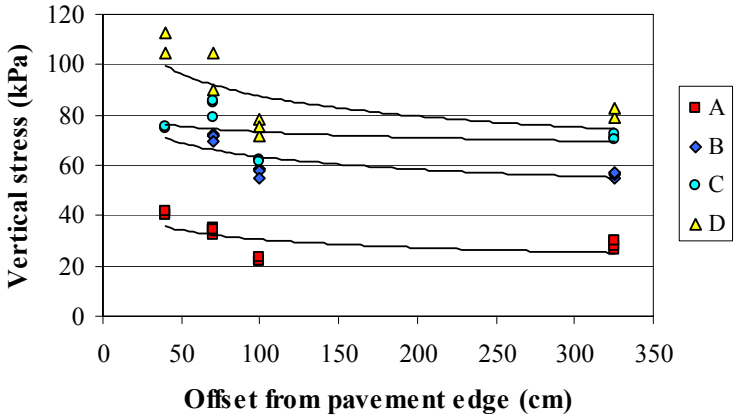

Figure 5-4: Measured vertical stresses directly under the right front wheel at the bottom of the subbase layer

One of the Geokon soil pressure cells, VPC 1, stopped functioning during the winter 1999-2000. This is the reason why measurements 40 cm from the pavement edge are missing in *Figure 5-4* for case B. All other cells were still in function during 2000.

The measurements show a clear tendency of increasing vertical stress towards the pavement edge, especially at the bottom of the base layer. This effect is particularly evident for wheel passages closer than ca. one meter from the pavement edge. Loading 40 cm from the pavement edge gave in average 68 % greater vertical stress below the base layer and 28 % greater vertical stress below the subbase layer compared to the corresponding measured values by wheel passages in the inner wheel path. Measured vertical stresses at the bottom of the base layer were approximately three times the corresponding values at the bottom of the subbase layer, independent of offset.

Measured maximum vertical stresses for load passages directly over and for passages 30 cm beside the different sensors are shown in *Figure 5-5* and *Figure 5-6.* Here, the values for load directly over the sensors are mean values for the duplicate readings in *Figure 5-3* and *Figure 5-4.*

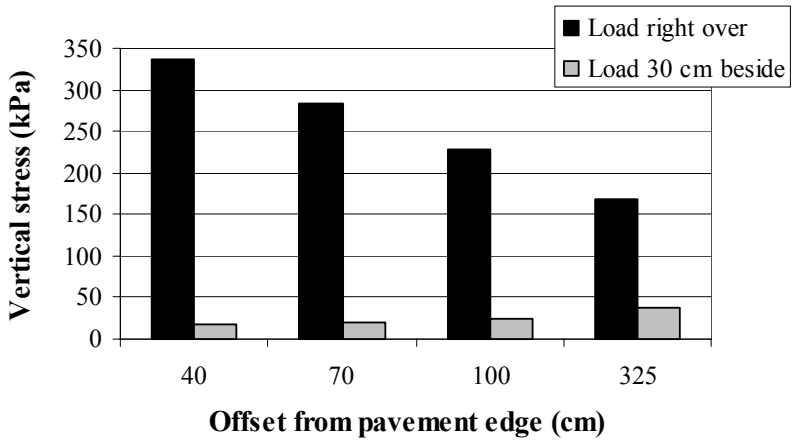

Figure 5-5: Measured vertical stresses at the bottom of the base layer for wheel load B (29.4 kN, 690 kPa)

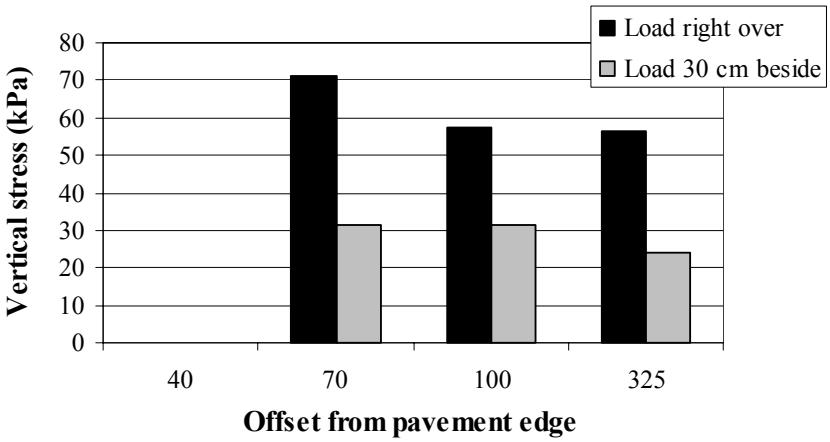

Figure 5-6: Measured vertical stresses at the bottom of the subbase layer for wheel load B (29.4 kN, 690 kPa)

Figure 5-5 shows that at the bottom of the base layer there was a high concentration of stresses directly beneath the load. When the wheel was passing 30 cm beside the sensor (transversally inwards), the measured maximum stress 40 cm from the pavement edge was reduced by 95 %, while in the inner wheel path the reduction was 78 %. The difference is supposed to be caused by decreasing confining pressure and hence decreasing load spreading properties for the base material towards the pavement edge. The average reduction of vertical stress at the bottom of the subbase layer for wheel passages 30 cm beside the sensor was 53 %.

5.2.2 Horizontal stress under wheel loading

Horizontal stresses were measured at the bottom of the base layer. Four Kulite soil pressure cells placed at different offsets from the pavement edge measured horizontal stresses in the transversal direction (HPC 1 – HPC 4), and one cell measured horizontal stresses in the longitudinal direction (HPC 5), see *Chapter 4.5*.

Figure 5-7 shows readings from HPC 1, HPC 2 and HPC 3 for one certain passage of the two-axle truck, with the right front wheel 70 cm from the pavement edge (directly over HPC 2). Load and tyre pressure of the front wheel was in this case 29.4 kN and 690 kPa, respectively (case B in Table 5-2).

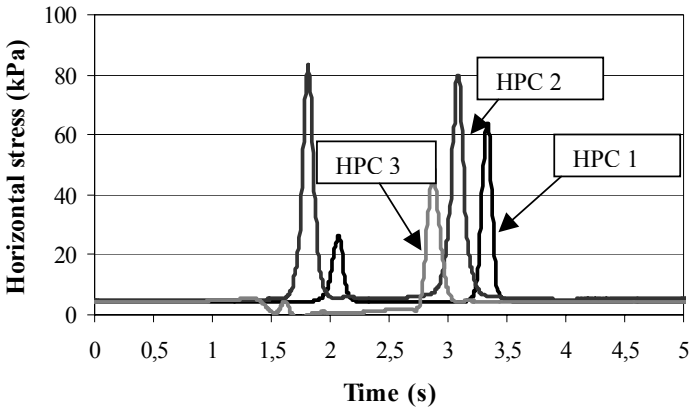

Figure 5-7: Example of logged horizontal stress under a two-axle truck

Figure 5-8 shows measured peak values of transversal stress for front wheel passages directly over each pressure cell. The labelling of the series relates to *Table 5-2*.
These readings can not be emphasized due to the general uncertainties connected to measurements in the horizontal direction in granular materials. It is nevertheless interesting to notice that the measured horizontal stress is lowest for the pressure cell 325 cm from the pavement edge. According to increased side support and thereby better load distribution properties of the granular base material towards the inner wheel path, the opposite result was expected.

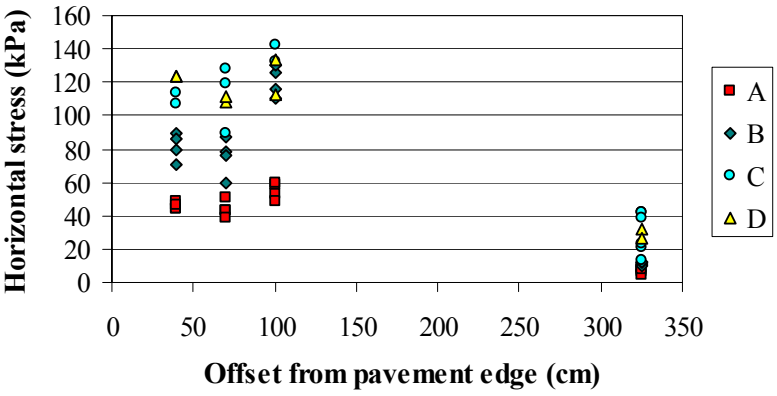

Figure 5-8: Measured transversal horizontal stresses at the bottom of the base layer

HPC 5, which measured horizontal stress in the longitudinal direction 325 cm from the pavement edge, gave a double-peak signal for wheel passages directly over the sensor. This is consistent with a rotation of principal stresses during a wheel passage. Double peak signals are not observed for HPC 4, measuring transversal stresses at the same distance from the pavement edge. *Figure 5-9* shows typical signal curves for these two sensors for the passage of a two-axle truck.

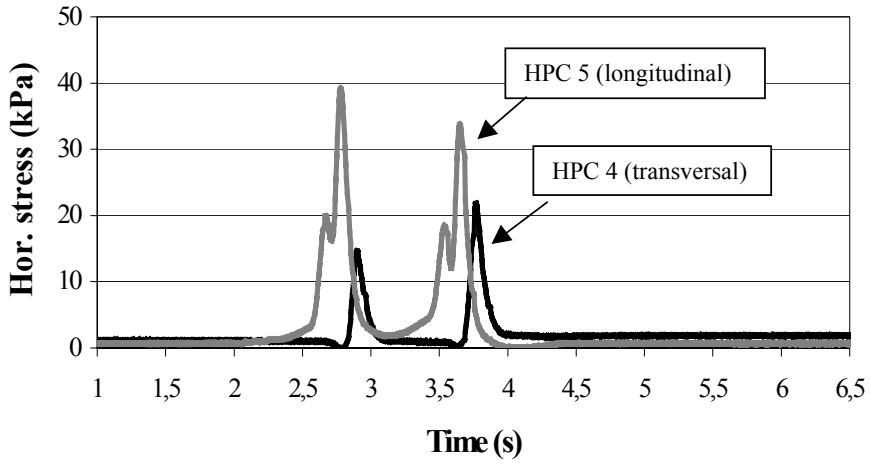

Figure 5-9: Example of logged horizontal stresses in longitudinal and transversal direction 325 cm from the pavement edge

For all combinations of wheel load and tyre pressure, the measured horizontal stresses in the longitudinal direction were greater than in the transversal direction. However, compared to the measurements closer to the pavement edge, the horizontal stress level under the inner wheel path, also in the longitudinal direction, was considerably lower. This is inconsistent with the theory, but since these were readings only from one single sensor in each direction, they should be repeated before any conclusions could be drawn.

5.2.3 Vertical strain under wheel loading

Examples of signal curves from the vertical deformation transducers placed in the subbase and base layer 40 cm from the pavement edge (VDT 1 and VDT 3) are shown in *Figure 5-10*. The signal curves give information on elastic, plastic and total deformation for each wheel passage.

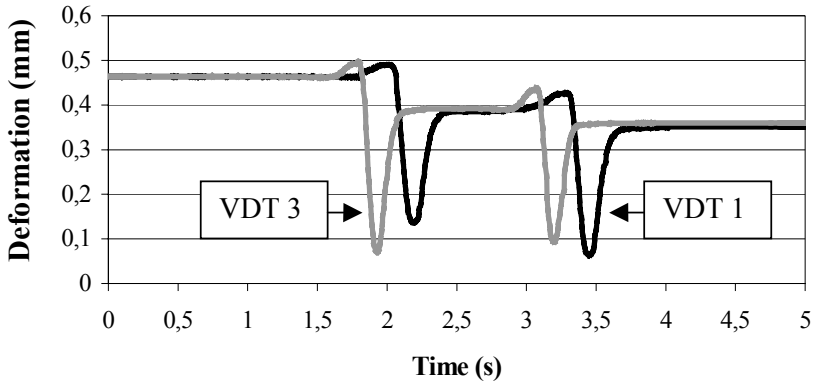

Figure 5-10: Example of logged vertical deformation 40 cm from the pavement edge

Measured vertical deformations are analysed for each combination of load and tyre pressure. The average results are converted into strain, and the results are shown in the following figures. Vertical strain values in the base layer are shown in *Figure 5-11*, while corresponding values for the subbase layer are shown in *Figure 5-12*.

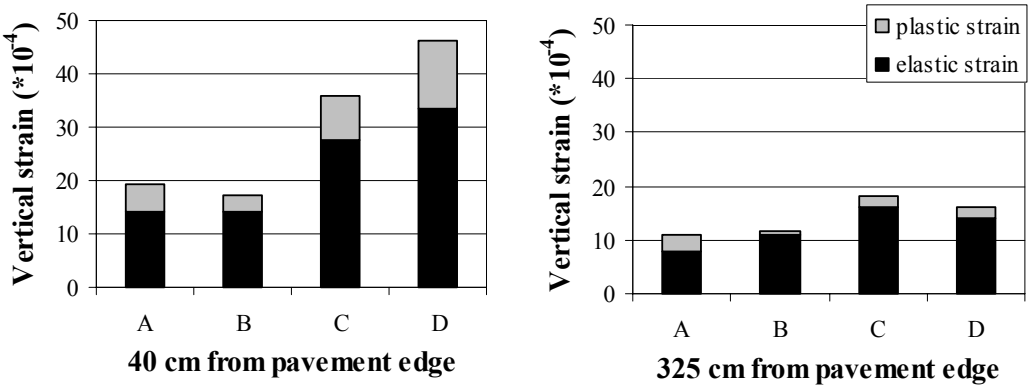

Figure 5-11: Measured vertical strain in the base layer directly under the wheel

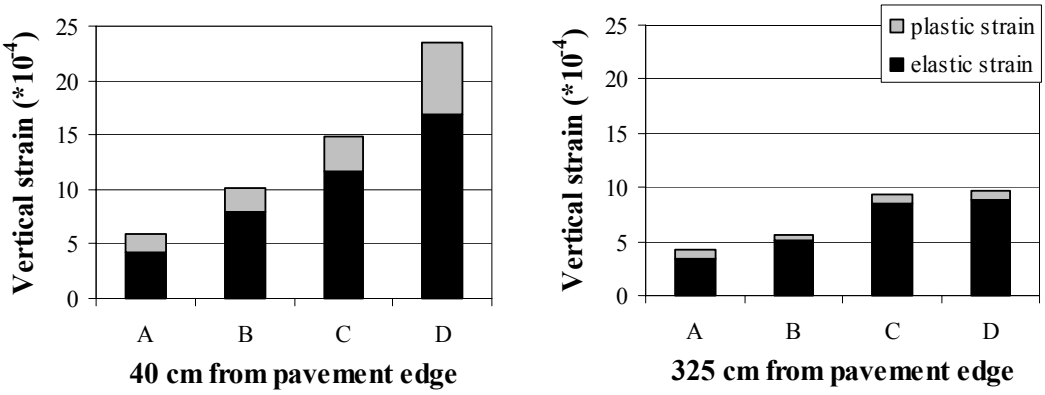

Figure 5-12: Vertical strain in the subbase directly under the wheel

The greatest values of vertical strain were found in the base layer for the load positioned close to the pavement edge. The difference between the inner wheel path and the pavement edge was clear from readings both in the base and the subbase layers. Loading 40 cm from the pavement edge also gave a greater relative component of plastic strain than in the inner wheel path. The largest difference was found for the heaviest wheel load.

5.2.4 Horizontal strain under wheel loading

Figure 5-13 shows horizontal strain in the transversal direction in the base layer for wheel passages directly over the sensors.

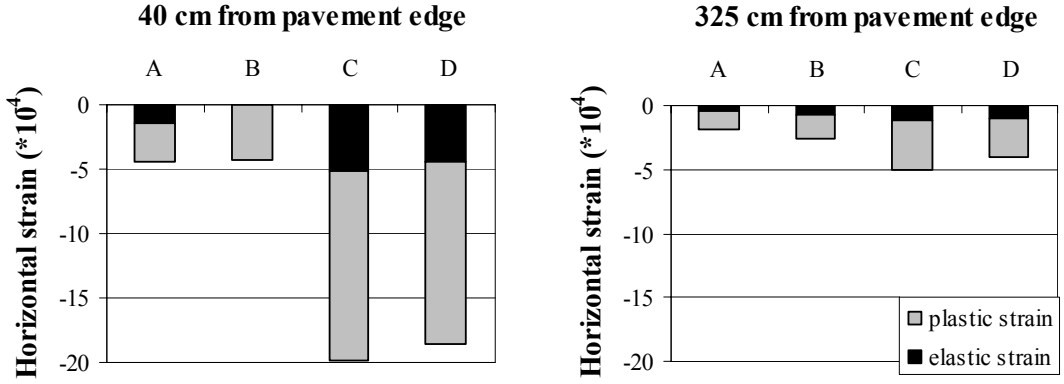

Figure 5-13: Horizontal strain in the base directly under the wheel

As expected, horizontal expansion was measured when the wheel passed directly over the sensor. In this case, the amount of plastic strain was very large, and for all load combinations, larger than the elastic component for wheel passages both near the pavement edge and in the inner wheel path. The measured levels of total strain were higher near the pavement edge than in the inner wheel path, especially for wheel loads C and D with high tyre pressure (900 kPa).

The general uncertainties connected to these measurements are demonstrated by the fact that greater strain is measured under wheel load C than under wheel load D.

5.3 FWD measurements

The FWD measurements at Sandmoen test field were carried out at two different occasions, 1999-09-28 and 2000-06-15. The same Dynatest FWD as referred to in *Chapter 3* was used. The load plate diameter was 30 cm as earlier, but at these occations the deflection sensors were located 0, 20, 30, 45, 65 and 90 cm from the plate centre, which is slightly different from the earlier sensor configurations.

Normal practice for FWD measurements is to place the apparatus in the longitudinal direction. This was done at the measuring points located 325 cm from the pavement edge. For the rest of the points, the apparatus had to be placed crosswise to the road in order to locate the loading plate of the FWD close enough to the paved edge, see *Figure 5-14*.

Figure 5-14 FWD measurement

5.3.1 Measured bearing capacity

The bearing capacity has been calculated by the same formula as given in *Chapter 3.4, Equation 3.2*. At Sandmoen, $AADT_h$ was set to be 100.

The average force for the 1999 measurements was 54.1 kN (765 kPa), while the measurements in 2000 were carried out with an average force of 72.9 kN (1031 kPa). *Figure 5-15* shows calculated bearing capacity including trendlines (2nd order polynomials) for the two test sections for the two measuring occasions.

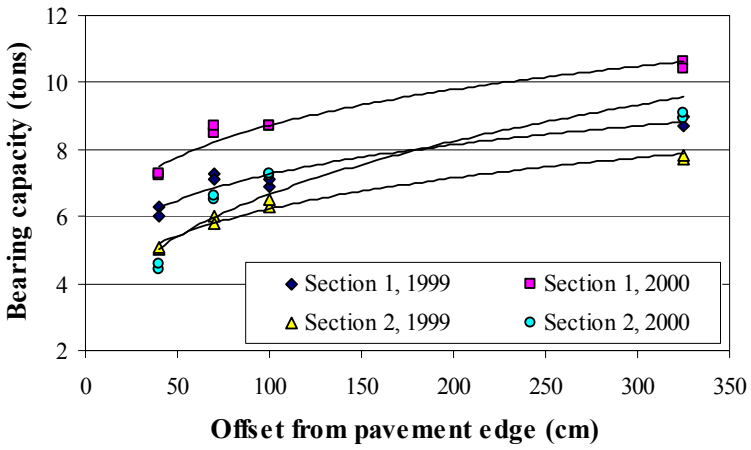

Figure 5-15: Calculated bearing capacity from FWD measurements

The measurements show a clear reduction of bearing capacity towards the pavement edge at both test sections. Compared to the value in the inner wheel path, the average reduction of bearing capacity 40 cm from the pavement edge is 30 % for Section 1 and 42 % for Section 2.

As expected, the bearing capacity is somewhat higher at Section 1 with crushed rock subbase layer than at Section 2 with gravel subbase layer. The difference is most evident for measurements with high force close to the pavement edge.

In all positions, with an exception for the point 40 cm from the pavement edge at Section 2, the calculated bearing capacity is higher for 2000 than for 1999. One

reason for this might be some secondary compaction from the traffic during the first months of service, another that the 2000 measurements were carried out with a higher force, giving a higher stress level and thus a stiffer behaviour of the structure.

The reduction of bearing capacity towards the pavement edge at the test field is comparable to the earlier measurements reported from Fv 462 in *Chapter 3.5*.

5.3.2 Vertical stress under FWD loading

An example of measured vertical stress at the bottom of the base layer during one single FWD deflection test is shown in *Figure 5-16*. The applied force for the first drop was in this case 68.0 kN.

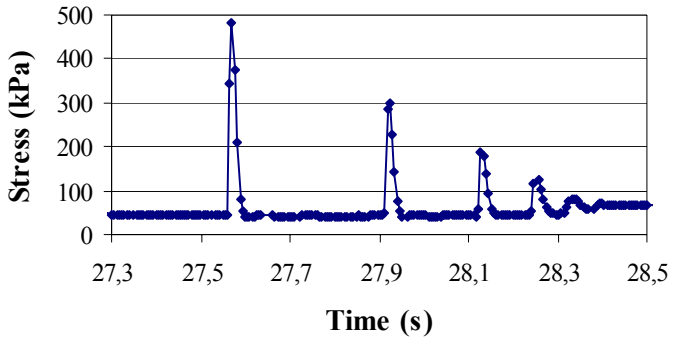

Figure 5-16: Logged vertical stress at the bottom of the base layer at VPC 5, 68.0 kN FWD load

The first peak appears when the falling weight hits the rubber buffers of the apparatus, and the following peaks are due to the fact that the weight bumps up and down on the buffers until it finally settles down. As can be seen from the figure, the sampling speed was not high enough to fully cover the stress peaks. Only a few points form the curve for each drop, and consequently the reading of the peak value became inaccurate. That is, the real peak value might lie between two points, and might therefore be somewhat higher.

Measured maximum (i.e. first drop) peak values of vertical stress are shown in *Figure 5-17*. Trend lines (2nd order polynomials) are added. Like the measurements under the

moving wheel, the FWD measurements showed that the vertical stress at the bottom of the base layer increases towards the pavement edge. At the bottom of the subbase layer this effect was not so evident.

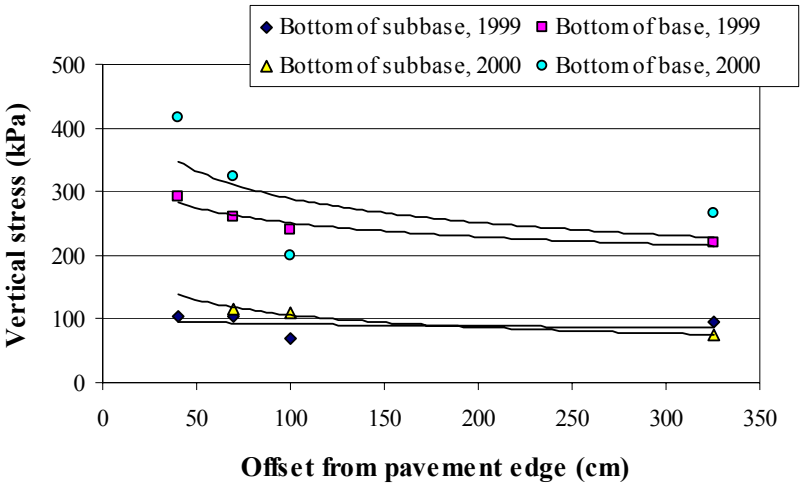

Figure 5-17: Measured vertical stress for FWD loading

It was expected that higher applied load for the 2000 measurements (72.9 kN) than for the 1999 occasion (54.1 kN) should give an clear effect on the measured vertical stress. The difference was evident at the bottom of the base layer, but not below the subbase layer, possibly due to the stiffening effect of the increased load, resulting in greater load spreading ability in the granular layers.

5.3.3 Horizontal stress under FWD loading

Peak values from measurements of horizontal stress in the transversal direction at the bottom of the base layer are shown in *Figure 5-18*.

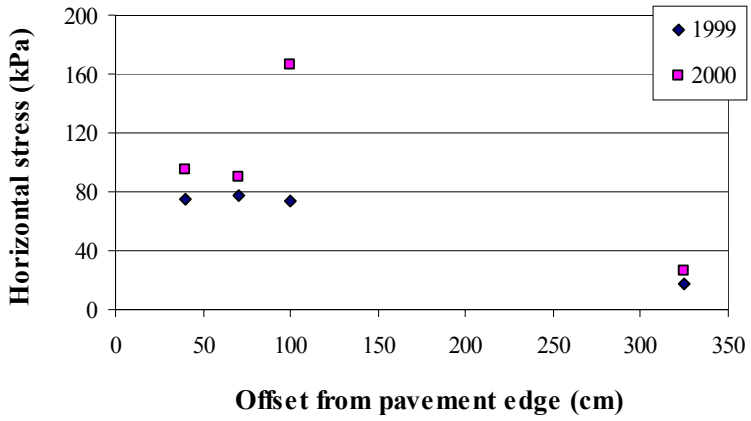

Figure 5-18 Measured horizontal stress for FWD loading

As explained for measurement of vertical stress, the high frequency of the FWD load causes uncertainty in the interpretation of the stress curves. The real peak values may be higher than shown in *Figure 5-18*.

There is no good explanation of why horizontal stress in the inner wheel path should be lower than values closer to the pavement edge. The opposite result is expected. Supplementary measurements should be carried out before any conclusions can be drawn.

5.3.4 Vertical and horizontal strain under FWD loading

Figure 5-19 shows compression of the subbase during one release of the falling weight. In this case (VDT 1, 1999-09-28) it can be read from the figure that approximately 2/5 of the total deformation is permanent, and the remaining 3/5 is elastic.

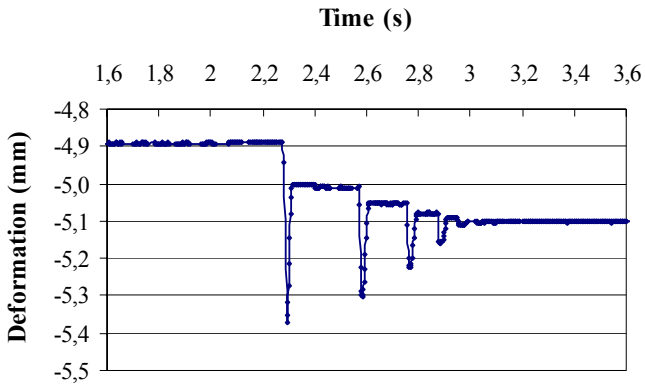

Figure 5-19: Logged vertical deformation in the subbase (VDT 1, 52.9 kN FWD load)

The measurements of vertical and horizontal deformation under FWD loading showed a great deal of scatter, and consequently there are no clear conclusions to be drawn. Still, from interpretation of the deformation curves it was clear that both vertical and horizontal strain tend to be higher near the pavement edge than under the inner wheel path, and that the plastic part of the total strain increases towards the pavement edge.

5.4 Plate loading

The plate loading test is usually carried out for compaction control of granular pavement layers during construction. At Sandmoen test field, the purpose of the plate loading tests was to measure structural response to static loading at different positions at the pavement surface. The tests were carried out in July 2000.

5.4.1 Description of the plate loading equipment

The plate loading equipment consists of a circular steel plate of diameter 30 cm and thickness 12 mm placed on the pavement surface. Vertical load is added to the plate using a hydraulic jack pressing against the rear of a loaded truck. The pressure is added in two subsequent loading sequences with the following nominal steps (kPa): 0–50–180–300–420–600-0-50-180-300-420-600-0. For every load step and after unloading, the surface deflection is measured with a Benkelman beam. An E1 value is computed from the first loading cycle and an E2 value from the second loading cycle. The E-modulus formula is given in *Chapter 3.5, Equation 3.4*.

A typical example of a load–deflection curve from the plate loading test is shown in *Figure 5-20*.

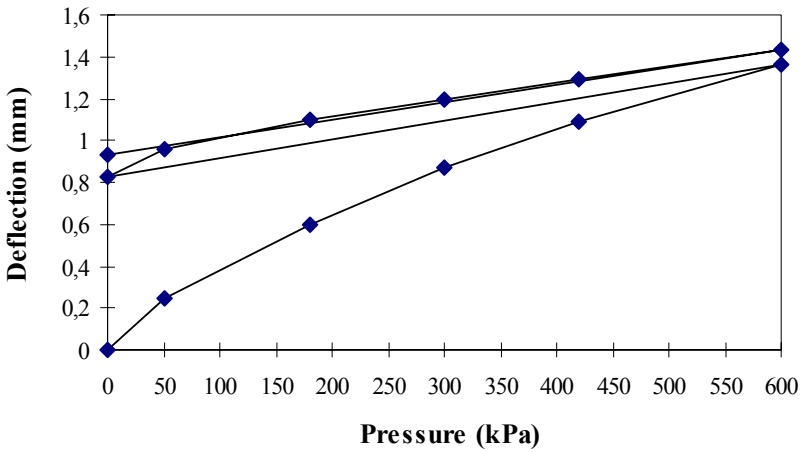

Figure 5-20: Typical load-deflection curve from the plate loading test

5.4.2 Calibration of the hydraulic jack

Comparison between the measured load responses from controlled wheel loads and plate loading gave some unexpected results that were difficult to explain. Seeking the cause of this, it was decided to do a recalibration of the hydraulic jack. This calibration was performed in April 2002 and revealed considerable deviation from the nominal load steps. The real load steps steps were (kPa): 0-39-124-206-284-410-0-39-124-206-284-410-0. In the following interpretation of the plate loading data, it is assumed that the deviation has been unchanged since the measurements were carried out at the test field.

5.4.3 Results from surface deflection measurements

Plate loading tests were carried out at both test sections 1 and 2 at different offsets from the pavement edge. The results presented in the figures below represent the average values from measurements at two different cross sections at each test section.

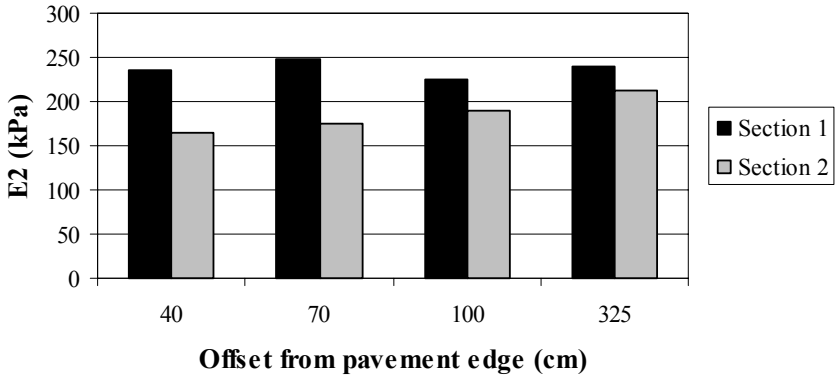

Figure 5-21: E2-values from plate loading tests

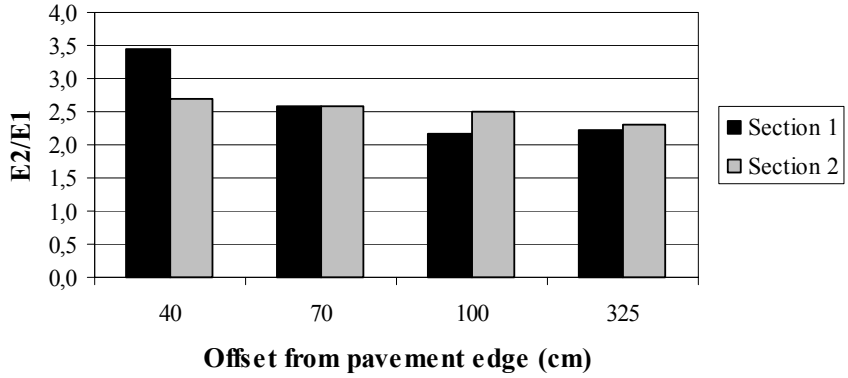

Figure 5-22: E2/E1-values from plate loading tests

For Section 1, the E2-value was not clearly influenced by the distance to the pavement edge, but an increase of E2/E1 towards the edge indicates that granular materials in this part of the structure were not so well compacted. For Section 2, the decrease of the E2-values towards the pavement edge was clear. An increase of E2/E1 towards the edge can be seen, although not so evident as for Section 1.

5.4.4 Vertical stress under plate loading

The procedure followed for the plate loading tests at Section 2 included testing with the plate first located directly over the actual sensor, and thereafter 30 cm further from the edge. *Figure 5-23* and *Figure 5-24* show measured vertical stresses at the bottom of the base and subbase layers for the maximum applied load at the surface, that is a plate contact pressure of 410 kPa (2^{nd} loading cycle). Readings from loading both directly over and 30 cm beside the sensors are presented. For comparison, the same scale is used for the vertical axis in both figures.

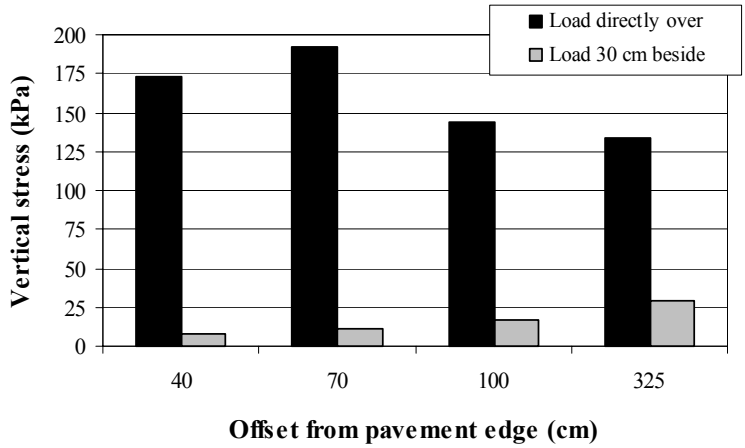

Figure 5-23: Vertical stress at the bottom of the base layer, 29.0 kN plate load

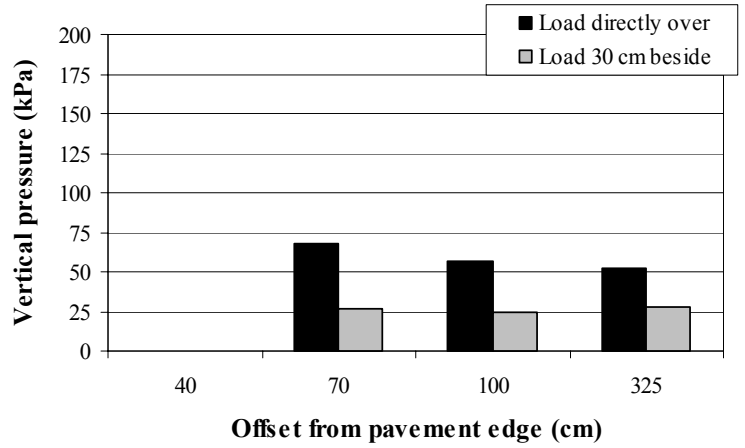

Figure 5-24: Vertical stress at the bottom of the subbase layer, 29.0 kN plate load

There is a clear tendency of increasing vertical stress towards the pavement edge when the load is placed directly over the sensor. It is, though, unexpected that the greatest value of vertical stress at the bottom of the base layer occurred 70 cm from the pavement edge.

Measured vertical stress at the bottom of the base layer when the load was placed 30 cm beside the sensor is very low, and decreases towards the pavement edge. As for truck loading, this is supposed to be caused by decreasing confining pressure and hence decreasing load spreading properties of the base material towards the pavement edge.

5.4.5 Horizontal stress under plate loading

Measured horizontal stress at the bottom of the base layer for maximum plate load, is shown in *Figure 5-25*. As for measurements under truck load and FWD, the horizontal stress was lowest in the inner wheel path, while the opposite result was expected.

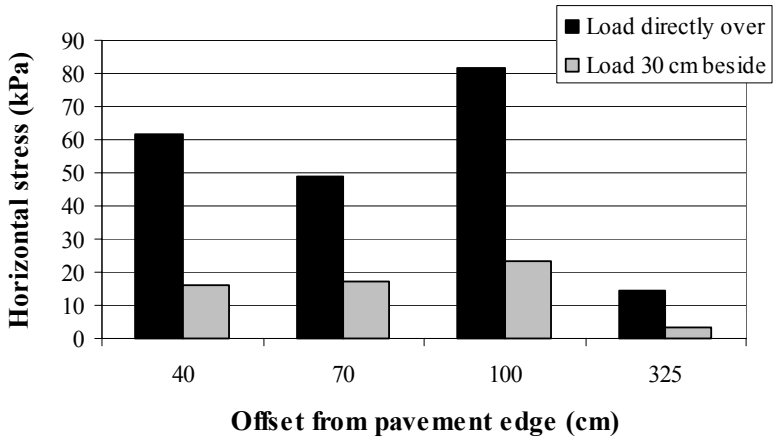

Figure 5-25: Horizontal stress at the bottom of the base layer, 29.0 kN plate load

Measured horizontal stress for each load step during one specific plate loading test being carried out 100 cm from the pavement edge is shown in *Figure 5-26*.

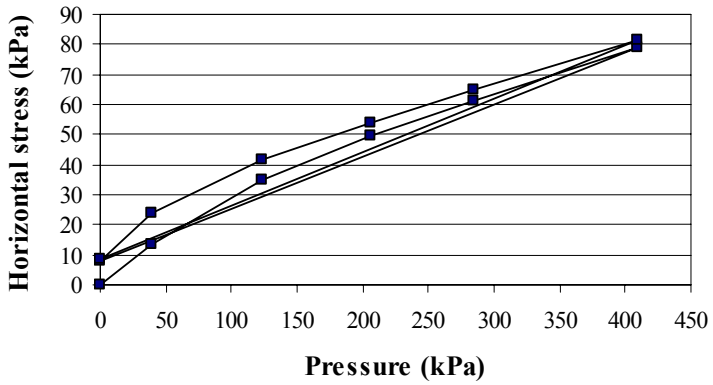

Figure 5-26: Horizontal stress at the bottom of the base layer for each load step

5.4.6 Vertical strain under plate loading

Figure 5-27 shows vertical strain in the base layer at VDT 4, 325 cm from the pavement edge, first with the plate placed directly over the sensor and secondly 30 cm beside it.

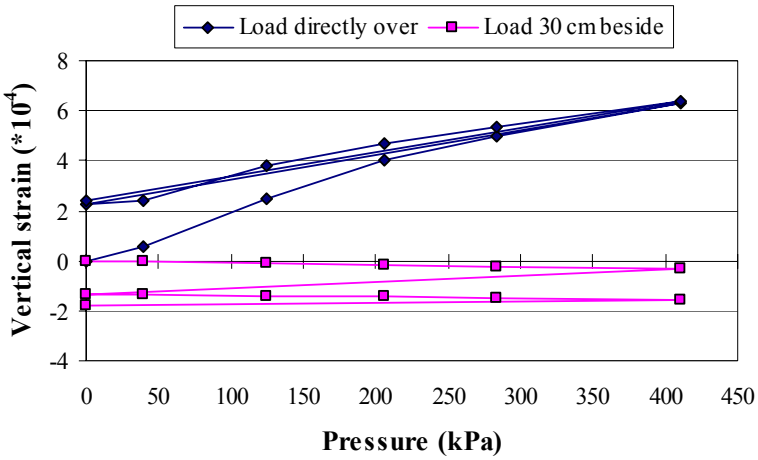

Figure 5-27: Vertical strain in the base layer at VDT 4

For loading directly over the sensor, a compression of the base layer was recorded. The total strain for maximum load consists of about 2/3 elastic and 1/3 plastic strain, most of the latter occurring during the first loading cycle. When the plate subsequently was placed 30 cm beside, most of the plastic compression strain recovered. This is an interesting observation, and especially that a considerable part of the plastic strain was recovered during unloading after the first cycle of loading.

Figure 5-28 shows vertical strain in the subbase layer at VDT 2, 325 from the pavement edge. The same load response pattern is seen here, but a less part of the plastic compression strain recovered for loading 30 cm beside the sensor.

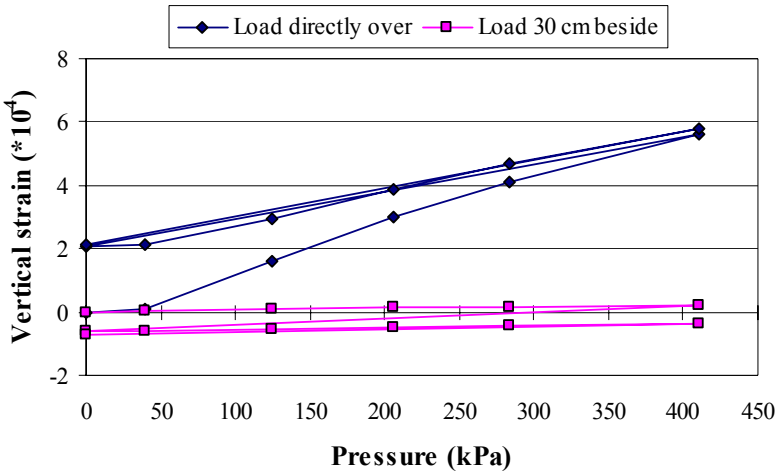

Figure 5-28: Vertical strain in the subbase layer at VDT 2

5.4.7 Horizontal strain under plate loading

Figure 5-29 and *Figure 5-30* show horizontal strain in the base layer at HDT 1 and HDT 2 for loading close to the pavement edge and in the inner wheel path, respectively. The same loading procedure as described earlier was used.

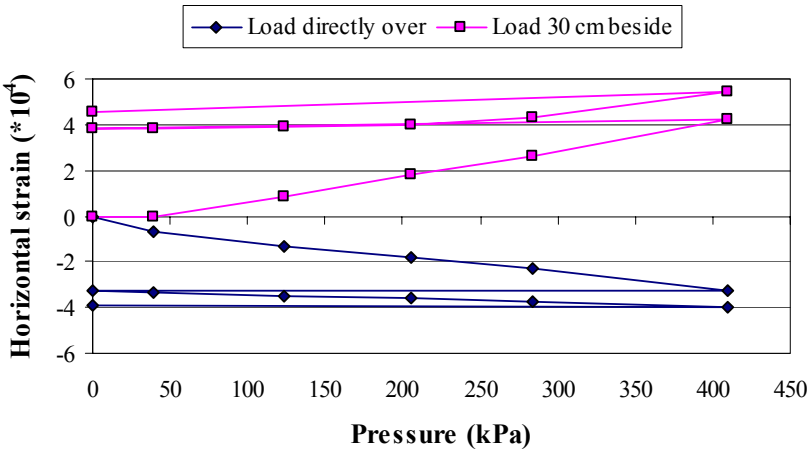

Figure 5-29: Horizontal strain in the base layer for loading at HDT 1

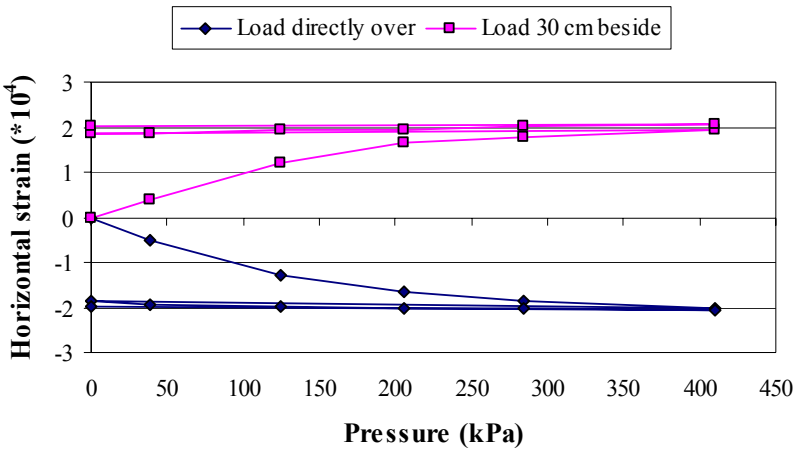

Figure 5-30: Horizontal strain in the base layer for loading at HDT 2

For loading directly over the sensors, horizontal tensile strain in the base layer was recorded. The elastic strain was close to zero. For two loading/unloading cycles, measured horizontal strain near the pavement edge was about twice as big as in the inner wheel path. When loading was carried out 30 cm beside the sensor, almost all plastic tensile strain recovered.

5.5 Comparison of measured responses from static plate and controlled wheel loading

The level of stresses and strains in the lower part of the base layer and further down in the pavement, is dominated by the total applied load. To compare measured load responses from controlled truck and plate loading, it is therefore most relevant to compare load cases of approximately equal total load.

Plate loading at 206 kPa gives a total load of 14.6 kN, which is close to wheel load A of 15.2 kN. Plate loading at 410 kPa gives a total load of 29.0 kN, which is close to wheel load B of 29.4 kN. In the following figures, readings from these combinations of static and moving load are compared.

Figure 5-31 shows measured vertical stress at the bottom of the base layer for the current load cases. Close to the pavement edge, there are considerable differences in measured stress under static plate loading and moving wheel load of comparable magnitude. The discrepancy is largest for the heaviest loads. Towards the inner wheel path, the differences are decreasing. Measured stresses under the wheel load are consistently higher than measured stresses for the corresponding static loads.

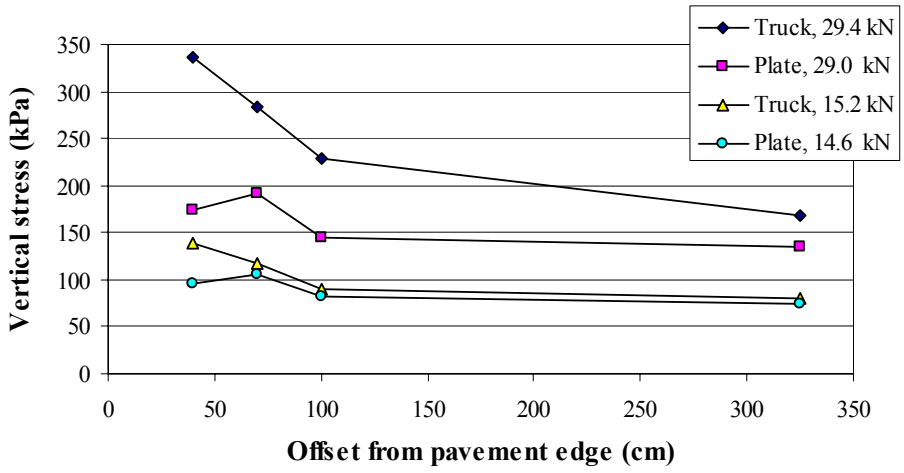

Figure 5-31: Measured vertical stress at the bottom of the base layer for comparable load cases

Figure 5-32 shows measured vertical stress at the bottom of the subbase layer for the same combinations of static and moving wheel load. The conformity is better here than below the base layer. Most of the measurements 40 cm from the pavement edge are missing due to the malfunction of VPC 1.

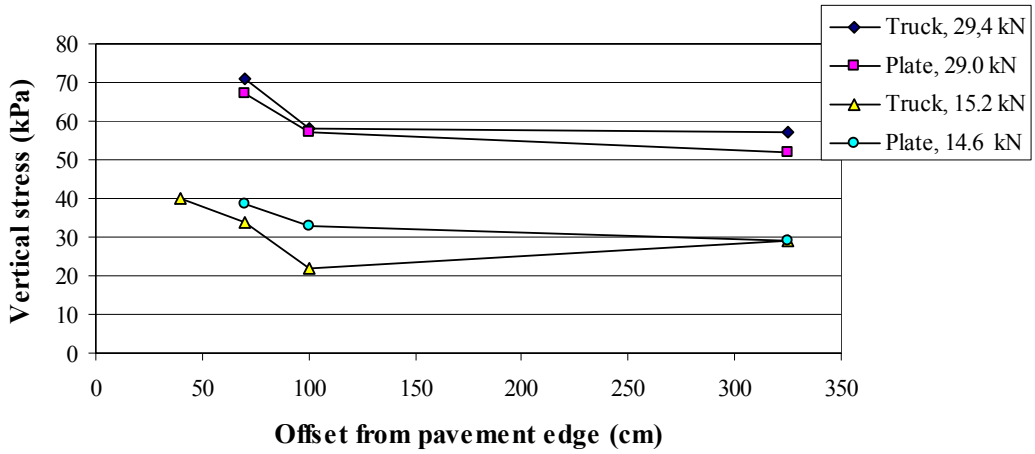

Figure 5-32: Measured vertical stress at the bottom of the subbase layer for comparable load cases

In *Figure 5-33* strains 325 cm from the pavement edge are presented. For plate loading, values from the second loading cycle are used. In the base layer, considerable differences in vertical strains are recorded. Here, the strains under the rolling wheel loads are 1.8 and 2.2 times as great as for the corresponding static loads. Better correlation is found for vertical strains in the subbase layer and for horizontal strains in the base layer.

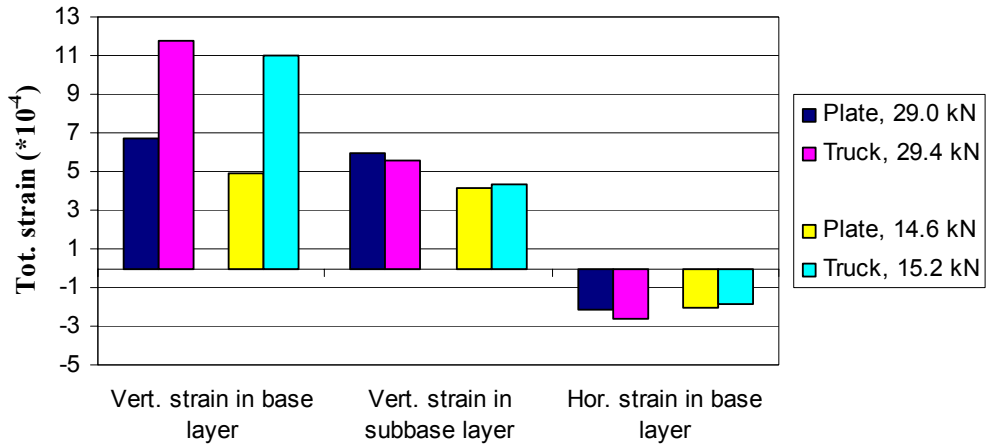

Figure 5-33: Strain 325 cm from the pavement edge for comparable load cases

The compared load cases were approximately equal as far as total load is concerned, but the contact pressure was quite different; that is 690 kPa for both wheel load A and B, and 206 kPa and 410 kPa for the current plate loading steps. Due to the small thickness of the surface layer, it is probable that these differences have influenced the stress and strain level in the base layer. This might explain most of the observed discrepancies.

Another uncertain factor is the real magnitude of the applied plate load. The deviation from the nominal load steps at the date of testing at Sandmoen in July 2000 might have been somewhat different than it was when the equipment was recalibrated in April 2002.

Variations in water content in the granular layers may also have influenced the test results as the compared measurements were carried out at different dates (plate loading in July 2000, and truck loading in November 1999 and May 2000). Even though the drainage system of the pavement was well functioning, some variations in water content may have occurred, especially in the zone close to the unpaved side slope.

There also were some variations in pavement temperature between the days of testing, but because the thickness of the asphalt surfacing was only 4 cm, this is assumed to have only a minor influence on measured stresses and strains.

6 COMPARISON OF CALCULATED AND MEASURED LOAD RESPONSES

6.1 Introduction

To be able to compare calculated and measured load responses, both multilayered elastic (ME) and finite element (FE) analyses are conducted. BISAR, described in *Chapter 2.5*, has been used for ME calculations, while the FE calculations have been performed using the finite element program ABAQUS.

In all calculations, the load is modelled as a static uniform contact pressure over a circular area. This is expected to be a good representation of the plate loading, but represents a simplification of a moving wheel and the FWD. Consequently, the correlation between measured and calculated stresses, strains and deformations is assumed to be better for the plate loading than for the other devices, and emphasis is put on the plate loading results.

All materials are modelled to be linear elastic, both in the ME and FE calculations. As described in *Chapter 4*, samples from all layers at Sandmoen test field are tested in the laboratory. Granular materials are tested in the triaxial apparatus, while parameters for the asphalt surfacing are found from indirect tensile tests.

The stiffness of crushed rock, natural gravel and sand is stress dependent. From the measured values of stress at the bottom of the base and subbase layers, the levels of mean stress within the different layers are estimated. This is the basis for the determination of the E-moduli for the granular materials that are used in the calculations.

The stiffness of the asphalt surfacing is determined from the indirect tensile test results, see *Chapter 4*. Because the temperature during the laboratory testing was

25 ^{o}C, while the pavement temperature during field testing varied from 10 to 15 ^{o}C, the E-modulus in *Table 6.1* is greater than the values from the indirect tensile testing.

The chosen material parameters for the theoretical analyses are shown in *Table 6.1*. The denotation of the different wheel loads corresponds to the denotation used in *Chapter 5*.

Table 6.1: E-moduli (MPa) for theoretical analyses of load responses

Type of loading	Load (kN)	Asphalt surfacing	Crushed rock 0-32 mm	Natural gravel	Sand
Max. plate load	29.0	3000	500	250	75
Wheel load A	15.2	3000	400	200	75
Wheel load B	29.4	3000	500	250	75
Wheel load C	30.6	3000	500	250	75
Wheel load D	42.9	3000	600	300	75

6.2 Finite element analysis

6.2.1 Geometric models of the pavement structure

As described in *Chapter 4.5*, the sensors at Sandmoen test field are placed along four longitudinal lines as illustrated in *Figure 6-1*. FE calculations are made for load positions at each of the four lines.

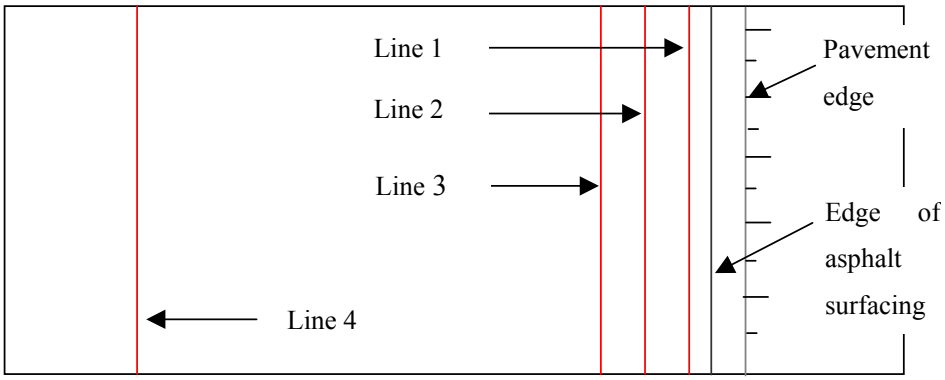

Figure 6-1: Lines where sensors are placed

Three different models are set up; of these are two 3-dimensional while the third is axisymmetric. Sketches of the models are shown in *Figure 6-2*.

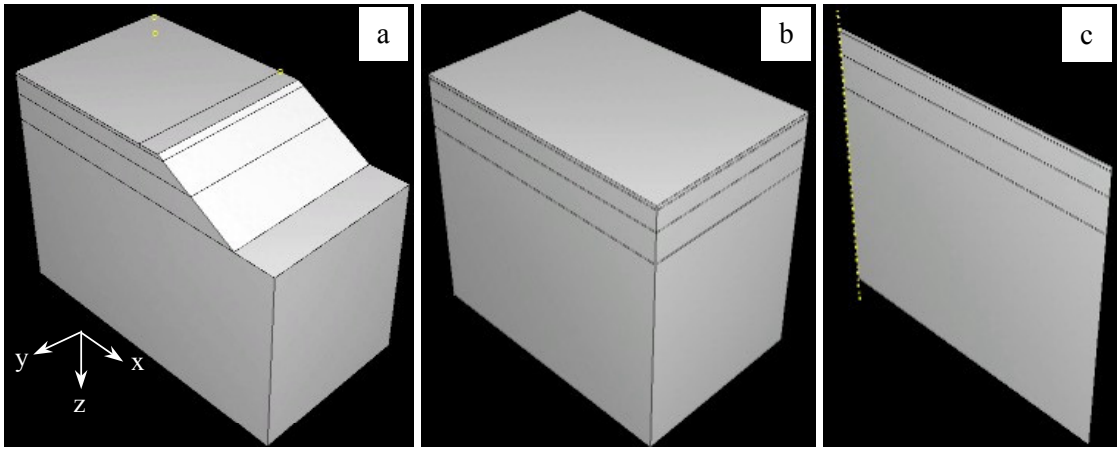

Figure 6-2: Geometric models used for the FE calculations; a: loads at line 1, 2 and 3, b and c: load at line 4

The model shown to the left of *Figure 6-2* is used for calculations when the load is situated at line 1, 2 and 3. It is divided into different partitions according to the layers in the real pavement at Sandmoen. The partitions on top of the model are the surfacing (2000x2000x40 mm) and the shoulder (250x2000x40 mm). The thickness of the base layer is 200 mm, and further down is the subbase of thickness 300 mm and the subgrade partition (3750x2000x2000 mm).

Line 4 is located so far from the pavement edge (325 cm) that the presence of the edge and side slope is supposed not to have any influence on the load induced stresses, strains and deformations. Consequently, a simpler model can be used for calculations when the load is placed in this position, shown in the middle of *Figure 6-2*. The dimension of this model is 3000x2000x2540 mm, and the layer thicknesses are as described earlier.

For a circular load situated at line 4 there is also a possibility to model the pavement as a layered axisymmetric structure. This model is shown to the right of *Figure 6-2*. This model is 3000 mm wide and 2540 mm high, as a "slice" of the second model.

For a load at line 4, calculations with both the 3-D and the axisymmetric model are performed. Comparisons of the results showed only insignificant differences. Therefore, the simpler axisymmetric model is used for this situation.

6.2.2 Symmetry

Symmetry characteristics are utilised to minimize the size of the 3D models. For a load at line 1, 2 and 3, the vertical plane in transversal direction through the load is a symmetry plane, and consequently only half of the pavement structure is modelled, see *Figure 6-3*.

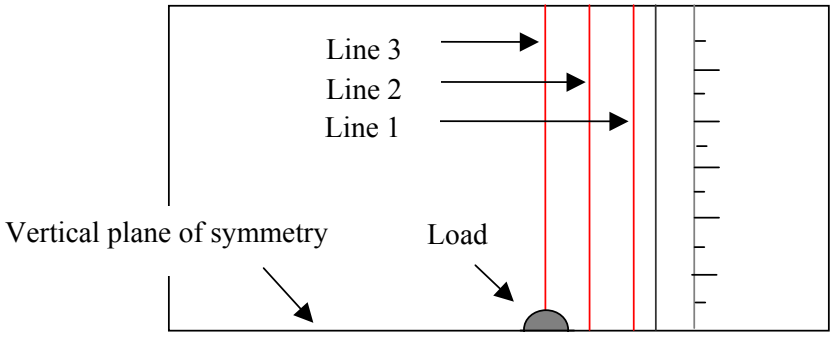

Figure 6-3: Symmetry plane of the 3D model including the pavement edge

The 3D-model for a load at line 4 utilises the fact that the vertical plane in both transversal and longitudinal direction through the load are planes of symmetry, thus this model represents only one quarter of the structure.

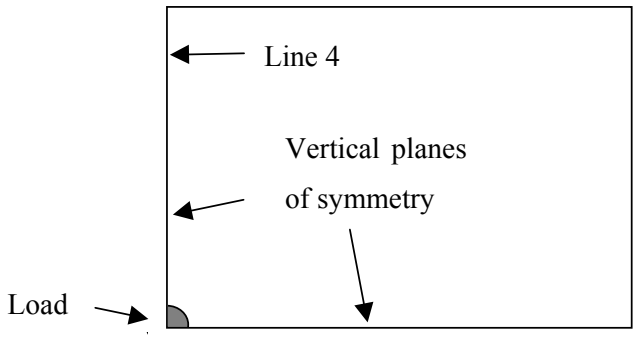

Figure 6-4: Symmetry planes of the 3D model for load at line 4

6.2.3 Load and boundary conditions

The surface loading is represented by a static uniform contact pressure acting normal to the surface over a circular area with a fixed diameter of 300 mm. In the calculations of truck loading, the contact pressure is adjusted to equal the total wheel load, not the tire pressure. For example, for wheel load C of 42.9 kN, the contact pressure in the FE-calculations is set to be $42.9/(\pi \cdot 0.15^2) = 606.9$ kPa.

At the bottom, the models are restricted from movement in all directions. All vertical surfaces are restricted from movements normal to the plane, but free to move in the other directions. The boundary conditions for the axisymmetric model are shown in *Figure 6-5*.

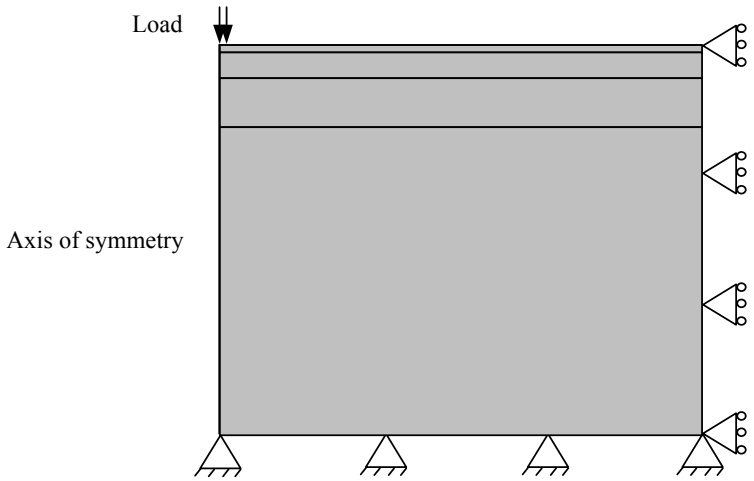

Figure 6-5: Boundary conditions for the axisymmetric model

6.2.4 Meshing and element types

A well adapted element mesh is of essential importance for the reliability of every FE-calculation. The model should not have too many elements because this will cause a very long calculation time, especially in 3-D analyses. On the other hand, the mesh must not be too coarse, since this will reduce the accuracy of the calculated stresses, strains and deformations. This means that the element mesh needs to be refined in parts of the structure where exact data are required, in this case in the area close to the load, and can be made coarser in other parts.

To be able to control the element meshing, especially near the load area, the 3-D models are sub-divided into several partitions. For the model including the pavement edge, the basic principle has been to define a semicircle of radius 150 mm around the load, and outside this another semicircle of radius 300 mm. The chosen partitions for the load placed at line 3 is shown in *Figure 6-6*.

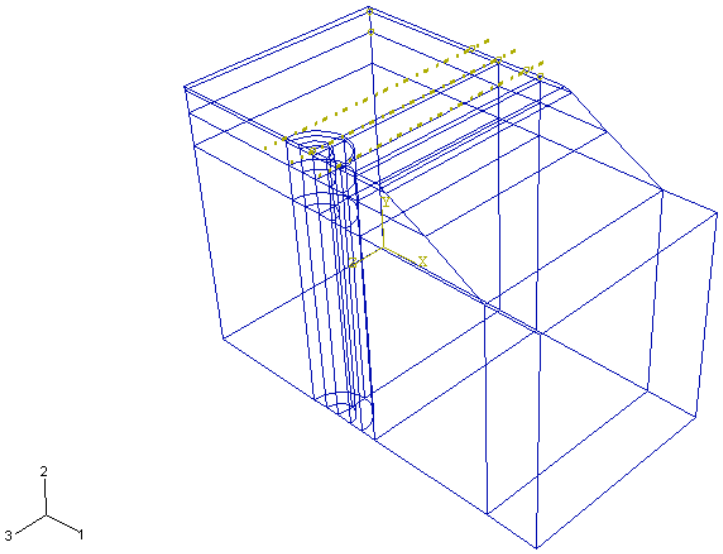

Figure 6-6: Model with chosen partitions for the load placed at line 3

In all 3D-models 20-noded continuum elements with reduced integration are used. For the axisymmetric model, 8-noded axisymmetric elements with reduced integration are used. The generated element mesh for each model is shown in *Figure 6-7* to *Figure 6-11*.

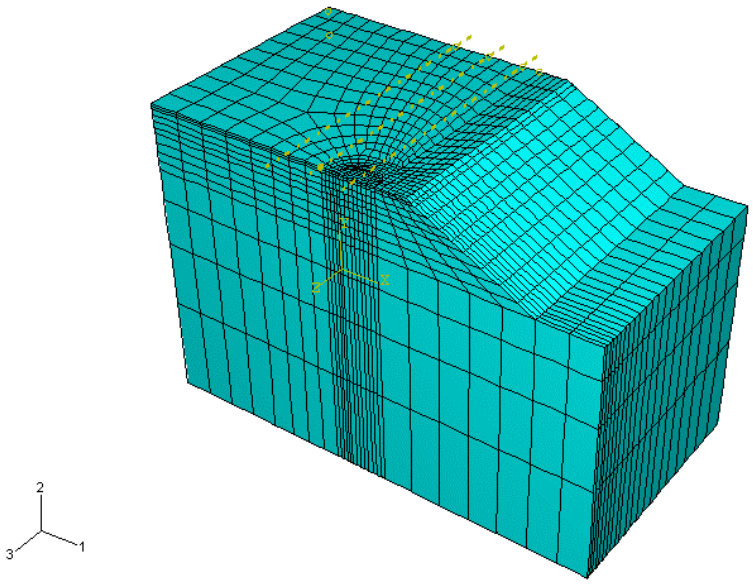

Figure 6-7: Mesh for load at line 1 (6020 elements)

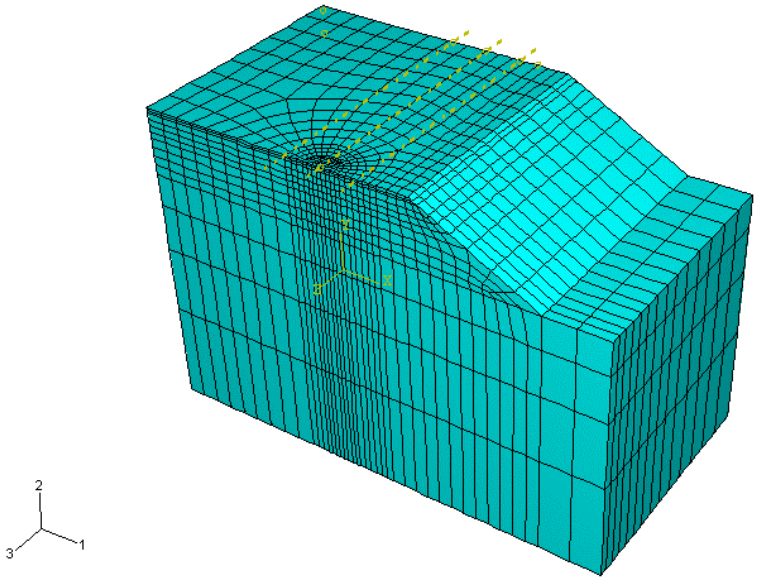

Figure 6-8: Mesh for load at line 2 (5432 elements)

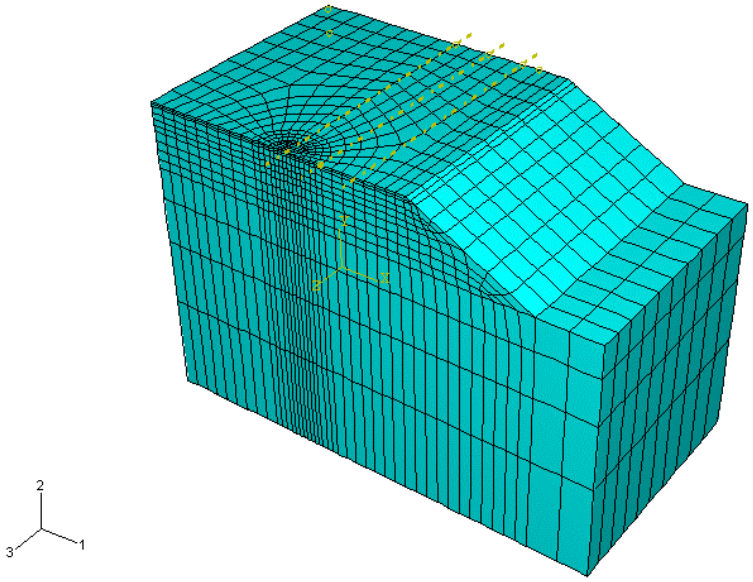

Figure 6-9: Mesh for load at line 3 (5250 elements)

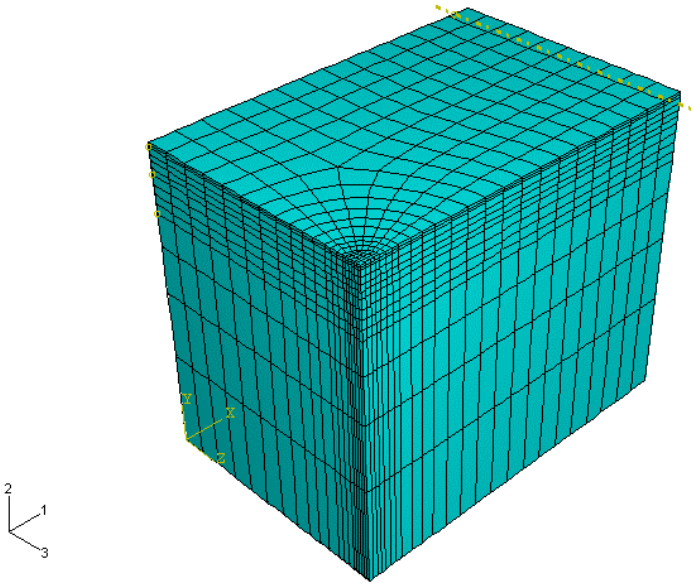

Figure 6-10: Mesh for load at line 4 (3080 elements)

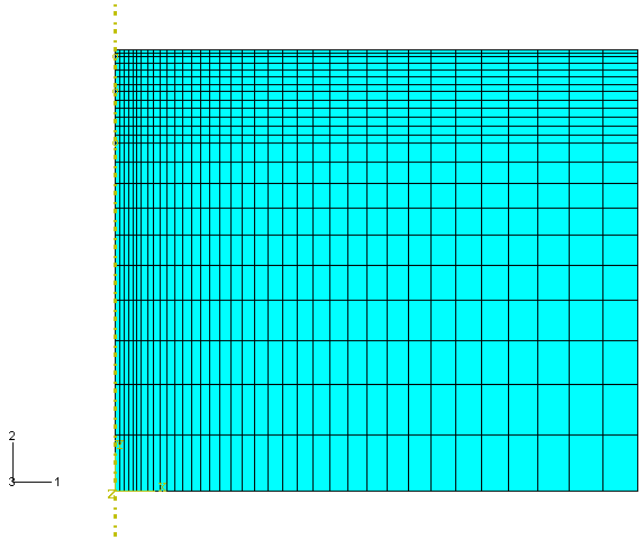

Figure 6-11: Mesh for load at line 4, axisymmetric model (828 elements)

6.2.5 Contour plots

Results from the calculations might be displayed in contour plots. A typical example is shown in *Figure 6-12* for loading at line 1. These kind of coloured plots may look quite impressive, and give a good picture of both deformed shape and distribution of the chosen variable. However, for comparison with measured values, specific information about calculated values at the same locations as the embedded sensors, is needed. To get this information, vertical paths through the model are made, and at certain points along these paths, values of stresses, strains and displacements are calculated.

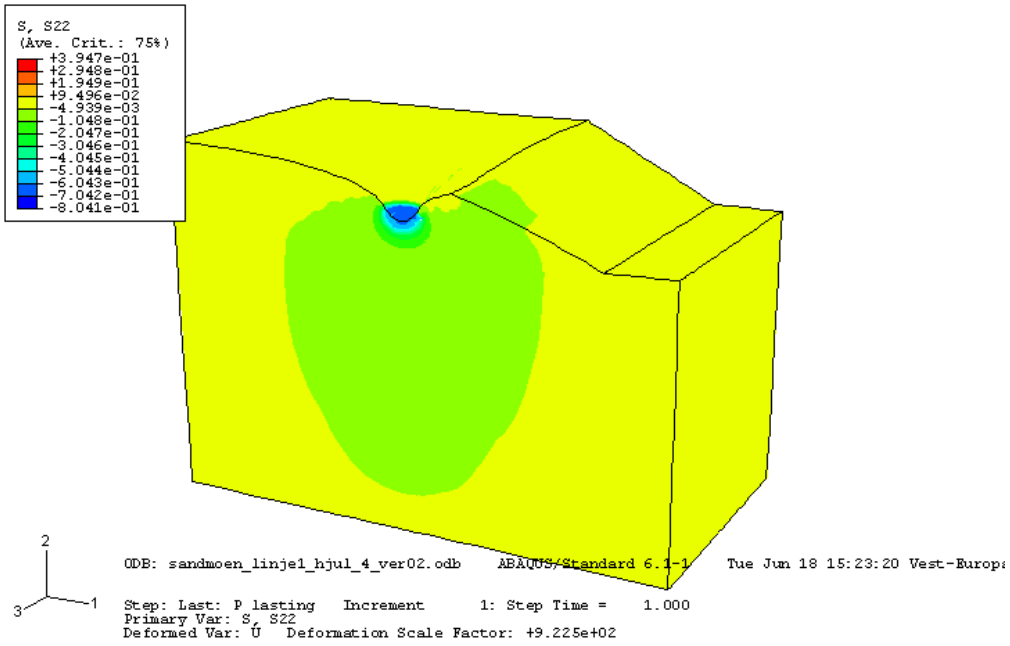

Figure 6-12: Contour plot of vertical stresses for loading at line 1, 42.9 kN load

6.3 Calculated and measured load responses

6.3.1 Surface deflection under plate loading

The surface deflection during the plate loading test is measured by the use of a Benkelman beam. The method is simple and gives very reliable data. The deflection readings give information on both total and elastic deflection since the remaining deflection after unloading of the plate is also noted. *Figure 6-13* shows measured deflections together with results from ME and FE calculations.

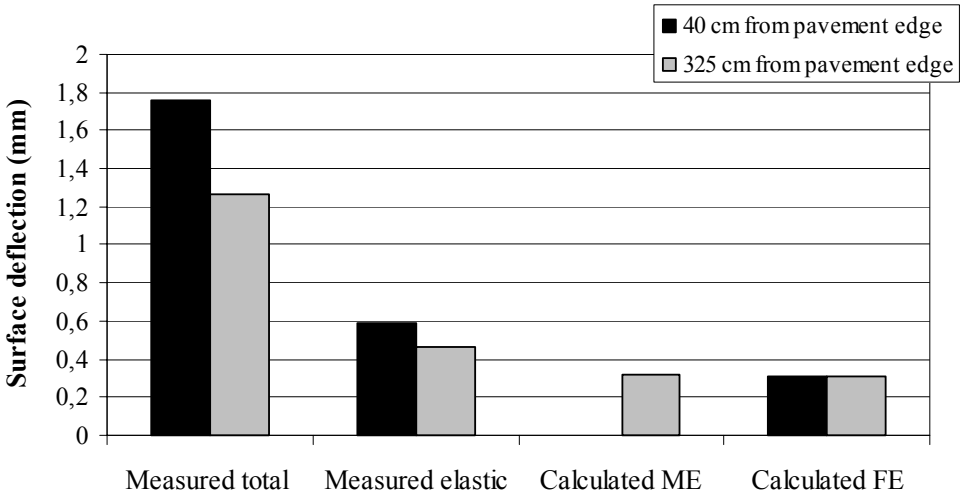

Figure 6-13: Measured and calculated surface deflection from maximum plate load

Measured total deflection is much greater than the calculated deflection. The differences are smaller between the elastic component of the measured deflection and the calculated values. The least deviation is found between calculated and measured elastic deflection 325 cm from the pavement edge.

The FE calculations with linear elastic materials in all layers give the same value of deflection close to the pavement edge as in the inner wheel path.

6.3.2 Vertical stress

Figure 6-14 and *Figure 6-15* show measured and calculated vertical stress at the bottom of the base layer directly under the load for maximum plate load and wheel load D, respectively. There is best accordance between measured and calculated values when the load is situated 325 cm from the pavement edge. In this position, the difference between calculated (FE) and measured vertical stress for maximum plate load is 14 %, while the corresponding difference for wheel load D is 15 %.

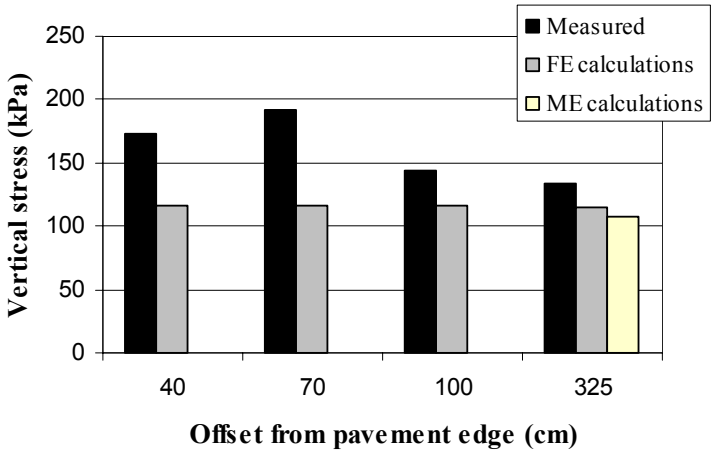

Figure 6-14: Measured and calculated vertical stress at the bottom of the base layer for maximum plate load (29.0 kN)

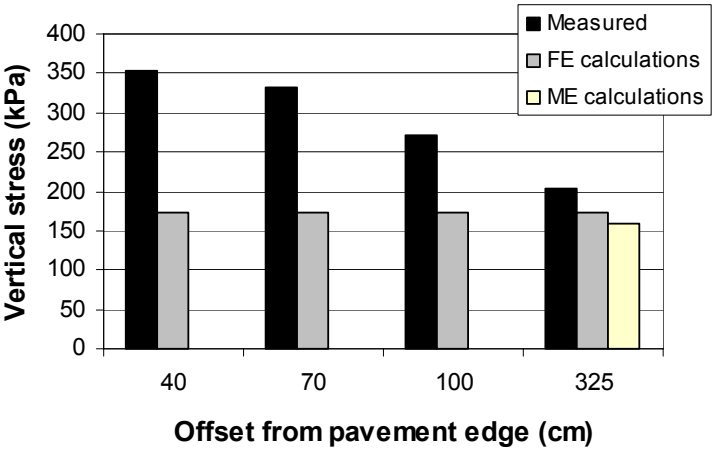

Figure 6-15: Measured and calculated vertical stress at the bottom of the base layer for wheel load D (42.9 kN)

In *Figure 6-16* and *Figure 6-17* are shown vertical stresses at the bottom of the subbase layer for the same loading situations. The differences between measured and calculated values are substantially larger here than at the bottom of the base layer. For loads 325 cm from the pavement edge, the calculated (FE) vertical stress is only 40 % and 35 % of the measured values for maximum plate load and wheel load D, respectively.

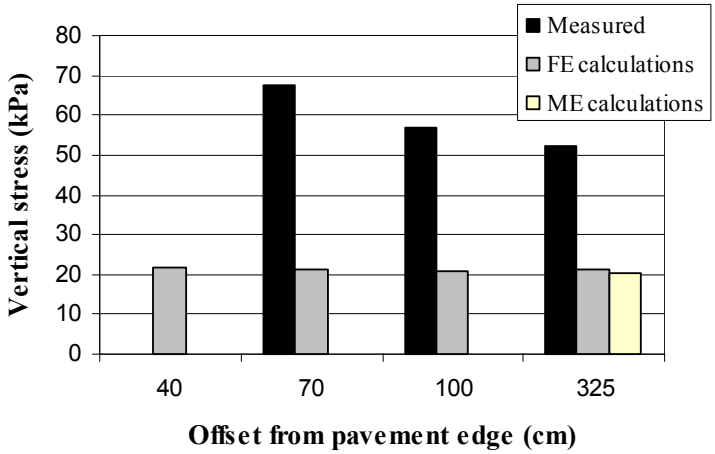

Figure 6-16: Measured and calculated vertical stress at the bottom of the subbase layer for maximum plate loading (29.0 kN)

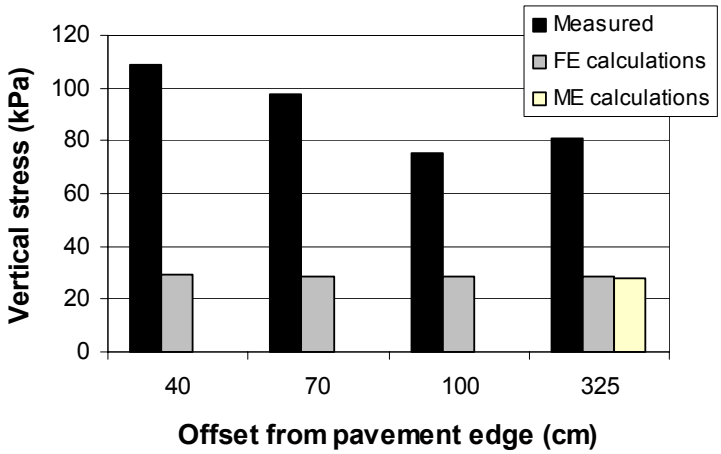

Figure 6-17: Measured and calculated vertical stress at the bottom of the subbase layer for wheel load D (42.9 kN)

Both at the bottom of the base and the subbase layers, the measured stresses are consequently greater than the calculated values. The linear elastic FE calculations show almost no increase in vertical stress towards the pavement edge neither at the bottom of the base nor at the bottom of the subbase layer. This causes greater discrepancies between measured and calculated vertical stresses near the pavement edge than in the inner wheel path.

In *Figure 6-18,* calculated (ME) vertical stresses from the surface and vertically down through the pavement structure are shown together with measured values at the bottom of the base and subbase layers for different loads situated/passing 325 cm from the pavement edge. For the structural analysis, the moduli are shown in *Table 6.1*. The figure shows that with the chosen set of input variables, the least deviations between measured and calculated vertical stress are found at the bottom of the base layer for all analysed load cases.

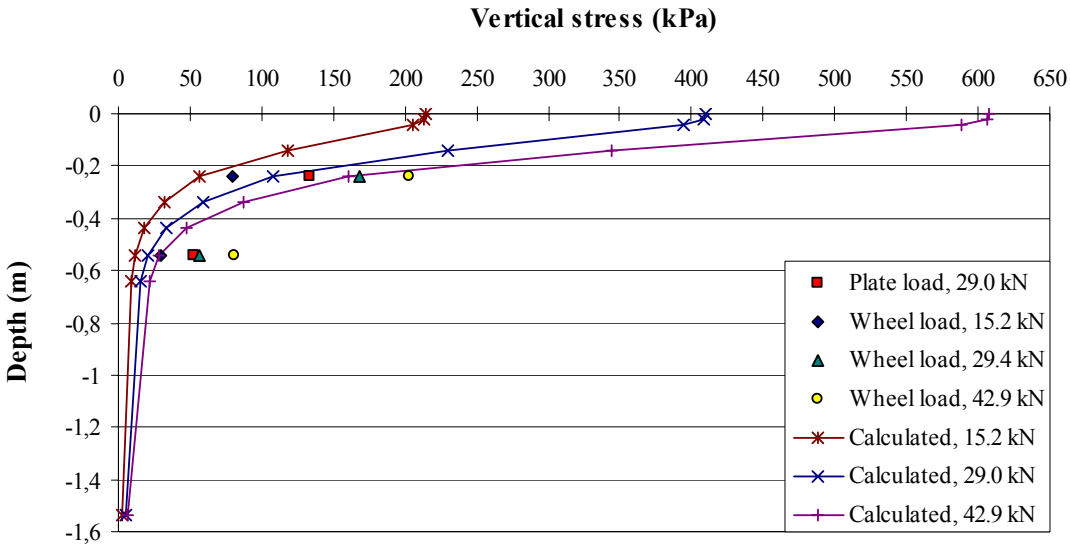

Figure 6-18: Measured and calculated (ME) vertical stresses for loads situated/ passing 325 cm from the pavement edge

6.3.3 Horizontal stress

Both the FE and ME calculations give horizontal tensile stresses in the lower part of the base and subbase layers, as shown in *Figure 6-19*. This is obviously not realistic, as unbound granular materials are unable to withstand tensile stresses. The measurements performed at the test field verify this, by the fact that horizontal compressive stresses are measured at the bottom of the base layer, see *Chapter 5*. Consequently, further comparisons between calculated and measured values of horizontal stress make no sense.

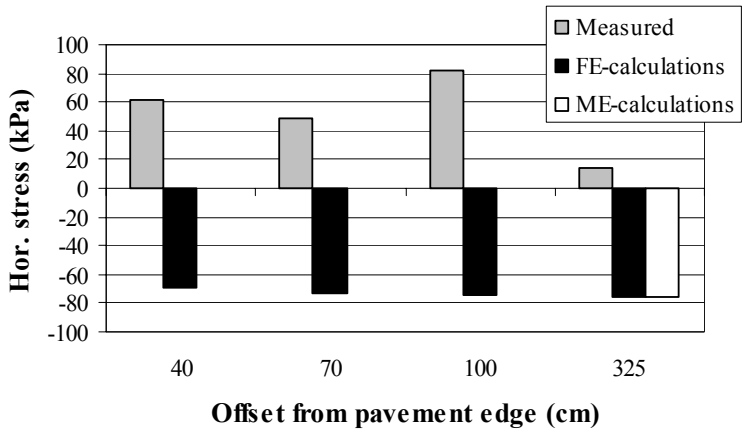

Figure 6-19: Measured and calculated horizontal stress at the bottom of the base layer for maximum plate load, 29.0 kN

6.3.4 Vertical strain

Figure 6-20 shows calculated vertical strain compared to values of total and elastic vertical strain derived from deformation measurements under the maximum plate load when situated 325 cm from the pavement edge.

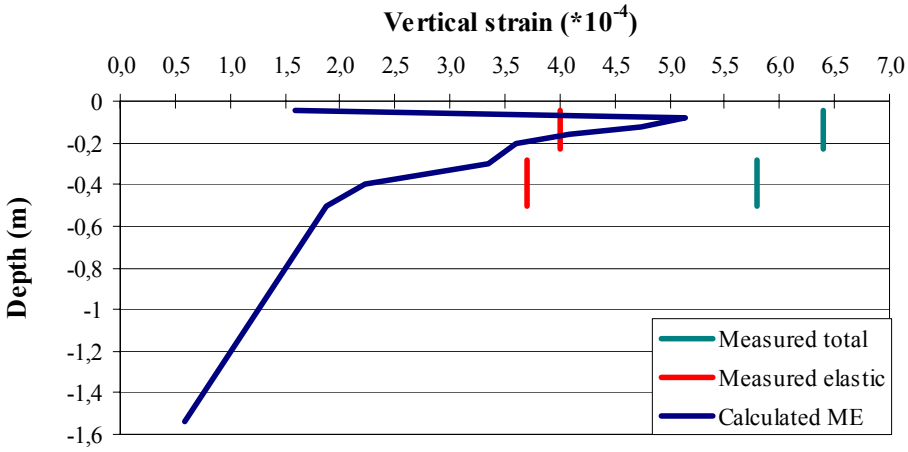

Figure 6-20: Measured and calculated (ME) vertical strain 325 cm from the pavement edge for maximum plate load, 29.0 kN

As stated in *Chapter 5.4*, the total vertical strain during plate loading is composed of approximately 2/3 elastic and 1/3 plastic strain. *Figure 6-20* shows that the calculated level of vertical strain is considerably lower than the total strains derived from the deformation measurements. The discrepancy is largest in the subbase layer.

6.3.5 Horizontal strain

Horizontal deformations are measured only in the base layer. As described in *Chapter 5*, the strains derived from these measurements were dominated by the plastic strain component, especially for plate loading. In *Figure 6-21,* calculated (ME) horizontal strain in the base layer is shown together with the measured values for maximum plate load situated 40 and 325 cm from the pavement edge. The calculated strain level is comparable to the measured total horizontal strain in the inner wheel path. Strains from deformation measurements close to the pavement edge are much higher.

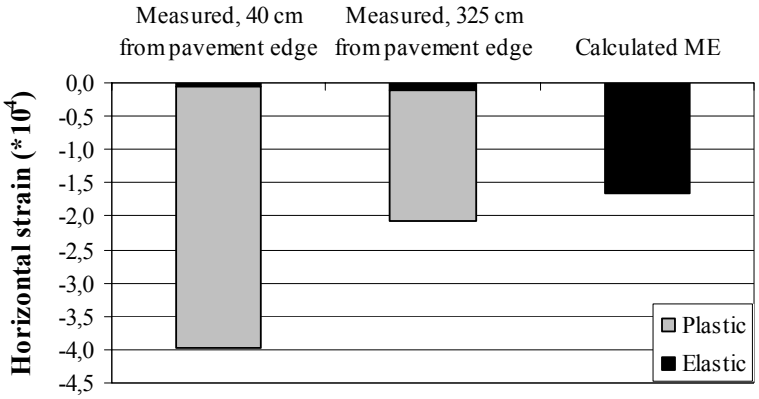

Figure 6-21: Measured and calculated horizontal strain in the base layer under maximum plate load, 29.0 kN

7 CONCLUSIONS AND RECOMMENDATIONS FOR FURTHER RESEARCH

7.1 Conclusions

The main objective of the present thesis work has been to improve the knowledge concerning pavement edge effects. This is done by studying how load responses develop towards the pavement edge, primarily by performing measurements at a full scale, instrumented test field.

Introductory field measurements

Performed FWD measurements at different road cross sections in Sør-Trøndelag county show a considerable decrease in bearing capacity towards the pavement edge. The edge effect is noticeable for loads situated less than about 1.0 m from the pavement edge, and the bearing capacity 50 cm from the pavement edge is reduced by approximately 40 % compared to the value at the centre line.

A limited field test including FWD and plate loading was performed to study the structural effect of varying the side slope of an existing road. The findings show that a gradually steepening of the side slope has little influence on the measured bearing capacity near the pavement edge.

Construction of a full scale test field at Sandmoen

A full scale test field with instrumentation for the measurement of stresses and strains has been constructed. Accurate levelling of the granular layers and installation of the sensors were demanding tasks, and required a high degree of accuracy and control. Through this project, valuable experience from the construction and instrumentation work was gained.

Results from Sandmoen test field

Vertical stress has been successfully measured at the bottom of both the base and the subbase layers, 24 cm and 54 cm below the surface, respectively. The results show increasing vertical stress as loads are applied closer to the pavement edge. This effect is evident at the bottom of the base layer for load positions closer than 1.0 m from the pavement edge. Controlled traffic loading 40 cm from the pavement edge gives in average 68 % greater vertical stress at the bottom of the base layer and 28 % greater vertical stress at the bottom of the subbase layer compared to the corresponding measured values in the inner wheel path.

Measured vertical stress at the bottom of the base layer is very low when the load is placed 30 cm beside the sensor, and decreases towards the pavement edge.

As expected, horizontal compressive stresses are recorded at the bottom of the base layer for loads applied on the pavement surface. However, the measurements of horizontal stress show some surprising results, and should be repeated before any conclusions can be drawn.

Measurements of vertical deformations in the base and the subbase layers show that the vertical strains are substantially greater and have relative greater plastic components near the pavement edge than in the inner wheel path. Parts of the plastic strains recover when the load position is changed.

Horizontal deformation measurements show expansion in the base layer directly under the surface load. As for measurements in the vertical direction, much greater strains are found near the pavement edge than in the inner wheel path, and for all combinations of applied load, the plastic strain component is greater than the elastic component. Also horizontal strains recover when the load position is altered.

Comparison of calculated and measured load responses

3D finite element (FE) models for the calculation of responses at different offsets from the pavement edge have been set up. Linear analyses are performed, and the calculated stresses, strains and deformations are compared to the measured values. In

addition, multilayered elastic analyses are performed for comparison with measured load responses in the inner wheel path of the test field.

The FE calculations show only insignificant changes in stresses, strains and deformations as the load is moved closer towards the pavement edge. Consequently, comparisons of measured and calculated load responses in this part of the structure show considerable discrepancies. Better accordance between measured and calculated values is found in the inner wheel path, except for horizontal stresses at the bottom of the base layer where *compression* is measured while *tension* is calculated.

The large differences between measured and calculated load responses revealed in this study demonstrate that linear elastic modelling of the granular layers is inadequate for the calculation of load responses under a load situated close to the pavement edge, even when the edge is modelled in 3D FE analysis.

Norwegian road design practice

One of the interesting findings from the Sandmoen test field was that the plastic strain components in the base and subbase layers are greater for loading close to the pavement edge than in the inner wheel path. Permanent deformation in granular layers is the main cause for most of the occurring pavement edge damages at the Norwegian road network. It is therefore obvious that a traffic load placed near the pavement edge has a much higher deteriorating effect than a load positioned in the inner wheel path where the side support is better.

According to the Norwegian Pavement Design Manual (NPDM) /31/ and the Road and Street Design Manual /30/, the requirement for the pavement and shoulder width is dependent on the traffic volume and the road classification. For two-lane roads in rural areas of Norway and with AADT less than 1500 vehicles, the requirement is a lane width of 2.75 m and a shoulder width of 0.5 m. Only half of the shoulder, i.e. 0.25 m, has to be paved, which implies that the total width of the paved surface is only 6.0 m. When two trucks meet at a road like this, the pavement will obviously be exposed to heavy traffic loads very close to the edge. In order to prevent the pavement from premature edge damages and reduce the maintenance costs, it is therefore likely

to believe that an increase of the shoulder width to 0.75–1.0 m would be beneficial. A wider shoulder is also favourable from a traffic safety point of view. On the contrary, construction of roads with wider shoulders will of course bring along higher investment costs.

7.2 Recommendations for further research

The present work has contributed to new and interesting knowledge concerning the variation of load responses towards the pavement edge. Nevertheless, a lot of both experimental and theoretical research still remains in order to give a more complete understanding of the subject for a wider range of pavement types, material qualities and layer thicknesses.

Some of the results from the Sandmoen test field, especially concerning the horizontal load response in granular layers, were quite unexpected. Therefore, complementary field measurements should be performed.

In theoretical studies, the effort should be concentrated on the development and implementation of stress dependent material models for granular materials, for use in FE analyses. Another important property of such models should be the ability to handle permanent deformations.

The consequences of increasing the required shoulder width of new Norwegian low volume roads should be evaluated through a life-cycle cost analysis including both the investment and future maintenance costs together with an evaluation of the effects regarding traffic safety issues.

REFERENCES

/1/ Baker, H. B., Buth, M. R., Van Deusen, D. A.: *Minnesota Road Research Project. Load Response Instrumentation Installation and Testing Procedures.* Report no. 94-01, Minnesota Department of Transportation, USA, 1994

/2/ Bakløkk, L., Slyngstad, T., Kristiansen, K. E.: *Bestemmelse av material-parametre for vegbyggingsmaterialer*. Report no. STF61 F83014, SINTEF, Trondheim, Norway, 1983

/3/ Biarez: *Contribution a l'Etude des Properietes in the Triaxial test*. Int. Conf. on Pore Pressure and Suction in Soils, 1962, pp 38-46

/4/ Boussinesq, J.: *Application des Potentiels à l'Ètude de l'Èquilibre et du Mouvement des Solides Èlastiques*. Paris, Gauthier-Villard, 1885

/5/ Boyce, J.R.: *A non-linear model for the elastic behaviour of granular materials under repeated loading*. Int. Symposium on Soils under Cyclic and Transient Loading, Swansea, 7-11 January 1980, pp 285-294

/6/ Burmister, D. M.: *The Theory of Stresses and Displacements in Layered Systems and Application to the Design of Airport Runways*. Highway Research Board, Proc. from 23rd Annual Meeting, 1943

/7/ Canadian Good Roads Association: *Pavement evaluation studies on Canada*. Technical publication no. 19, Ottawa, Canada, 1963, pp 191-193

/8/ Dunnicliff, J.: *Geotechnical Instrumentation for Monitoring Field Performance*. 577 p. ISBN 0-471-09614-8. Wiley, New York, 1988.

/9/ Gullberg, G.: *Bæreevne over vegens tverrprofil.* Hovedoppgave, Department of Road and Railway Engineering, The Norwegian Institute of Technology, Trondheim, 1980

/10/ Hanna, T. H.: *Field Instrumentation in Geotechnical Engineering*. Series of Rock and Soil Mechanics, Vol. 10. 843 p. ISBN 0-87849-054-X. Trans Tech Publications, Germany, 1985.

/11/ Hibbit, Karlsson & Sorensen Inc.: *ABAQUS/Standard User's Manual*. Version 5.8, USA, 1998

/12/ Hoff, I.: *Exclay Internordic Geoproject Field Test at Sandmoen, Norway, Construction and Instrumentation*. Report no. STF22 F00612, SINTEF, Trondheim, Norway, 2000

/13/ Hoff, I.: *Material Properties of Unbound Aggregates for Pavement Structures*. Doctoral thesis, Department of Road- and Railway Engineering, The Norwegian University of Science Technology, Trondheim, 1999

/14/ Hoff, I.: *Optiroc Geolight, Sandmoen test field, Surface icing and friction measurements*. Report no STF22 F02101, SINTEF, Trondheim, Norway, 2002

/15/ Hoff, I., Watn, A.: LWA Geolight - LWA for roads and Railways, Internordic *research and development project - Testfield Sandmoen, excavation and load tests.* Report no. STF22 F02107, SINTEF, Trondheim, Norway, 2002

/16/ Hvorslev, M. J. *The Changeable Interaction Between Soils and Pressure Cells; Tests and Reviews at the Waterways Experiment Station*. Technical report S-76-7. 274 p. U.S. Army waterwas Experiment Station, Vicksburg, Missisippi, 1975.

/17/ Lampinen, A.: *Variation av bärigheten i vägens tvärprofil.* Technical Research Centre of Finland (VTT), Research report 222, Finland, 1983.

/18/ Lehtipuu, E.: *Bearing capacity of road shoulders.* Proceedings from the 1st International symposium on Bearing Capacity og Roads and Airfields (BCRA) 1982.

/19/ Lekarp, F., Isacsson, U. and Dawson, A.: *State of the Art I: Resilient Response of Unbound Aggregates.* ASCE Journal of Transportation Engineering, vol. 126, no. 1/2000, pp 66-75

/20/ Lerfald, B. O.: *A study of Ageing and Degradation of Asphalt Pavements on Low Volume Roads.* Doctoral thesis, Department of Road and Railway engineering, The Norwegian University of Science Technology, Trondheim, 2000

/21/ Harichandran, S., Baladi, G. Y., Yeh, M. S.: *Mich-Pave User's Manual*. Michigan State University, Department of Civil Engineering, Michigan, USA, 1989.

/22/ Nordal, R. S., Hansen, E. K.: *Vormsund test road , Part 3: Observations and results.* Meddelelse nr. 57, Norwegian Road Research Laboratory, 1984.

/23/ Nordal, S.*: Soil modelling.* Class notes from EEU course / dr.ing. course 33584, Department of Geotechnical Engineering, The Norwegian Institute of Technology, October 1994

/24/ Odemark, N.: *Undersökning av elasticitetsegenskaperna hos olika jordarter samt teori för beräkning av beläggningar enligt elasticitetsteorin*. Statens Väginstitut, Meddelande 77, Sweden, 1949

/25/ Opplysningsrådet for vegtrafikken: Bil- og vegstatistikk 2002. Oslo, 2002

/26/ Peattie, K. R., Sparrow, R. W.: *The Fundamental Action of Earth Pressure Cells*. Journal of Applied Mechanics, Vol. 18, 1951.

/27/ Selig, E. T.: *In Situ Stress Measurements.* State of the Art of Pavement Response Monitoring Systems for Roads and Airfields. CRREL Special Report 89-23, p. 162-170. USA, 1989.

/28/ Statens vegvesen: *Håndbok 014 Laboratorieundersøkelser*. Vegdirektoratet, Oslo, 1997

/29/ Statens vegvesen: *Håndbok 015, feltundersøkelser.* Vegdirektoratet, Oslo, 1997

/30/ Statens vegvesen: *Håndbok 017 Veg og gateutforming*. Vegdirektoratet, Oslo, 1993

/31/ Statens vegvesen: *Håndbok 018 Vegbygging*. Vegdirektoratet, Oslo, 1999

/32/ Timoshenko, S.: *Theory of elasticity*. McGraw-Hill Book Company, New York, 1934

/33/ Thompson, M. R.: *Illi-Pave User's Manual*. University of Illinois at Urbana, Illinois, USA, 1984.

/34/ Tory, A. C., Sparrow, R. W.: *The Influence of Diaphragm Flexibility on the Performance of an Earth Pressure Cell*. Journal of Scientific Instruments, Vol. 44, No. 9, p. 781-785. 1967.

/35/ Ullidtz, P.: *Modelling of Granular Materials Using the Discrete Element Method.* Proceedings from the 8th International Conference on Asphalt Pavements, Vol. 1 pp 757-769, Seattle, 1997

/36/ Van Deusen, D. A., Newcomb, D. E., Labuz, J. F.: *A Review of Instrumentation Technology for the Minnesota Road Research Project*. Final report. Research Administration and Development Section, Office of Materials and Research, Minnesota Dept. of Transportation, 1992.

/37/ Vägverket: *Bärighet nära vägkant.* DDa-rapport, B-project 199, delrapport 2, 83609-27, Sweden, 1983.

/38/ Vägverket: *Bärighet nära vägkant.* DDa-rapport, B-project 199, delrapport 3, 85604-27, Sweden, 1985.

/39/ von Mises, R.: Mechanik der plastischen Formänderung von Kristallen. Zamm, 1928

/40/ Weiler, W. A., Kulhawy, F. H.: *Factors Affecting Stress Cell Measurements in Soil*. Proceedings ASCE, Journal of Geotechnical Engineering Division, Vol 108, No. GT12, p. 1529-1548. 1982.

Reports from The Department of Road and Railway Engineering

Report no.	Author	Title	Year
1	Kummeneje, Ottar	Rutebilstasjoner	1949
2	Riise, T.B.	Terrengets innflytelse på vindens retning og hastighet styrke	1950
3	Lærum og Ødegård	Grunnlag for vurdering av den økonomiske verdi av vegforbedringer	1957
4	Ødegård, Erik	Vegen som forretning	1959
5	Ording, Jørgen	Undersøkelser av asfaltdekker i Trondheim	1961
6	Riise og Heim	Undersøkelse av torvmatters innflytelse på faste dekker	1962
7	Gustavsen, Øyvind	En analyse av trafikkutviklingen ved overgang fra ferje- til bruforbindelse	1964
8	Sagen, Ragnvald	Traffic Simulation	1967
9	Riise, T.B.	Blandingsjordarters telefarlighet	1968
10	Kvåle, Kjell	Studiereise på veganlegg i Alpeland	1972
11	Norem, Harald	Utforming av veger i drivsnøområder	1974
12	Svennar, Odd	Nærtrafikkbaner	1975
13	Arnevik, Asbjørn	Overflatebehandling	1976
14	Noss, Per Magne	Poresug i jordarter	1978
15	Slyngstad, Tore	Filler i bituminøse vegdekker	1977
16	Melby, Karl	Repeterte belastninger på leire	1977
17	Tøndel, Ingvar	Sikring av veger mot snøskred	1977
18	Angen, Eigil	Fukttransport i jordarter	1978
19	Berger, Asle Ketil	Massedisponering. Beregning av kostnadsminimale transportmønstre for planering av fjell- og jordmasser ved bygging av veier	1978
20	Horvli, Ivar	Dynamisk prøving av leire for dimenjonering av veger	1979
21	Engstrøm, Jan Erik	Analyse av noen faktorer som påvirker anleggskostnader for veger	1979
22	Hovd, Asbjørn	En undersøkelse omkring trafikkulykker og avkjørsler	1979
23	Myre, Jostein	Utmatting av asfaltdekker	1988
24	Mork, Helge	Analyse av lastresponsar for vegkonstruksjonar	1990
25	Berntsen, Geir	Reduksjon av bæreevnen under teleløsningen	1993
26	Amundsen, Ingerlise	Vegutforming og landskapstilpassing, Visuelle forhold i norsk vegbygging fra 1930 til i dag	1995
27	Sund, Even K.	Life-Cycle Cost Analysis of Road Pavements	1996
28	Hoff, Inge	Material Properties of Unbound Granular,	1999

URN:NBN:no-3347

		Materials for Pavement Structures	
29	Lerfald, Bjørn Ove	Study of Ageing and Degradation of Asphalt Pavements on Low Volume Roads	2000
30	Løhren, Alf Helge	Økt sidestabilitet i kurver med små radier	2001
31	Hjelle, Hallgeir	Geometrisk modellering av veger i 3D	2002
32	Skoglund, Kjell Arne	A Study of Some Factors in Mechanistic Railway Track Design	2002
33	Garba, Rabbira	Permanent Deformation Properties of Asphalt Concrete Mixtures	2002
34	Thordarson, Skuli	Wind Flow Studies for Drifting Snow on Roads	2002
35	Aksnes, Jostein	A Study of Load Responses towards the Pavement Edge	2002

URN:NBN:no-3347